Journal Of Applied Chemistry

Vol. 24 No. 6

THE ROLES OF OXIDATION VOLUME AND OF A SEPARATE DENITRATOR IN A SULFURIC ACID TOWER SYSTEM

M. E. Pozin and N. E. Kirichenko

As we know, the higher the percentage of nitrogen in the cycle, the greater the efficiency of the Mills-Packard process, the nitric acid losses depending largely upon concentration ratio of the nitrogen oxides to the sulfur dioxide in the gas phase. Correcting this ratio in time as the concentration of the sulfur dioxide fluctuates ensures minimum losses of nitric acid. A change in the concentration of the sulfur dioxide is due to the irregular supply of pyrites to the furnaces and occurs in all sulfuric-acid plants.

Changes in the required ratio between the concentrations of the nitrogen oxides and the sulfur dioxide result in periods of operation of tower installations during which the losses of nitrogen oxides rise sharply. It is certain that the absorption of the nitrogen oxides is most complete when they exist as an equimolecular mixture of NO and NO_2. When the SO_2 concentration rises, the extent of oxidation of the nitrogen oxides is too low, the NO predominating, while a drop in the SO_2 concentration causes the nitrogen oxides to reach the absorption zone primarily as NO_2. Careful maintenance of the required concentration ratio ensures a low consumption of nitric acid even at extremely high operating loads, while a departure from this ratio results in a high loss of nitric acid even at low operating loads.

At the present time, as the result of accumulated experience, we possess various means of correcting the degree of regeneration of the nitrogen acids in the tower system. In addition to the use of a regulating oxidizing space in the shape of a special non-trickling tower between the production and absorption zones of the system, these means include: regulating the concentration of H_2SO_4 in the nitroses; employing a sulfur dioxide by-pass; feeding the mixture into the next to the last tower; using the unregulated space above the brickwork in the first absorption tower for the complete oxidation of the nitric oxide; using this same volume, but regulating the passage of all or part of the gas through it; varying the nitrose trickling rate in the towers, varying the temperature of the nitroses supplied to the production towers; varying the quantity of furnace gas by regulating the

streams entering the first two parallel production towers.

There are other ways of regulating the regeneration of the nitrogen oxides, such as: wetting part of the furnace gas in a special device (by spraying hot water or passing the gas through trickling checkerwork, or by using an ejector), thus making it possible to vary the density of the nitrose in the reaction zone rapidly; regulating the concentration of SO_2 in the gas by pumping air ahead of the production or absorption towers; varying the concentration of the sulfur dioxide produced in the pulverized-combustion furnaces by regulating the pyrites supply automatically (provided preliminary drying and screening are not omitted); and correcting the SO_2 concentration in the furnace gas by means of special evaporating or combustion chambers for sulfur.

The degree of processing of the nitrogen oxides before they reach the absorption towers may also be controlled by regulating the temperature of the gas passing through the unregulated or regulated oxidation space. This may be done by means of water-cooled coolers set up within the oxidation space or by spraying cold weak sulfuric acid or a high-nitrose acid that had been previously cooled in a cooler.

The same purpose may be served by feeding into the first absorption tower nitric oxide (especially the oxide obtained from the ammonia-oxidizing installation of the sulfuric acid plant) or nitric-acid vapor produced by heating the mixture with steam or water in a special installation.

This list of the methods available to regulate the processing of the nitrogen oxides before regeneration need not be extended. There are enough methods available all of them aimed at solving a single problem in the operation of a sulfuric acid plant: achieving an efficient composition of the nitrose gasses ahead of the absorbers.

It should be stressed, however, that this problem is not directly related to the problem of increasing production. Preparing the nitrogen oxides for absorption is an elementary requirement in the operation of any sulfuric acid plant, no matter how high its load factor. We therefore believe that the endeavor to regard the preliminary preparation of the nitrogen oxides before their absorption in a hollow non-trickling oxidizing tower as "one of the decisive factors in intensifying the tower process" [1] is erroneous. The controversy on the role of the oxidation space has for many years diverted the attention of workers in scientific organizations and plants from the solution of important, fundamental problems involved in increasing the rate of sulfuric acid production.

In the paper cited, Baleev writes: "One of the decisive factors in intensifying the tower process of producing sulfuric acid is the preliminary oxidation of the nitrogen oxides to an <u>equimolecular</u> ratio of the NO and NO_2 before they are absorbed" (our emphasis – M. P. and N. K.). The idea of achieving an equimolecular ratio of the NO and NO_2 before their absorption and the installation of a regulating oxidation space for this very purpose in the shape of a special non-trickling tower is basically faulty, as has been confirmed by the experience of several factories. As a matter of fact, the supporters of this idea believe that the nitrose gases leaving the production zone, most of whose nitrogen oxides are in the form of NO, can be oxidized to a ratio of $NO:NO_2 = 1$ in a small oxidation space installed ahead of the absorption zone. They forget that the free space ahead of the absorption tower is about 3 times as large as the volume of the oxidation tower they recommend. Hence, the gas must stay in the first absorption tower three times as long as in the oxidation tower. This cannot be disregarded in the belief that the

nitrogen oxides oxidized in a special tower to an equimolecular ratio of the NO and NO_2 will retain this degree of oxidation during their long sojourn in the free space in the absorption zone. It is obvious that if a gas processed until its $NO:NO_2$ ratio is equimolecular is fed into the absorption zone, it will be further enriched with nitric acid in that zone. In other words, the nitrose gas will be greatly overoxidized, resulting in the appearance of a dark-red "tail" in the waste tower gases, which is evidence of an inadmissible increase in the consumption of nitric acid.

We might agree to the advisability of processing the nitrose gases in a special oxidizing tower until their $NO:NO_2$ ratio was equimolecular if the champions of this idea proposed to eliminate, or at least to retard sharply, the further oxidation of the nitric oxide in the regeneration zone by resorting to such measures as: sharply reducing the free space in the absorption-tower packing; greatly increasing the specific surface of absorption, thus making it possible to increase the absorption rate of the nitrogen oxides greatly and thus shorten the time the gas stays in the towers; and using a concentrated furnace gas that is so processed as to leave 1-2% oxygen in the gas leaving the production zone instead of the usual 6-8%.

But neither these measures nor any others having the same objective are proposed by the champions of preparing the nitrogen oxides to an equimolecular mixture in a special oxidation space. In any event, no such measures are mentioned in the articles published in defence of the oxidation space.

Calculations indicate that if the nitrogen oxides are in the form of nitrogen trioxide ahead of the regeneration zone, the further oxidation in that zone will be so pronounced that the excess of NO_2 above the equimolecular ratio may be as high as 15-20%, in spite of the marked retardation of oxidation due to the decrease in the NO concentration. This figure is 1% and more in terms of absolute concentrations by volume, representing disastrous losses of nitrogen oxides in the waste gases. It should be borne in mind that this also involves a drop in the absorption rate due to the appearance of nitric acid in the nitrose, and not merely because of a departure from the ideal $NO:NO_2$ ratio in the gas.

We cite below an illustrative rough calculation of the oxidation of the nitrose gas in the free space in the packing of the first absorption tower, based on the operating data for a tower system in October 1938 at a rate of 100 kg of H_2SO_4 per cu m per day. This calculation shows the extent of the post-oxidation of the nitric acid occurring in the absorption space.

Initial data: SO_2 concentration in the furnace – 9.6%; system load – 235 t H_2SO_4 per 24 hours; characteristics of the first absorption tower: $D_{inc.} = 6.5$ m, $H_{tot.} = 14$ $H_{packing} = 11.5$ m; packing – ceramic rings 50 x 50 mm; mean gas temperature inside the tower – 75°, pressure – 9700 mm water column; per cent nitrogen oxides in the gas entering the tower – 6.7%, in the gas leaving the tower 1.9%, including 0.2-0.3% NO_2.

Free space in the tower = 260 cu m; specific volume of gases at 75° = 3078 cu m per ton; gas volume per second = $\frac{235 \cdot 3078}{24 \cdot 3600}$ = 8.4 cu m per sec; time gas stays in the tower = $\frac{260}{8.4}$ = 31 sec. The oxygen concentration in the gas entering the first absorption tower was 3.6%.

Notation: $\underline{x}$ = % NO in the gas entering the first absorption tower; $\underline{y}$ = % NO_2 produced by post-oxidation of the gas in that tower.

It is obvious that the gas entering the tower contains $(6.7 - \underline{x})\%$ NO_2. The NO_2 absorbed $= \frac{6.7 - 1.9}{2} = 2.4\%$. 0.3% remained unabsorbed. The NO_2 material balance (disregarding the change in the overall gas volume) is: $6.7 - \underline{x} + \underline{y} = 2.4 + 0.3$, whence $\underline{x} = 4 + \underline{y}$.

In this case, at 75° the velocity constant of NO oxidation, $\underline{K}_p = 24$; $\tau = 31$ sec; the pressure $\underline{P} = 0.94$ atm; the initial oxygen concentration $\underline{b} = 0.036$; half the mean concentration[1] of NO in the tower, $a = \frac{x - 1.6}{2 \cdot 100 \cdot \ln \frac{x}{1.6}}$ (where 1.6 is the NO concentration in the outlet gas); and the degree of oxidation (in this case the extent of post-oxidation within the tower) $\alpha = \frac{y}{2a \cdot 100}$, or, since $\underline{y} = \underline{x} - 4$, $\alpha = \frac{x - 4}{2a \cdot 100}$.

Substituting these values in the equation for the rate of NO oxidation:

$$K_p \cdot \tau \cdot P^2 = \frac{1}{(b - a)^2} \left[\frac{(b - a)\alpha}{(1 - \alpha)a} + \ln \frac{1 - \alpha}{1 - \frac{a\alpha}{b}} \right],$$

and solving, we get $\underline{x} = 4.7$.

Hence, the gases entering the first absorption tower contain 4.7% NO and $6.7 - 4.7\% = 2\%$ NO_2, while the post-oxidation of the gas in the free space of this tower's packing yielded $\underline{y} = 4.7 - 4 = 0.7\%$ NO_2.

It is apparent that the gases entering the regenerator will be oxidized to nearly the equimolecular ratio only when the nitrose process is superefficient, with the free space in the absorption zone so small that the degree of oxidation remains practically unchanged while the gas stays in it. When these conditions are satisfied, a special oxidation space, exceeding by far the free space in the absorption zone, is a convenient means of regulating the composition of the gas. It is one such method applicable to existing tower systems as well, but it cannot be regarded as the decisive factor in raising the load carried by such systems.

Other critical comments may be made concerning the views set forth in the cited paper by Stupnikov and Baleev.

The notion that the oxidation volume cannot be placed behind the third tower in a five or six-tower system is debatable, since it is not the number of towers that matters but rather the composition of the gas. As a matter of fact, when the third tower is operating essentially as an absorber of the nitrogen oxides, the effectiveness of an oxidation space installed behind it will be low, owing to the low concentration of the nitrogen oxides in the gases entering it. But when the gases entering the third tower still contain an appreciable percentage of SO_2 (as is usually the case), the effectiveness of an oxidation space installed behind the third tower will still be low, for the sulfur dioxide paralyzes the action of the oxidation space by strongly deoxidizing the nitrogen

[1] We used half the mean concentration instead of the initial concentration because the fall in the NO concentration during the passage of the gas through the tower is due to absorption as well as oxidation; this procedure is not entirely accurate, but the error involved is slight.

dioxide. This impairs the absorption of the nitrogen oxides, owing to their insufficient oxidation as well as to the excessive heating of the nitroses because of the SO_2 in the gas. This will make the oxidation space installed behind the third tower operate poorly, unless its location strictly conforms to the chosen operational regime of the system, with no departures from this régime allowed.

Though the authors believe that the procedure followed by one plant, where the oxidation space was converted into a tower with a trickle packing, is inefficient, basing their conclusion upon the fact that the SO_2 concentration ahead of the first absorption tower was not reduced and the consumption of nitric acid was not diminished, they are forced to admit that this increased the system's output by 25-30%. To be sure, the authors believe that there is no relationship between the substitution of trickling for the oxidation space and the increase in the system output. But there is only one possible conclusion, namely, that the provision of free oxidation space is completely unnecessary for the satisfactory and efficient operation of present-day tower systems. In the concluding paragraph of their paper, the authors also come to this conclusion, although their article is devoted to a defense of the necessity of oxidation space.

The authors regard the introduction of trickling oxidation space into the system as a return from "short" to "long" systems, identifying the former with high-load systems and the latter with low-load systems. In support thereof they print a table containing information on the number of towers in various systems, their load factors, and their consumption of nitric acid. But the figures in the table are no evidence, for they are incommensurable. The table gives no data on the operating conditions in the systems compared: the quality of the nitrose, the trickling rate, the composition of the furnace gas, the provision of furnace gas for the system, the gas flow rate, the nitrose temperature, the cleanliness of the packing, the true surface of the tower packing, and the like. In other words, nothing is said about the most important factors governing the load factor of each system. For this reason the cited table can hardly serve to prove that "short" systems are the high-load ones, and hence that "short" systems are superior to "long" ones.

We cannot subscribe to the view that the longer a system is, the more uneconomical it is. Modern engineering does not strive necessarily to reduce the number of details in an object. It is frequently better to perform individual processes in specially adapted apparatus than to combine them in a single apparatus. An instance in point is the first production tower, which fulfils contradictory functions. This tower has to supply the system with a large quantity of denitrated acid, which is incompatible with the requirement of complete denitration; hence, assigning these functions to two separate, specialized installations would doubtless increase the efficiency of the system, even though it lengthened the latter.

The advisability of a tower installation providing for a special denitrator tower connected in parallel with the first tower has been discussed more than once. Kuzminykh, in his paper [2], again offers convincing proof of the efficiency of operation with a special denitrator. We fully agree with the arguments adduced in this paper and are only compelled to cast doubt upon the small volume that Kuzminykh believes is needed for the denitrator, which he therefore calls a "little tower".

We know from experience that the volume of the first tower is sometimes insufficient to ensure the production of a well-denitrated output, notwithstanding the fact that it constitutes 5 to 7% of the total system volume. We think that the 10-15% of the furnace gas that it is proposed to pass through the denitrator will not ensure satisfactory denitration. Nor must we lose sight of the fact that passing a small amount of gas through the denitrator will sharply increase the concentration of the nitrogen oxides in the gas, thus retarding the denitrating process.

If a nitrose containing only 4% HNO_3 (nominal) is fed into the denitrator in a high-load system, the concentration of nitrogen oxides in the denitrator outlet gases will be:

$$\frac{1000 \cdot 0.04 \cdot 22.4 \cdot 100}{0.75 \cdot 63 \cdot 250} = 8\%.$$

(In this case: 250 cu m of gas per ton of product = 10% of 2500 cu m per ton; acid concentration = 75%). So high a nitrosity of the gas is encountered only after the second production tower, which supplies a nitrose with a concentration of 4-6% HNO_3 even with counterflow. The concentration of nitrogen oxides in the gases coming from the towers that furnish the product is no more than 1.5-2%. To ensure a concentration of this magnitude, the portion of the gas that passes through the denitrator must not constitute 10-15%, but four to five times as much, that is 50-60%. When we remember that the gas concentration varies logarithmically with the tower height and start out with the mean concentration of nitrogen oxides in the gas in the special denitrator at the same level as in the operating producing towers, the percentage of the gas passed through the denitrator is 30-50%.

Hence, about half of the furnace gas should be passed through the denitrator. Therefore, the problem boils down to the restoring of parallel operation of the production towers by utilizing the available towers correctly.

When a little tower is used as a special denitrator, with only 10-15% of the furnace gas passed through it, satisfactory denitration may be achieved, as N. I. Kuzminykh asserts, provided a separate cycle is used for trickling a low-nitrose acid through the denitrator and tapping off the product at intervals. It must be borne in mind however, that the latter condition complicates manufacture by interrupting the continuous operation of the system.

LITERATURE CITED

[1] S. D. Studnikov and A. V. Baleev, Jour. Chem. Ind. 7, 195 (1949).

[2] N. I. Kuzminykh, Jour. Chem. Ind. 7, 196 (1949).

Received June 28, 1950.

THE PHYSICAL CHARACTERISTICS OF FINE-GRAINED CRYSTALLINE MASSES IN RELATION TO REACTIONS OF THEIR MIXTURES

A. M. Ginstling

The Lensoviet Institute of Technology, Leningrad

Reactions in mixtures of solid, fine-grained substances, called solid-phase reactions, are of great importance industrially at the present time.

As a rule, the mechanism of these reactions "in the solid state" are treated, as the direct interaction of solids, as proposed by Tammann, involving the detachment of particles (atoms, molecules, ions or complexes) from the crystal lattice of one reagent and their penetration into the lattice of the other reagent without any preliminary conversion into the gaseous or liquid state.

In this connection one of the basic factors governing the reaction rate in powder mixtures is held to be the surface of contact between the solid particles (grains) of the components in the initial mixture.

The present paper is an endeavor to discuss these problems in the light of data obtained in a study of the reactions occurring in mixtures of solids.

As we know, the surface of contact between the grains of a solid dispersed mass, which is an extremely small part of the total surface of these grains, depends largely upon the form, dimensions, and spatial arrangement of the grains, and may vary over a very wide range.

In the simplest case, when the grains are spherical and of identical diameter, each grain is in contact with its neighbors at 6,8, or 12 points, on the whole, depending upon the nature of their spatial arrangement, the amount of free space (the porosity) between the particles varying accordingly from 47.64 to 25.95%. These figures which apply to the geometrically perfect spatial arrangement of absolutely smooth, incompressible, dry spheres, which touch at individual mathematical points, hardly correspond, of course, to the properties and behavior of real, crystalline, free-flowing masses. We cannot secure the ideal dense arrangement of these particles (corresponding to the free space value of $V_{free} = 25.95\%$) in practice, nor can we count on their geometrically perfect free arrangement (corresponding to $V_{free} = 47.64\%$), because of the irregularity of form and the surface roughness of the particles in fine-grain substances and because of the existence of frictional and adhesion forces between them. In actual masses the various constituent grains are spaced at varying distances: some of the adjacent grains being in rather close contact with one another, while the distance between other adjacent grains is rather great, and so forth. The irregularity of form and the roughness of surface of the grains in real masses result in the distance between various portions of the surface of any one grain and the surface of the surrounding grains fluctuating within the

widest limits.

In general, however, when we consider any fine-grain mass, we may speak of a mean value representing the distance between the surfaces of its constituent grains. This value, which is extremely important in analyzing the interactions occurring within solid mixtures, may be readily found as follows.

If a unit total volume of a free-flowing mass consists of n spherical grains with a mean diameter of $d_{gr.}$ and, correspondingly, n spaces with a mean diameter of $d_{sp.}$, constituting together the free space with a volume of V_{free} (in fractions of unity), the volume of the grains proper will be:

$$1 - V_{free} = n \frac{\pi d^3_{gr.}}{6} \qquad (1)$$

and the volume of the empty space will be:

$$V_{free} = n \frac{\pi d^3_{sp.}}{6}. \qquad (2)$$

When the mean diameter of a single space $d_{sp.}$ or, in other words, the mean distance l between the grains will be:

$$l = d_{sp.} = d_{gr.} \left(\frac{V_{free}}{1 - V_{free}} \right)^{1/3}. \qquad (3)$$

Moreover, if $\delta_{wt.}$ is the mean apparent specific gravity of a particle (a grain), then the total volume of all the fine-grain material, consisting of the aggregate volume of the particles proper $\frac{1}{\delta_{wt.}}$ and the aggregate volume of the spaces between the particles, will be:

$$V_{total} = \frac{\frac{1}{\delta_{wt.}}}{1 - V_{free}}. \qquad (4)$$

And as the unit weight of the dry, granular material,

$$\gamma_{gr.} = 1 : \frac{\frac{1}{\delta_{wt.}}}{1 - V_{free}} = (1 - V_{free})\, \delta_{wt.}, \qquad (5)$$

we get

$$V_{free} = 1 - \frac{\gamma_{gr.}}{\delta_{wt.}}. \qquad (6)$$

Substituting (6) in (3), we get:

$$l = d_3. \left(\frac{\delta_{wt.} - \gamma_{gr.}}{\gamma_{gr.}} \right). \qquad (7)$$

Therefore, once we know the weight per cubic meter of the dry, granular material, the mean diameter of its constituent grains, and the latter's apparent specific gravity, we can estimate the mean distance between the surfaces of adjacent grains in the material.

Equation (7), which is correct for spherical grains, expresses the mean distance between the surfaces of adjacent grains in a fine-grain mass with sufficient accuracy for practical purposes, no matter what the grain shape may be.

Determining the value of $\underline{l}$ in real masses may be complicated somewhat only by the difference between the true and apparent density of the substance's particles and by errors in determining the latter. The aggregate volume of the inter-particle spaces that govern this difference usually is 0.5 to 15% of the grain volume, as is proved by experimental data on inorganic crystalline substances [1, 2], however, and hence does not exceed 7% of the poured volume of all the grains (the only exceptions to this rule are sorbents, refractories, heat insulators, and other materials whose porosity has been increased artificially). When we remember that the volume of the inter-particle space does not exceed 50% of the poured volume of the grain mass, as a rule (see the experimental data cited below, by way of example), we readily see that the true density of the substance comprising the particles may be substituted for $\gamma_{wt.}$ in Equation (7) in ascertaining the <u>order of magnitude</u> of the values applying to the grain mass.

It is interesting to demonstrate, on the basis of experimental data, the order of magnitude of the mean distance between the surfaces of adjacent grains in actual masses to characterize the properties of crystalline, fine-grained materials in the reactions occurring in their mixtures. With this as our objective, a great number of crystalline, fine-grained substances has been investigated in the present research.

All these substances were carefully classified according to size to determine the weight per unit volume of the dry, granular material. Then 2,3,4 narrow fractions were selected for each substance. The mean diameter of the grains within each narrow fraction, determined by the size of the openings in the coarser and finer screens, was calculated from the equation:

$$d_{ave.} = \sqrt[3]{\frac{2d^2_{max.}}{d_{max.}} \frac{d^2_{min.}}{+ d_{min.}}}, \qquad (8)$$

where $\underline{d}_{max.}$ and $\underline{d}_{min.}$ are the diameters of the largest and smallest grains in the fraction, corresponding to the size of the openings in the coarser and finer screens; and the number of nominal grains of the average diameter $\underline{d}_{ave.}$, as calculated from this equation, is equal to the actual number of particles in the fraction. Table 1 describes the principal selected fractions of fine-grained substances.

TABLE 1

Characteristics of Tested Fractions of Fine-Grained Substances

Size range of grains in the fraction, (mm)	Average grain size, (mm)
0.350-0.270	0.306
0.350-0.250	0.294
0.270-0.250	0.259
0.250-0.200	0.223
0.200-0.135	0.163
0.135-0.120	0.127
0.102-0.088	0.095
0.088-0.060	0.072

The weight per unit volume of the "coarse" and "fine" fractions and of equal-volume mixtures of the two was determined for each substance in order to find the variation of $\gamma_{gr.}$, V_{free}, and $\underline{l}$ with particle size in the fine-grained mass. Some of the results of these determinations are listed in Table 2, which deals with no more than 20 inorganic substances of industrial importance, for reasons of space.[1] In accordance with the foregoing, $\gamma_{wt.}$ in the table denotes the true specific gravity of the substance making up the particles, while $\underline{V}_{free}$ is the aggregate (intra-particle and inter-particle) porosity of the mass. The third line

1) See following page for footnote.

in the entry for each substance represents a mixture of equal volumes of the two fractions represented by the first two lines of the entry.

The $d_{ave.}$ of the grains in this mixture is calculated as a weighted-mean dimension, based on the following considerations.

If $d_{max.}$ and $d_{min.}$ are the mean diameters of the grains in the "coarse" and "fine" fractions, and $n_{max.}$ and $n_{min.}$ are the numbers of particles in equal volumes of these fractions, the mean size of the grains in the mixture will be:

$$d_{ave.\ mix.} = \frac{n_{max.}\, d_{max.} + n_{min.}\, d_{min.}}{n_{max.} + n_{min.}}. \qquad (9)$$

The ratio between the numbers of grains in equal volumes of the fractions may be taken to equal:

$$\frac{n_{max.}}{n_{min.}} = \frac{d^3_{min.}}{d^3_{max.}}. \qquad (10)$$

Solving (9) and (10) simultaneously, we get:

$$d_{ave.} = \frac{d^3_{min.}\, d_{max.} + d^3_{max.}\, d_{min.}}{d^3_{min.} + d^3_{max.}} \qquad (11)$$

The experimental data listed in Table 2 indicate that:

1) The spatial arrangement of grains in real fine-grained masses seems to differ essentially from any "theoretical" arrangement of smooth spherical particles.

2) The porosity of these masses is 50-80%, as against 26-48% for the porosity of a mass of smooth spheres.

3) The mean distance l between the surfaces of adjacent grains in the real mass and the average grain diameter $d_{ave.}$ are of the same order of magnitude, l being 120-150% of $d_{ave.}$

4) The porosity of the mass is greater when its component grains are all of the same size than when their sizes differ.

5) If the mass consists of particles (grains) of about the same size, the porosity of the mass and, hence, the mean distance between the surfaces of its grains increase as the grain size decreases.

These findings are in full agreement with the theory. The impossibility of close contact between rough surfaces naturally results in an appreciable increase in the free space between them. It is obvious that a diminution in the size of the particles in the mass, resulting in an increase in the surface of these particles per unit weight, produces a corresponding increase in internal friction and in the stability, the "strength", of the mass. This latter fact is borne out by the data in Table 3 on the angle of repose of some fine-grained substances. One result of this increase in the "strength" of the mass is an increase in its porosity. The lower porosity of a polydisperse mass than that of a monodisperse

1) The properties of the overwhelming majority of the tested substances not included in the table resemble those of the 20 compounds listed.

TABLE 2

Physical Characteristics of Crystalline, Fine-Grained Substances

Free-flowing substance	Average grain size. (mm)	Specific gravity of the substance, γ wt.	Weight per unit volume of the dry, granular material, δ gr.	Porosity of the mass, V_{free} (%)	Mean distance between surfaces of adjacent grains, l, (mm)
1	2	3	4	5	6
Al_2O_3	0.095	4.05	0.998	75.3	0.14
	0.072		1.00	75.3	0.10
	0.079		1.013	75.1	0.11
$Al(OH)_3$	0.127	2.26	1.21	46.5	0.12
	0.072		1.11	50.9	0.07
	0.082		1.18	49.8	0.08
$Al_2(SO_4)_3$	0.163	2.71	0.532	80.4	0.26
	0.095		0.518	80.9	0.15
	0.107		0.550	79.8	0.17
AlF_3	0.127	2.50	0.671	73.2	0.18
	0.095		0.648	74.1	0.13
	0.107		0.675	73.0	0.15
$BaSO_4$	0.259	4.46	1.20	73.1	0.36
	0.072		1.05	76.4	0.10
	0.076		1.20	73.1	0.11
Fe_2O_3	0.163	5.10	1.04	79.7	0.26
	0.072		0.99	80.6	0.12
	0.078		1.12	78.0	0.12
KNO_3	0.306	2.11	0.975	53.7	0.32
	0.095		0.720	65.8	0.12
	0.104		0.827	60.7	0.12
$K_2Cr_2O_7$	0.294	2.70	1.26	53.3	0.31
	0.095		0.94	65.2	0.12
	0.108		1.21	55.2	0.12
$CaSO_4 \cdot 2H_2O$	0.306	2.20	0.89	59.6	0.35
	0.095		0.69	68.7	0.12
	0.104		0.85	61.4	0.12
$CaCO_3$	0.163	2.71	0.506	81.3	0.27
	0.095		0.507	81.3	0.16
	0.107		0.515	81.0	0.17
CaF_2	0.163	3.10	1.15	63.0	0.19
	0.095		1.11	64.2	0.11
	0.107		1.16	62.6	0.13

TABLE 2 contd.

1	2	3	4	5	6
SiO_2	0.306 0.095 0.209	2.65	1.42 1.40 1.48	46.5 47.2 44.2	0.29 0.09 0.18
MgO	0.306 0.127 0.195	3.45	0.204 0.188 0.230	94.09 94.56 93.86	0.77 0.33 0.47
$MgSO_4 \cdot 7H_2O$	0.306 0.095 0.163	1.68	0.725 0.477 0.677	56.9 71.7 59.7	0.33 0.13 0.19
$CuSO_4 \cdot 5H_2O$	0.306 0.095 0.163	2.2[illegible]	1.04 0.715 1.02	54.6 58.8 55.5	0.33 0.12 0.18
$Na_2SO_4 \cdot 10H_2O$	0.163 0.095 0.107	1.46	0.70 0.66 0.72	51.7 55.0 50.4	0.17 0.10 0.11
NaF	0.095 0.072 0.077	2.[illegible]3	0.952 0.952 1.0	65.2 65.2 63.4	0.12 0.09 0.09
NaCl	0.163 0.095 0.107	2.16	0.927 0.843 0.892	57.1 61.0 58.8	0.18 0.11 0.12
$(ClF)Ca_5(PO_4)_3$ (apatite)	0.163 0.095 0.107	3.2	1.56 1.54 1.59	51.1 52.0 50.4	0.17 0.10 0.11
$mAl_2O_3 \cdot 2H_2O \cdot nFe_2O_3 \cdot qSiO_2$	0.259 0.095 0.147	2.58	1.10 0.98 1.04	56.9 61.6 59.2	0.29 0.11 0.17

mass of the same substance is naturally due to the small grains filling up the spaces between the coarse grains, etc.

The fact that the relative increase in the surface of contact between the particles of a fine-grained material as the grain size decreases may be wiped out by the relative growth in the surface of these particles in an essential practical corollary flowing from the cited data.

But what is most important for further analysis, however, is the conclusion that follows from the experimental findings that the surface of the particles in fine grained solid reagents (particularly powdered ones), when mixed together, are spaced on the average a distance that is 1.2 to 1.5 times the diameter of these particles.

TABLE 3

Angles of Repose of Free-flowing Masses at Different Grain Sizes

Freeflowing substance	Grain size (mm)	Angle of repose
$BaSO_4$	0.25 -0.060	41°60'
	0.088-0.060	45°
KNO_3	0.35 -0.27	38°40'
	0.102-0.088	45°
NaCl	0.20 -0.135	39°42'
	0.102-0.088	41°60'
$AlNH_4(SO_4)_2 \cdot 12H_2O$	0.35 -0.27	36°53'
	0.20 -0.135	45°

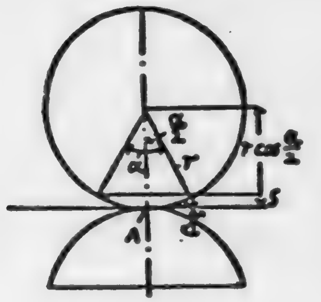

Fig. 1. Contact between two spherical particles.

Let us estimate the possible surface of contact between grains of a free-flowing mass. We shall regard the surfaces as in contact whenever the distance between them does not exceed the action radius of the molecular forces. We know that this radius is measured in Angstroms, i.e., is of the order of 10^{-8} cm. As for the grain size of the initial reagents, this dimension may be said to be of the order of 10^{-1} - 10^{-3} cm in various solid-phase processes in practice (in the technology of silicates, alumina, electrothermal manufacture, and other industries [3,4,5]).

Let us now return to the smooth, dry, spherical particles (grains) of uniform diameter. Let two such particles of radius r be in contact at some point A (Fig. 1). Let S be the radius of action of the molecular forces, and α the central polyhedral angle subtending the spherical surface of either of the grains that falls within the radius of action of the other grain's molecular forces. The cosine of half of this angle may be found from the equation:

$$S = r\left(1 - \cos\frac{\alpha}{2}\right) . \tag{12}$$

With $S = 10^{-8}$ cm and $r = 10^{-1} - 10^{-3}$ cm, we find from (12) that α may range from a few (1-2) seconds of arc to a few minutes, which is equivalent to a theoretically possible surface of contact between the particles that ranges from 10^{-7} to 10^{-4} of the total surface of these particles.

The results of various investigations [6] indicate that the contact surface between the grains of real masses is of the order of millionths of the total surface of the grains.

If we assume that the grains are spherical and consider the free space between them to be 50% of the aggregate volume of the free-flowing mass constituted by them, and if we bear in mind that the contact surface between them is of the order of 10^{-4}% of their total surface, according to the experimental findings, we can readily obtain the approximate surface of contact between grains in masses containing particles of different size, as shown in Table 4.

It is obvious that the rough surface of the particles in a real mass is much greater than their apparent surface and still greater than the surface of

TABLE 4

Approximate Surface of Contact Between Particles in a Fine-Grained Mass[1]

Grain diameter, in cm	Grain volume, cm^3	Grain surface, cm^2	Number of grains per cu cm of the mass	Surface of grains in 1 cu cm of the mass, sq cm	Approximate surface of contact between grains in 1 cu cm of the mass, sq cm
1	$5.23 \cdot 10^{-1}$	3.14	$9.57 \cdot 10^{-1}$	3	$3 \cdot 10^{-6}$
$5 \cdot 10^{-1}$	$6.54 \cdot 10^{-2}$	$7.84 \cdot 10^{-1}$	7.64	6	$6 \cdot 10^{-6}$
$1 \cdot 10^{-1}$	$5.23 \cdot 10^{-4}$	$3.14 \cdot 10^{-2}$	$9.57 \cdot 10^{2}$	$3 \cdot 10$	$3 \cdot 10^{-5}$
$5 \cdot 10^{-2}$	$6.54 \cdot 10^{-5}$	$7.84 \cdot 10^{-3}$	$7.64 \cdot 10^{3}$	$6 \cdot 10$	$6 \cdot 10^{-5}$
$1 \cdot 10^{-2}$	$5.23 \cdot 10^{-7}$	$3.14 \cdot 10^{-4}$	$9.57 \cdot 10^{5}$	$3 \cdot 10^{2}$	$3 \cdot 10^{-4}$
$5 \cdot 10^{-3}$	$6.54 \cdot 10^{-8}$	$7.84 \cdot 10^{-5}$	$7.64 \cdot 10^{6}$	$6 \cdot 10^{2}$	$6 \cdot 10^{-4}$

spheres of the same size. This same roughness, however, hinders contact between the particles, disengaging them (examples of the arrangement of particles in a real fine-grained mass are given in Fig. 2, a, b, c, d. See Plate p. 773). We may therefore consider the order of magnitude of the surface of contact between the particles in a fine-grained mass to be the same as those indicated in Table 4, without significant error.

Now let us consider the treatment of the interaction between solids proposed by Tammann[7], which has received wide acceptance, in the light of these findings.

In this treatment the amplitude of the vibrations of the crystal-lattice elements (atoms, molecules, ions, or complex ions) of a substance (which increases, of course, as the substance is heated) at some temperature reaches values that suffice to detach these elements from the crystal lattice and shift them to the lattice of another substance.

Following this theory and bearing in mind that the order of magnitude of the lattice vibrations (10^{-8} cm) is 10^5 to 10^7 times as small as the mean distance between the surfaces of adjacent grains of the reacting substances usually encountered in practice (10^{-3} to 10^{-1} cm), we can admit of the existence of only one path of mass transfer between the grains of the initial reagents in a solid-phase reaction: a substance penetrates from one lattice to that of another substance through the area where their grains are in contact.

The part possibly played by this path in actuality is disclosed by the following data, however. The surface of contact between solid reagents when the size of their grains ranges from 1 to 10^{-3} cm is given by quantities of the order of 10^{-4} to 10^{-6} sq cm per cu cm of the reaction mass (Table 4). The values of the diffusion coefficients from solid to solid lie within the range of 10^{-4} to 10^{-8} sq cm per sec [8, 9, 10, 11].

Bearing in mind these figures and remembering that the density of the substances and the driving force behind the process are measured by quantities of the order of magnitude of unity, we may conclude, after a simple calculation,

1) Calculated on the assumption that the grains are spherical and that $V_{free} = 50\%$.

that the per cent conversion of solids per hour will range from 10^{-8}% to 3-5%, depending upon the values of the diffusion coefficient.

In actuality, as we know, conversion of the initial reagents is practically complete within 20-30 minutes, however, in many of the solid-phase processes employed in industry.[1] In other words, the actual rate of these processes is at least 100 times (and much more often 1000 times) as high as the rate that is theoretically conceivable in the light of the concept of the mechanism underlying these processes set forth above.

It should be noted that the stirring of the reacting substances usually practiced, which greatly increases the intensity of their reaction in general, introduces no fundamental change into the reasoning and conclusions set forth above. The point at issue is that stirring, though it constantly renews the contact surface between the grains of the reagents and thus largely facilitates the uniform growth of the diffusion layer in these grains, does not affect the order of magnitude of the surface of contact between them, which remains a negligibly small quantity at any given instant.

The discrepancy between the theoretical feasibility of mass transfer in the manner considered and the practical data is evidence of the limited role of this method in many processes that involve interaction between solids.

The establishment of this fact naturally gives rise to the question of how mass transfer actually takes place in processes of this type.

The treatment of the mechanism and kinetics of reactions "in the solid state" proposed by Tammann affords no answer to this question. This is because the researches of Flavitsky [12], Cobb [13], Tammann [7], Hedvall [14], and other researchers, which established the basic feasibility of reactions between solids, often ignored or incorrectly evaluated the part played by liquid and gaseous phases in many reactions of that type.

It may be noted in passing that intensive mass transfer between solid granular reagents may be realized at another order of magnitude of the diffusion coefficients or with a much larger surface taking part in the mass-transfer process (in practice one is always related to the other), i.e., whenever the process, in one way or another, breaks out of the bonds set by the bonds between the elements of the crystal lattice. The conditions governing the braking of these bonds are, however, the conditions under which the substance is converted from the solid to the liquid or gaseous state.

As a matter of fact, is suffices to admit that the gas or liquid phase takes part in a reaction between solid substances for the problem of intensive mass transfer from one reagent to the other in the course of the reaction to be cleared up entirely.

Let A_s, say, react with B_g as follows:

$$A_s \rightarrow A_g; \quad A_g + B_s \rightarrow AB_s,$$

---

1) Reagents are usually kept in the reactor (furnace) for 1 or 2 hours under industrial conditions. In most instances, however, the actual reaction between the substance takes only a very small fraction of this time. The rest of the time is consumed in heating the initial reagents to the reaction temperature, dehydrating them, and so forth.

where the subscripts s and g denote solid and gaseous, respectively.

In this case, as in many other instances of interactions in mixtures of solids, the initial reagents and the end products of the process are solids. Reagent A sublimes, however, under the process conditions. As a result its particles come into contact with the entire surface of the grains of reagent B, form a layer of the AB product on these grains, and then diffuse through the entire surface of B at a rate that is characteristic of the diffusion of a gas into a solid. Thus, the high process rate is ensured in this case by the large surface of contact between the reagents, the large cross-sectional area of the diffusion flow, and the high diffusion coefficient.

Many other variants of reactions in solid mixtures, in which gases and liquids that arise and disappear during these reactions, are, of course, conceivable. The mechanism involved in these reactions will be the topic of a separate report.

The only point worth noting here is that in all these variants, reactions in mixtures of granular or powdered solids may take place at a high rate though the mean distance between the grains of the initial reagents is considerable and the surface of contact between the grains negligibly small, as has been shown in the example cited.

The foregoing discussion does not refute, in principle, the rigidly solid-phase mechanism involved in reactions occurring in mixtures of solids, but has as its objective defining the possible part played by this mechanism in such reactions under practical conditions.

SUMMARY

1. It has been shown that the mean distance between the surfaces of adjacent particles in real fine-grained masses is 10^5 to 10^7 as great as the radii of action of the atomic and other forces binding together the elements in a crystal lattice.

2. It has been found that in mixtures of this sort the rate of mass transfer by means of a "jump" (as advanced by Tammann and others) of lattice elements of one reagent into the lattice of the other reagent (without the emergence and participation of gaseous and liquid substances) is limited by the extremely small surface of contact between the grains in the reaction mixture and by the low diffusion coefficients, which may reduce it to an extremely low value.

3. It has been shown that intensive mass transfer during chemical interaction in mixtures of solids is quite possible provided the gas or liquid phase enters into these processes.

4. It has been established that the relative part played by a strictly solid-phase reaction mechanism in the intensive interaction of solid substances under actual conditions must be extremely small.

LITERATURE CITED

[1] K. A. Polyakov. Nonmetallic chemically resistant materials. (1947).

[2] C. Hardy, Iron Age, 154, 11, 57 (1944).

[3] P. P. Budnikov, ed. General Course of silicate technology. Vols I-II (1948), Vols. III-IV (1949).

[4] S. I. Volfkovich. General chemical engineering, II, 197 (1946).

[5] W. A. Mazel. The technology of alumina production, 134-141, 171-172 (1937).

[6] M. Yu. Balshin. Powder metallurgy (1948).

[7] G. Tamman, Z. anorg. allg. Ch., 126, 119 (1923); 149, 21 (1925); 157, 321 (1926).

[8] Ya. S. Umansky, B. N. Finkelshtein, and M. E. Blanter. Physical principles of metallography (1949).

[9] V. Z. Bugakov. Diffusion in metals and alloys (1949).

[10] W. N. Kondratyev, Jour. Techn. Phys. 13, 59 (1943).

[11] R. Berrer. Diffusion in solids (1948).

[12] F. M. Flavitsky. Jour. Russ. Phys. Chem. Soc. 41, 2, 205 (1909).

Received June 3, 1950

BLANK PAGE

THE DEHYDRATING PROPERTIES OF SOME CLAYS AND OPOKAS

N. Z. Kotelkov

Chair of Chemistry, Saratov Agricultural Institute

The catalytic [1,2,4] and, especially, the dehydrating properties of activated natural clays – Georgian bentonite [3,4,5,6] – have been described in the chemical literature. We have made a study of the dehydrating properties of some refractory Voronezh clays and Saratov clays and opokas.[1]

The chemical composition of clays in percent of the dry substance are given in Table 1.

TABLE 1

Chemical Composition of Clays Tested

Sample No.	Moisture	Calcining losses	SiO_2	Al_2O_3	Fe_2O_3	CaO	MgO	SO_3
Voronezh refractory clays								
1	2.38	9.74	53.19	35.51	0.25	0.41	0.[illegible]	0.77
3	5.29	12.49	50.38	36.46	–	0.36	0.[illegible]	0.22
Saratov clays								
1	4.06	6.11	61.25	7.62	20.13	1.53	2.[illegible]	0.91
2	4.34	22.21	41.71	2.93	11.99	2.19	1.[illegible]	1.56
Saratov opokas								
1	2.90	3.74	89.70	3.58	0.32	3.07	0.[illegible]	–
2	3.40	3.89	87.06	3.80	1.50	1.60	1.[illegible]	1.03
86	3.05	6.48	77.99	5.95	4.60	1.91	1.[illegible]	2.57
215	3.48	3.07	87.40	3.17	2.06	1.50	2.[illegible]	0.86
251	2.95	3.75	90.78	2.10	0.21	2.00	0.[illegible]	1.46

The catalytic properties of the opoka No. 1 have already been investigated in part [7].

EXPERIMENTAL

Method 1. The catalyst was ground to a fine powder, mixed with water, molded into balls 3-4 mm in diameter, and then dried at 100°. The dried balls were placed in a quartz tube 60 cm long and 14 mm in internal diameter, the quantity used ranging from 1.75 g (or 1 part by weight) to 14 g (or 8 parts by weight).

[1] "Opoka – a rock consisting principally of silica and a plastic material containing grains of quartz, glauconite, and feldspar." The bleaching earths of the USSR. A symposium edited by Prof. N. M. Fedorovsky and others (1933).

The tube was heated in an electric furnace, the temperature being measured with a nichrome-constantan thermocouple.

Method 2. A compound nichrome helix 7 cm long and 14 mm in diameter (wound with 560 cm of 0.6 mm wire; volume 1.583 cu cm; surface 105.5 sq cm) [8], with 1 part by weight of the catalyst applied to it, was placed in a quartz tube 50 cm long and 14 mm in internal diameter, which was connected to a receiver by a ground-glass connection. Tightly wedged inside the compound coil was a quartz pocket containing a thermocouple at one side and quartz plug 6 mm in diameter at the other. The coil was connected to the electric circuit, the lead wires being passed through holes melted into the tube. The condensate receiver was water-cooled at operating temperatures up to 350°, water and ice being employed for cooling above that temperature. The gaseous products were collected in a measuring gas buret with a capacity of 750 ml. The airtightness of the equipment was determined by means of an aspirator with a 1-meter difference in water level. Isopropyl alcohol, with a b.p. of 81.6-81.8° at 745.6 mm; d_4^{20} 0.7887; n_D^{20} 1.3774 was used in this research.

The objective of our research was to determine how dehydration is affected by temperature, the amount of catalyst, and the alcohol's rate of feed, as well as the life of the catalyst, the feasibility of regenerating it, and the advisability of mounting the catalyst on the heating coil. The experiments were made as straight-run tests, the rate of feed of the alcohol being 0.05 ml per minute, unless otherwise stated, at temperatures ranging from 250 to 450°.

The fresh catalyst was conditioned in a current of air (1 liter/hour) at 250° for 1 hour and 450° for 1 hour, followed by a current of electrolytic hydrogen for 1 hour at the rate of 1.25 liter/hour at 250°. The catalyst was kept in an atmosphere of hydrogen between the individual runs and was conditioned for about 1 hour in a current of hydrogen at the test temperature before each run. The gas volume was read every 2 minutes. The runs lasted 1.5 hours. The initial portions of gas and condensate were discarded, only the succeeding portions being analyzed. The refraction of the condensate was measured. The gas was analyzed in an improved VTI (All-Union Institute of Heat Engineering) gas analyzer [9].

Test Results

The dehydrating properties of the catalysts listed, shaped into balls, have been investigated, and the course of the process has been plotted as a function of the amount of catalyst and the temperature (Table 2 and Fig. 1).

As we see in Fig. 1, dehydration is a nearly straight-line function of the amount of catalyst at 250° C, when Voronezh clay No. 1 is used. This linear relationship is disturbed, however, as the temperature is raised.[1]

As for the variation of the reaction velocity with temperature, these same clays obey the Arrhenius equation satisfactorily, lg $\underline{K}$ being a linear function of $1/\underline{T}$ for all the catalyst proportions investigated (Fig. 2).

---

1) The kinetics of dehydration with the catalysts listed will be dealt with in a separate paper.

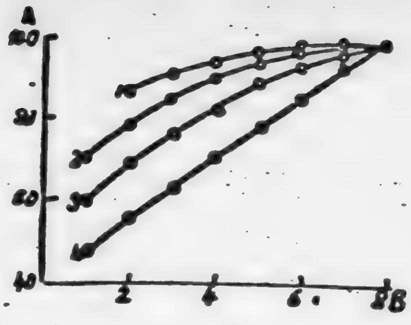

Fig. 1. Per cent dehydration as a function of the amount of catalyst and the temperature. A – Per cent dehydration; B – Proportion of catalyst, parts by weight. Temperatures, °C: 1 – 400; 2 – 350; 3 – 300; 4 – 250.

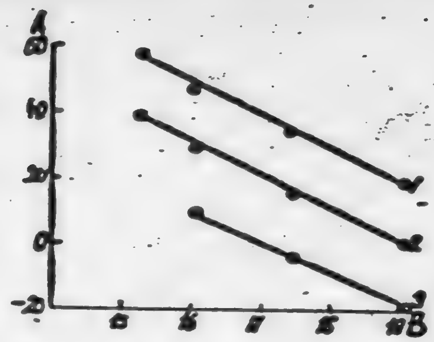

Fig. 2. lg K as a function of 1/T for various proportions of catalyst. A – $10^2 \cdot \lg K$; B – $1/T \cdot 10^4$. Proportion of catalyst (parts by weight): 1 – 5; 2 – 3; 3 – 1.

A similar relationship prevails for the other clays and opokas studied.

The activation energy, as found from the Arrhenius equation, is shown in Table 3.

The activation energies of the clays and opokas are nearly alike at the catalyst proportions employed, totaling about 4150 cal/mole. They are about 16,000 cal/mole for alumina [10]. It follows that the nature of the active centers in alumina is different from that in the clays and opokas. Chemical analysis appears to indicate that in the last-named it is governed by the silicon compounds.

The Voronezh clay, the Saratov clay No. 1, and the opoka No. 86 were found to be best.

The optimum temperature is 350° for low proportions of catalyst (1.75 g or 1 part by weight), dehydration not being increased by raising the temperature any higher. At medium proportions (3 to 5 parts by weight), the per cent dehydration rises with temperature up to 400 . At 8 parts by weight (14 g) of the Voronezh and Saratov No. 1 clays, the optimum temperature is 300°, nearly 100% dehydration being attained.

As for the German alumina, its activity is always some 32% lower than that of Voronezh clay at 250°, its activity increasing much faster with rising temperature, however, exceeding the activity of the best clay by some 20% at 400° and 1 part by weight of the catalyst. As the proportion of catalyst is increased, however, this difference grows smaller, nearly disappearing at 350° and 8 parts of catalyst by weight.

It should be noted that the Voronezh clays exhibit a ripening or induction period [11], during which activity rises some 4%, attaining a maximum after about 30 hours of operation, the activity remaining constant thereafter (for some 90 hours in our tests) (Table 4).

TABLE 2[1]

Per Cent Dehydration With Various Catalysts as Affected by Temperature and the Amount of Catalyst

Tempera-ture, °C	Catalyst and sample number							
	Voronezh refractory clay		Saratov clay		Saratov opoka			German Al_2O_3
	Amount of catalyst ≃ 1.75 g (1 pt. by wt.)							
250	(16) 47.78	(235) 48.02	(185) 41.23	(205) 33.86	(255) 31.52	(275) 37.48	(295) 38.83	(106) 16.35
300	(18) 60.43	(236) 60.64	(186) 53.12	(206) 44.20	(256) 41.39	(276) 48.40	(296) 50.18	(107) 49.68
350	(20) 71.35	(237) 71.43	(187) 63.56	(207) 54.14	(257) 51.02	(277) 58.73	(297) 60.74	(108) 88.07
400	(21) 72.51	(238) 72.58	(188) 65.63	(208) 55.72	(258) 53.81	(278) 60.26	(298) 62.28	(110) 92.97
	Amount of catalyst ≃ 5.25 g (3 pts. by wt.)							
250	(31) 63.86	(240) 64.00	(190) 59.74	(210) 47.72	(260) 45.49	(280) 51.43	(300) 53.14	(116) 32.08
300	(33) 76.40	(241) 76.54	(191) 72.47	(211) 59.96	(261) 57.53	(281) 64.03	(301) 65.87	(117) 77.53
350	(34) 85.38	(242) 85.47	(192) 82.25	(212) 70.55	(262) 68.17	(282) 74.53	(302) 76.33	(118) 99.05
400	(35) 91.49	(243) 91.55	(193) 89.13	(213) 79.08	(263) 76.89	(283) 82.67	(303) 84.27	(119) 99.99
	Amount of catalyst ≃ 8.75 g (5 pts. by wt.)							
250	(51) 78.75	(245) 78.84	(195) 74.17	(215) 58.84	(265) 56.75	(285) 63.52	(305) 64.31	(125) 46.63
300	(52) 88.83	(246) 88.90	(196) 85.34	(216) 71.45	(266) 69.28	(286) 76.02	(306) 76.81	(126) 91.03
350	(53) 94.74	(247) 94.78	(197) 92.36	(217) 81.24	(267) 79.35	(287) 85.26	(307) 85.90	(128) 99.95
400	(54) 97.71	(248) 97.73	(198) 96.30	(218) 88.26	(268) 86.76	(288) 91.43	(308) 91.89	(130) 99.99
	Amount of catalyst ≃ 14 g (8 pts. by wt.)							
250	(62) 99.67	(250) 99.69	(200) 95.52	(220) 78.13	(270) 76.23	(290) 82.64	(310) 84.12	(137) 67.06
300	(63) 99.97	(251) 99.98	(201) 98.78	(221) 88.30	(271) 86.90	(291) 91.64	(311) 92.64	(138) 98.67
350	(63a) 99.98	(252) 99.98	(202) 99.73	(222) 94.30	(272) 93.38	(292) 96.42	(312) 96.97	(138-a) 99.98
400	-	(253) 99.97	(203) 99.97	(223) 97.44	(273) 96.90	(293) 98.59	(313) 98.88	-

[1] In this and the following tables, the test numbers are given in parentheses.

TABLE 3

Activation Energy (in cal/mole) of Various Catalysts as a Function of the Proportion of Catalyst

Name of catalyst and number of sample		Proportion of catalyst, parts by weight: 1	Proportion of catalyst, parts by weight: 8	Name of catalyst and number of sample		Proportion of catalyst, parts by weight: 1	Proportion of catalyst, parts by weight: 8
Voronezh clay	1	4200	4160	Opoka	1	4100	4100
	3	4200	4100		2	4130	4120
Saratov clay	1	4150	4165		86	4150	4160
	2	4115	4100	Alumina		16020	16150

TABLE 4

Activity of Voronezh Clays as Affected by Length of Operation and Temperature

Temperature ° C.	Per cent dehydration: Fresh Clay	Per cent dehydration: Clay after 30 hours of operation
250	(51) 86.43	(181) 90.37
300	(52) 98.42	(182) 93.51
350	(53) 93.49	(183) 96.69

TABLE 5

Effect of the Rate of Alcohol Feed Upon Dehydration

Temperature ° C	Rate of feed, ml/min	Per cent dehydration: Voronezh clay No. 1	Per cent dehydration: Saratov clay No. 2
300	0.05	(63) 99.97	(221) 97.89
300	0.1	(66) 99.04	(225) 97.56
300	0.2	(67) 71.63	(226) 69.31
300	0.3	(68) 48.25	(227) 46.64
350	0.3	(69) 61.12	(228) 59.73
400	0.3	(70) 75.31	(229) 73.85

The effect of the rate at which the alcohol is fed upon dehydration when 13.93 g of catalyst are used is illustrated in Table 5.

A rate of 0.1 ml/min is satisfactory at 300°.

The activity of the catalyst drops off considerably after a high rate of alcohol feed has been employed, but its activity may be readily restored by passing 3 liters of air (2 liters per hour) at 450° through the tube containing the catalyst (Table 6).

Tests were made, using the same catalyst applied to the nichrome coil (Table 7).

TABLE 6

Per Cent Dehydration at High Rates of Alcohol Feed and After Regeneration

Tempera-ture ° C.	Catalyst		
	Fresh	After operating at a rate of 0.3 ml/min	After regeneration
250	(51) 86.43	(175) 70.32	(178) 88.93
300	(52) 89.42	(176) 73.59	(179) 92.47
350	(53) 93.49	(177) 77.84	(180) 95.68
250	(220) 78.13	(230) 60.48	(232) 78.53
300	(221) 97.89	(231) 79.27	(233) 97.94

Comparison of tables 2 and 7 indicates that applying the catalyst to the coil increases the efficiency some 800%. We also investigated the dehydration of isopropyl alcohol with a plain nichrome coil [8], finding it to be 0.89% at 300° and 2.19% at 400°.

The process resulted in decomposition of the alcohol into water and propylene in all the tests we ran, at temperatures ranging from 250 to 450°. This was proved by analysis of the gas and determination of the condensate's refraction. The differences between the per cent dehydration as calculated from the volume of gas and from the refraction, were negligible, not exceeding the experimental margin of error (see, for instance, opoka No. 1 and alumina in Table 7).

SUMMARY

1. A study has been made of the dehydrating properties of some Voronezh refractory clays and Saratov clays and opokas. The process involves no side reactions. The best catalysts were found to be the Voronezh clays, the Saratov clay No. 1, and the opokas No. 86 and No. 215.

2. A temperature of 350° is close to the optimum value for the catalysts tested, when the proportions specified are employed. Dehydration is close to 100% when 14 g of catalyst are used. A rate of 0.1 ml of alcohol per minute is efficient enough.

3. Voronezh clays exhibit a ripening period, which is followed by a period of constant activity, lasting about 90 hours.

The catalyst may be regenerated quite satisfactorily in a current of air at 450°.

4. When the catalyst is applied to a compound nichrome helix, the amount employed may be reduced 800%, the optimum temperature is 250°.

5. The variation of the reaction velocity with temperature conforms to Arrhenius's Equation.

In conclusion, I wish to express my profound gratitude to N.S.Nedina, senior laboratory assistant, for her assistance in the experimental work, to V.I. Astrakhanov, geologist of Saratov State University, for supplying the samples of clay and opoka, and to A.A.Tolstopyatova (of the N.D.Zelinsky Laboratory of Organic Catalysis) for supplying the alumina.

TABLE 7

Per Cent Dehydration When Catalyst Is Applied to the Nichrome Coil

Temperature °C	Per cent dehydration					
	Voronezh clay		Saratov clay		Opoka	
	No. 1 (1.748 g)	No. 3 (1.620 g)	No. 1 (1.763 g)	No. 2 (1.749 g)	No. 1 (1.784 g)	
	By n_D^{23} condensate					By volume of gas
250	(176) 99.60	(329) 99.67	(317) 95.46	(299) 77.60	(72) 76.21	76.15
300	(178) 99.96	(331) 99.97	(318) 98.75	(300) 87.89	(72) 86.80	86.71
350	(177) 99.97	(332) 99.98	(319) 99.71	(301) 94.04	(74) 93.29	93.22
	Opoka				German alumina (1.75 g)	
	No. 2 (1.780 g)	No. 86 (1.760 g)	No. 215 (1.895 g)	No. 251 (1.798 g)		
250	(284) 82.50	(269) 84.00	(272) 85.12	(287) 82.08	(153) 66.92	66.89
300	(285) 91.69	(270) 92.43	(273) 93.39	(288) 91.17	(154) 98.60	98.58
350	(286) 96.22	(271) 97.03	(274) 97.32	(288a) 96.09	(155) 100.00	100.00

LITERATURE CITED

[1] A. F. Nikolaeva and A. V. Frost, JGC 13, 739 (1943).

[2] A. F. Nikolaeva, V. M. Tatevsky, and A. V. Frost, JGC 15, 796 (1945).

[3] M. B. Turova-Polyak and N. I. Ziminova, JAC 1946, No. 9, 954.

[4] M. B. Turova-Polyak and O. B. Latich, JAC 1947, No. 3, 251.

[5] Kh. I. Areshidze and E. K. Tavartkiladze, JAC 18, 271 (1945); JAC 21, 281 (1948); JAC 22, 119 (1949).

[6] A. S. Nekrasov and B. A. Krentsel, JGC 19, 948 (1949).[1]

[7] N. Z. Kotelkov. Trans. Saratov Agric. Inst. 4 (1940).

[8] Ibid. 9 (1947).

[9] N. Z. Kotelkov, Jour. Anal. Chem. 5, 48 (1950).

[10] A. Kh. Bork and A. A. Tolstopyatova, JAC 12, 245 (1938).

[11] B. N. Dolgov. Catalysis in organic chemistry. State Chemical Press (1949)

Received June 15, 1950.

1) See Consultants Bureau English Translation, p. 937.

BLANK
PAGE

INVESTIGATION OF AQUEOUS SOLUTIONS OF SELENIC ACID BY THE SPECIFIC-GRAVITY METHOD

A. F. Kapustinsky and A. N. Zhdanova

The D. I. Mendeleev Institute of Chemical Engineering, Moscow.

The classic researches of Mendeleev on the specific gravity of aqueous solutions laid the foundations of the hydrate theory of solutions [1]. He discovered that a series of hydrates exists in the sulfuric acid – water system. These researches were continued later [2, 3, 4, 5, 6, 7].

We set as our objective similar investigations of the closest analog of sulfuric acid, <u>viz</u>.: selenic acid. This investigation was all the more necessary as the available material in this field was inadequate. The earlier researches not only did not use the standard temperature of 25° C, but were also inaccurate, as may be seen if we plot the product of specific weight by composition from the data secured by Cameron and Macallan [8] and by Diemer and Lehner [9]; the broad scattering of the points renders any conclusion at all impossible. Still, the experimental techniques of measuring the densities of liqudd systems have made considerable progress in recent years. Moreover, the experimental results may be analyzed in the light of the thermodynamics of partial molal quantities.

EXPERIMENTAL

The Washburn and Smith method [10] was used as the basis for measuring density. We did not use dual pyknometers, however, but rather a single quartz pyknometer with a capillary neck and a ground quartz stopper. The temperature in the thermostat was held within $\pm 0.005°$ C. Weighing was done to the nearest 0.0001 g. A correction was made for reduction to vacuum. The level of the liquid in the capillary was read with a cathetometer, which enabled us to make readings to the nearest 0.05 mm. The pyknometer was calibrated with repeatedly distilled water. All densities were referred to that of water, which was taken as 1 at 4° C. The analysis of the accuracy of determination was made with an error of ± 0.00001.

Of the various methods described in the literature for preparing selenic acid, we selected the Gilbertson and King method [11], involving the oxidation of selenium dioxide with hydrogen peroxide. A feature of this method is that the reaction yields no other products than H_2SeO_4 and water, thus guaranteeing the purity of the resulting preparation. The selenium dioxide required for the synthesis was prepared by the Meyer method [12] of oxidizing chemically pure elementary selenium with oxygen at 450-500° in the presence of nitrogen dioxide as a catalyst.

The hydrogen peroxide employed in this synthesis was distilled in vacuo to free it of the stabilizer always present in a hydrogen peroxide reagent. Completeness of oxidation was checked by quantitative determination of the unreacted SeO_2 [13]. The selenic acid we produced contained less than 1% SeO_2.

The synthesized solution of selenic acid was concentrated by prolonged (several days) distillation at a pressure of 4-6 mm of mercury and a temperature of 150°.

The concentrations of the initial solutions of selenic acid were determined analytically by the volumetric method, by titration with a 0.1N solution of sodium hydroxide, using methyl orange as an indicator.

The results of our determinations of specific gravity and the derivative $(\partial d/\partial p)_t$ calculated therefrom of aqueous solutions of selenic acid at 25° C are listed in Table 1.

TABLE 1

Density and Derivative of Density with Respect to Composition of Aqueous Solutions of Selenic Acid at 25° C

Concentration of H_2SeO_4, % by weight	Density d^{25}_4	$(\partial d/\partial p)_t$	Concentration of H_2SeO_4, % by weight	Density d^{25}_4	$(\partial d/\partial p)_t$
92.97	2.6175_7	0.0205	64.92	1.7868_5	
94.33	2.5573_1	0.0248	63.92	1.7664_4	0.0283
92.36	2.5081_7	0.0264	63.02	1.7458_2	0.0198
90.31	2.4541_1	0.0286	60.98	1.7067_8	0.0191
89.25	2.4235_5	0.0278	57.88	1.6514_7	0.0178
88.25	2.3958_4	0.0291	52.90	1.5709_0	0.0161
87.23	2.3660_0	0.0292	46.97	1.4785_0	0.0155
83.37	3.2531_4	0.0317	41.81	1.4079_0	0.0134
81.38	2.1898_3	0.0287	36.70	1.3444_5	0.0124
80.34	2.1600_9	0.0268	30.77	1.2756_8	0.0116
79.34	2.1331_1	0.0273	25.36	1.2185_7	0.0105
77.33	2.0781_8	0.0255	20.71	1.1724_4	0.0099
74.14	1.9965_7	0.0241	14.11	1.1120_5	0.0092
71.00	1.9207_5	0.0228	9.12	1.0698_8	0.0085
68.95	1.8739_2	0.0222	4.23	1.0310_2	0.0080
67.45	1.8405_7	0.0212	3.32	1.0239_3	0.0076
65.99	1.8096_4	0.0213			

The specific volumes and apparent molal volumes of the solutions of H_2SeO_4, calculated from the specific gravities, are listed in Table 2.

In view of the fact that selenic acid constitutes various hydrates with water, which are unstable compounds according to the structural diagram [14], we were interested in exploring the density of aqueous solutions of selenic acid at a lower temperature. We therefore made a study of the density of these solutions at 0° C.

A pyknometer with a capacity of about 15 cu cm, a capillary neck, and a ground stopper, was employed in these measurements. The temperature of the

TABLE 2

Density, Specific Volume, and Apparent Molal Volume of Aqueous Solutions of Selenic Acid at 25° C

Concentration %	Molal, M	$\sqrt{M}$	Specific Gravity d^{25}_{4}	Specific Volume, v^{25}_{4}	Apparent molal volume, φ
97.27	244.85	15.65	2.61757	0.38203	52.850
94.33	115.41	10.72	2.55731	0.39104	51.382
92.36	83.570	9.14	2.50817	0.39862	50.556
90.31	64.447	8.03	2.45411	0.40747	49.833
89.25	57.248	7.57	2.42355	0.41262	49.506
88.25	51.811	7.20	2.39584	0.41738	49.210
87.23	47.054	6.86	2.36600	0.42265	48.940
83.37	34.600	5.88	2.25314	0.44382	48.182
81.38	30.140	5.48	2.18983	0.45665	48.076
80.34	28.180	5.30	2.16009	0.46294	47.949
79.34	24.102	4.91	2.13311	0.46879	45.801
77.33	23.526	4.85	2.07819	0.48118	47.581
74.14	19.782	4.45	1.99657	0.50858	48.740
71.00	16.889	4.11	1.92075	0.52062	46.918
68.95	15.320	3.91	1.87392	0.53363	46.723
67.45	14.200	3.76	1.84057	0.54330	46.374
65.99	13.381	3.66	1.80964	0.55259	46.350
64.92	12.761	3.58	1.78685	0.55964	46.403
63.92	12.220	3.49	1.76664	0.56610	46.315
63.02	11.755	3.42	1.74582	0.57279	46.455
60.98	10.781	3.28	1.70678	0.58587	46.248
57.88	9.477	3.08	1.65147	0.60552	45.855
52.90	7.747	2.78	1.57090	0.63725	45.190
46.97	6.109	2.47	1.47650	0.67635	44.587
41.81	4.957	2.22	1.40790	0.71027	43.937
36.70	3.999	2.00	1.34445	0.74379	43.035
30.77	3.066	1.75	1.27566	0.78389	42.201
25.36	2.343	1.53	1.21857	0.82063	41.443
20.71	1.802	1.34	1.17244	0.85292	40.450
14.11	1.133	1.06	1.11205	0.89923	38.901
9.12	0.693	0.832	1.06988	0.93468	37.681
4.23	0.305	0.552	1.03102	0.96990	32.470
3.31	0.236	0.486	1.02393	0.97662	30.070
3.00	0.208	0.459	1.02136	0.97908	27.338
1.51	0.106	0.325	1.01005	0.99004	21.760
	–	–	0.99707	1.0029	–

ice thermostat was kept constant to within ±0.02°. To eliminate the effect of any error in determining the composition (as is unavoidable in titration) upon the course of the curve of the derivative of density with respect to composition, we employed the following method in preparing our solutions. The dried and weighed pyknometer was filled with an acid solution whose concentration had been determined as accurately as possible (by titration). After the density had been measured, a small amount of the solution was taken from

the pyknometer with a capillary pipet, the pyknometer was weighed, and then a calculated quantity of water was added to the pyknometer, which was immersed in a freezing mixture (-10°), causing the level of the liquid to fall below the neck, the liquid within the pyknometer being stirred by rotating a platinum wire within the pyknometer about its own axis by means of an electric motor. The action of centrifugal force caused the platinum wire to bend inside the pyknometer, thus stirring the liquid vigorously. After these operations were completed, the pyknometer was reweighed. Thus all the solutions whose density was measured were prepared from the same initial solution within the pyknometer itself; though this did not eliminate an error in the titration of the initial solution, it rendered the error constant throughout all the meansurements, and, hence, it did not affect the shape of the density-composition curve. The accuracy of determination at 0° is, of course, lower than that at 25°, by one order of magnitude.

The results of our determinations of specific gravity and the calculated derivatives of density with respect to composition for aqueous solutions of selenic acid at 0° C are listed in Table 3.

TABLE 3

Density and Derivative of Density With Respect to Composition of Aqueous Solutions of Selenic Acid at 0° C

H_2SeO_4 concentration, % by weight	Density d_4^0	$(\partial d/\partial p)_t$
93.30	2.5599	
92.58	2.5433	0.0231
92.01	2.5345	0.0157
91.49	2.5262	0.0159
91.01	2.5181	0.0169
89.79	2.4885	0.0241
88.06	2.4650	0.0136
86.99	2.4343	0.0285
85.75	2.4125	0.0177
84.10	2.3795	0.0200
82.64	2.3498	0.0203
81.44	2.3254	0.0202
80.11	2.3092	0.0121
78.95	2.2734	0.0308
77.66	2.2429	0.0237
75.84	2.1888	0.0295
73.93	2.1377	0.0264

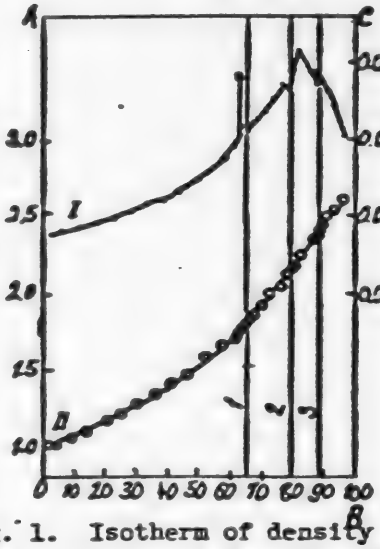

Fig. 1. Isotherm of density and derivative of density with respect to composition of aqueous solutions of selenic acid at 25° C.

A – Specific gravity (d),
B – per cent H_2SeO_4 by weight,
C – Derivative of density with respect to composition $(\partial d/\partial p)_t$ · I–$(\partial d/\partial p)_t$; II–d; 1–$H_2SeO_4$; 2–$H_2SeO_4 \cdot 2H_2O$; 3–$H_2SeO_4 \cdot H_2O$.

Figures 1 and 2 show the specific gravities of the aqueous solutions of selenic acid, measured at 25° and 0° C, and the derivative of density with respect to composition. The breaks in the curve are not shown very clearly in the 25° C isotherm (Fig. 1), but the derivative curve exhibits the discontinuities

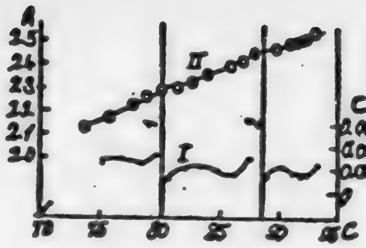

Fig. 2. Isotherm of density and derivative of density with respect to composition of aqueous solutions of selenic acid at 0° C.

A – Specific gravity (d);
B – per cent H_2SeO_4 by weight;
C – derivative of density with respect to composition $(\partial d/\partial p)_t$;
I-$(d/p)_t$; II-d; 1-$H_2SeO_4 \cdot 2H_2O$; 2-$H_2SeO_4 \cdot H_2O$.

corresponding to the stoichiometrical composition of the hydrates, viz.: $H_2SeO_4 \cdot H_2O$; $H_2SeO_4 \cdot 4H_2O$; and a hydrate $H_2SeO_4 \cdot 2H_2O$ as yet unknown in the literature.

The points of inflection on the density isotherm for 0° C (Fig. 2) and the striking discontinuities manifested on the curve of the derivative of density with respect to composition refer to the following hydrates of the selenic acid: $H_2SeO_4 \cdot H_2O$ and $H_2SeO_4 \cdot 2H_2O$, thus corroborating the existence of the latter. The more pronounced display of the points of inflection on the isotherm of the density of aqueous solutions of selenic acid at 0° C is evidence of the decrease in the dissociation of selenic acidhydrates as the temperature goes down.

The results of our determinations of density at 0 and 25° C are listed in Table 4, the specific gravities for 25° being interpolated from the data given in Table 1 for solution concentrations the density of which had been measured at 0°. The table shows the specific volumes of solutions of the stated concentrations at 0 and 25°, their differences, and their coefficients of volumetric expansion.

TABLE 4

Thermal Expansion of Aqueous Solutions of Selenic Acid

H_2SeO_4 concentration, % by weight	d_{25}, interpolated	d_0	v_{25}	v_0	$v = v_{25} - v_0$	$\frac{dv}{dt} \cdot 10^4$ cu cm per gram per degree
93.30	2.53317	2.5599	0.39476	0.3906	0.00412	1.647
92.58	2.51413	2.5433	0.39775	0.3932	0.00456	1.823
92.01	2.49829	2.5345	0.40027	0.3946	0.00571	2.28
91.49	2.48471	2.5262	0.40246	0.3970	0.00542	2.17
91.01	2.47191	2.5181	0.40450	0.3971	0.00738	2.95
89.79	2.43875	2.4885	0.41004	0.4018	0.00819	3.47
88.06	2.39030	2.4650	0.41835	0.4057	0.01268	5.07
86.99	2.35911	2.4343	0.42388	0.4108	0.01309	5.23
85.75	2.32293	2.4125	0.43049	0.4141	0.01640	6.57
84.10	2.27467	2.3795	0.43962	0.4202	0.01938	7.75
82.64	2.22996	2.3498	0.44843	0.4256	0.02286	9.14
81.44	2.19197	2.3254	0.45621	0.4300	0.02618	10.47
80.11	2.15390	2.3092	0.46426	0.4330	0.03122	12.48
78.95	2.12244	2.2734	0.47115	0.4398	0.03130	12.52
77.66	2.08730	2.2429	0.47908	0.4458	0.03323	13.29
75.84	2.04003	2.1888	0.49018	0.4569	0.03332	13.32
73.93	1.99131	2.1377	0.50218	0.4678	0.03440	13.76

The coefficient of volumetric expansion of aqueous solutions of selenic acid between 0 and 25° is plotted in Fig. 3 for the concentration range of 73.9-93.3% by volume of H_2SeO_4. The discontinuities on the curve once more lie at the $H_2SeO_4 \cdot H_2O$ and $H_2SeO_4 \cdot 2H_2O$ compounds of selenic acid.

The application of the modern theory of strong electrolytes to the analysis of the properties of solutions, particularly volumetric and heat-capacity properties, has been most successful in systems in which no clearly marked chemical action takes place. It was to be expected (and this has been borne out by experiment) that whenever different, clearly distinct, compounds are formed in the solution, Mason's rule [15] and other analogous functions of $\sqrt{M}$ will not apply at all or, in any event, will hold good only in a narrow concentration range. We see in Fig. 4, as a matter of fact, that the variation of the apparent volumes with $\sqrt{M}$ (a constant according to the figures in Table 2) is far from linear. The figure shows that the emergence of the hydrates is accompanied by an anomalous course of the curve. This is shown clearly enough in the case of the tetrahydrate and dihydrate, while as far as the monohydrate is concerned, it is manifested by the intersection of two clearly different curves. Even systems in which the chemical action is less manifest, such as the system of a uranyl salt and water, exhibit an appreciable departure from the linearity rule, as has been proved in the paper by Kapustinsky and Lipilina [16], linearity being maintained only in a narrow concentration range. The Mason equation, which was first derived empirically [17], was later derived theoretically by Redlich [18]. This conclusion holds good for highly dilute solutions. We also know [19] that the linear variation of the apparent volumes with $\sqrt{M}$ applies to dilutions no lower than $\sqrt{M} = 0.05$. Extrapolated values of the apparent volumes are therefore usually obtained by extrapolating the linear relationship secured in a concentration range that does not extend to excessively high dilutions.

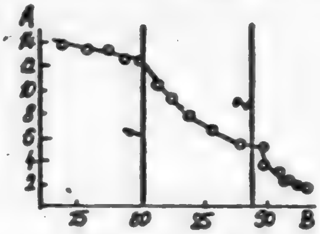

Fig. 3. Coefficient of thermal expansion of aqueous solutions of selenic acid (in the range of concentrations from 73.93 to 93.3% by weight).

A – ($\Delta v/\Delta t$)·10^4 cu cm per gram per degree; B – per cent H_2SeO_4 by weight. 1 – $H_2SeO_4 \cdot 2H_2O$; 2 – $H_2SeO_4 \cdot H_2O$.

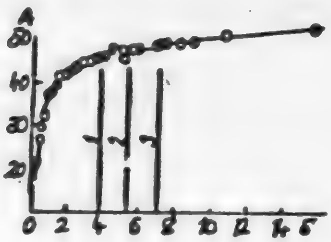

Fig. 4. Variation of the apparent molal volume φ with $\sqrt{M}$ for aqueous solutions of selenic acid at 25° C.

A – φ, cu cm; B – $\sqrt{M}$.
1 – $H_2SeO_4 \cdot 4H_2O$; 2 – $H_2SeO_4 \cdot 2H_2O$, 3 – $H_2SeO_4 \cdot H_2O$.

We have made the following analysis of our measurements in the light of the foregoing. Figure 5 is a plot of 13 points representing the left-hand portion of the curve in Fig. 4. We see in this large-scale graph that the first 4 points accurately fit a linear function; we may add that treatment by the method of least squares yields the following equation: $\varphi_v = 7.37 + 44.6 \cdot \sqrt{M}$.

Fig. 5. Variation of the apparent molal volume with $\sqrt{M}$ in the 0 – 1.13 concentration range (straight line plotted by the method of least squares).

A – cu cm; B – $\sqrt{M}$.

This equation cannot be employed, however, to secure extrapolated estimates, for the reasons given above. As a matter of fact, it applies to dilutions where we must expect the curve to drop off and depart from linearity as $\sqrt{M}$ diminishes. We undertook no tests of still weaker solutions, since the measurement errors in this dilution range rise sharply as the molality of the solution is diminished. In conformity with the foregoing, we employed the concentration range that precedes the region of ultimate dilution (as has been done in other researches), where the linear relationship is still preserved, even though only roughly. We see from Fig. 5 that the first six points satisfactorily lie along a straight line, extrapolation of which gives us $_v{}^{o}$ = 18.1. The following reasoning may be cited in support of this rough estimate of the apparent volume of the selenate ion at infinite dilution.

In an ultimately dilute solution, selenic acid (which is a strong electrolyte as has been proved by Khodakov and Agafonova [20, 21]) may be regarded as fully dissociated into $H^{\cdot}$ and SeO_4^{--} ions. Then the ultimate apparent volume must be the sum of the respective ionic volumes $\varphi^{o}_{H_2SeO_4} = 2\ ^{o}_{H^{\cdot}} + \ ^{o}_{SeO_4^{--}}$. Fajans and Johnson [22] give a list of ionic volumes. Using their value for the volume of $H^{\cdot}$ together with the value we have obtained for $\varphi^{o}_{H_2SeO_4}$, we get $^{o}_{SeO_4}$ = 17.6, or 8.8 per equivalent. Fajans and Johnson do not give any value for the selenate ion, nor is it found anywhere else in the literature, so that our estimate is the first to be published. The reality of our estimate may be judged by comparing the apparent volumes and ionic radii of the sulfate and selenate ions.

The volumes are to each other as the cubes of the radii. Kapustinksy and Yatsimirsky [23] have found the SO_4^{--} radius to be 2.30 and the SeO_4^{--} radius to be 2.44. On the assumption that the ratio of the ion volumes in the lattice is the same as the ratio of the apparent volumes, we get: $\frac{r^3 SeO_4^{--}}{r^3 SO_4^{--}} = \frac{\varphi^{o} SeO_4^{--}}{\varphi^{o} SO_4^{--}}$,

and substituting the known values from the papers by Fajans and Johnson [22] and Kapustinsky and Yatsimirsky [23], we find $^{o}_{SeO_4^{--}}$ = 9.1, as against our experimental determination of 8.8, the difference being only 0.3. In view of the rough and approximate nature of the extrapolation itself as well as the method of comparison employed, we may consider the agreement fully satisfactory.

SUMMARY

1. The density isotherms at 0 and 25° C of aqueous solutions of selenic acid show that the following hydrates of selenic acid exist: $H_2SeO_4 \cdot H_2O$, $H_2SeO_4 \cdot 2H_2O$, and $H_2SeO_4 \cdot 4H_2O$. The hydrate $H_2SeO_4 \cdot 2H_2O$ has been discovered for the first time.

2. The measured specific gravities of aqueous solutions of selenic acid have been utilized to find the apparent molal volume of the SeO_4^{--} ion, equaling 8.8.

LITERATURE CITED

[1] D. I. Mendeleev. Selected Works, III. United Scientific and Technical Press (1934); N. S. Kurnakov. Introduction to physico-chemical analysis. USSR Acad. Sci. Press (1940).

[2] M. A. Pickering, J. Chem. Soc. 57, 331 (1890).

[3] E. V. Biron, J. Russ. Chem. Soc. 31, 517 (1898).

[4] Knietsch, Ber. 34, 4100 (1901).

[5] N. I. Podkopayev, J. Russ. Phys. Chem. Soc. 44, 481, 1005 (1912).

[6] O. Hulsmann u. Biltz, Z. anorg. allg. Chem. 218, 369-378 (1934).

[7] Bright, Hutchison a. Smith, J. Soc. Chem. Ind. 65, 385 (1946).

[8] C. A. Cameron a. J. Macallan, Chem. N. 59, 230 (1889).

[9] M. E. Diemer, V. Lehner, J. Phys. Chem. 13, 505 (1909).

[10] Washburn a. Smith, Bull. Bureau Standard. J. of Res. 11, 4, 453 (1933), 12, 3, 305 (1934).

[11] L. J. Gilbertson a. G. B. King, J. Am. Chem. Soc. 58, 180 (1936).

[12] J. Meyer, Ber. 55, 2082 (1922).

[13] W. F. Hillebrand and G. Lundell. Applied Inorganic Analysis (Russ. ed.). United Scientific and Technical Press (1937).

[14] R. Kreman, F. Hofmeier, Sitzber. Akad. Wien, 117, 735 (1908).

[15] D. O. Mason, Phil. Mag. 8, 49, 218 (1929).

[16] A. F. Kapustinsky and I. I. Lipilina, Proc. USSR Acad. Sci. 58, 4, 485 (1948).

[17] H. S. Harned a B. B. Owen, The Phys. Chem. of Electrolytic Solutions (1943)

[18] O. Redlich u. P. Rosenfeld, Z. Phys. Ch. (A), 155, 65 (1931).

[19] M. Randall a. M. D. Taylor, J. Phys. Chem. 45, 6, 959 (1941).

[20] A. L. Agafonova and Yu. V. Khodakov, Proc. USSR Acad. Sci. 40, 9, 399 (1943).

[21] A. L. Agafonova J. Gen. Chem. 17, 6, 1055 (1947).

[22] K. Fajans a. O. Johnson, J. Am. Chem. Soc. 64, 668 (1942).

[23] A. F. Kapustinsky and B. K. Yatsimirsky, J. Gen. Chem. 19, 2191 (1949).[1]

Received July 21st, 1950.

1) See Consultants Bureau Translation, p. a-665

CONDUCTANCE AND VISCOSITY IN THE KOH – K_2CO_3 – H_2O SYSTEM

M. I. Usanovich and T. I. Sushkevich.

We have investigated the conductance and viscosity of aqueous solutions of KOH, containing various proportions of K_2CO_3, in concentrated KOH solutions, because solutions of these concentrations are employed in the industrial electrolysis of water.

The KOH and K_2CO_3 employed in our research came from the firm of Kahlbaum. The solutions were prepared with water that had been double-distilled with $KMnO_4$ and $Ba(OH)_2$, the conductance of which ranged from 0.8 to $1.5 \cdot 10^{-5}\ \Omega^{-1}$. In preparing the solutions the caustic alkali was first washed repeatedly with the bidistillate to remove the superficial crust of carbonate, inasmuch as we were interested in the influence of the K_2CO_3 upon conductance, and we wanted to begin with solutions that contained only small percentages of K_2CO_3. The solutions prepared in this manner contained 0.3 to 0.5% potassium carbonate. The conductance was measured at three temperatures: 25, 50, and 97°,[1] and in the KOH concentration range from 18.86% to 41.59%, the potassium carbonate content ranging from 1% to 31%.

TABLE 1

Conductance at a KOH Concentration of 18.86%

No.	Per cent K_2CO_3	$k_{25°}$	$k_{50°}$	$k_{97°}$
1	–	0.6042	0.8769	1.4143
2	2.00	0.5893	0.8588	1.3815
3	9.76	0.5289	0.7864	1.2759
4	21.50	0.4329	0.6612	1.1304
5	25.97	0.3933	0.6134	1.0510

TABLE 2

Conductance at a KOH Concentration of 21.95%

No.	Per cent K_2CO_3	$k_{25°}$	$k_{50°}$	$k_{97°}$
1	–	0.6527	0.9637	1.5506
2	3.54	0.6225	0.9240	1.3880
3	6.26	0.5959	0.8912	1.4458
4	14.20	0.5233	0.7959	1.3329
5	18.20	0.4789	0.7452	1.2590
6	31.10	0.3457	0.5708	1.0420

Our findings indicate that increasing the percentage of potassium carbonate in the alkali lowers the specific conductance of the solution.

At first sight, this is surprising. It would seem that adding one electrolyte to another that does not react chemically with it should increase the conductance of the solution, but the contrary is observed to happen. The only possible explanation

[1] The boiling point of water under the conditions of the experiment.

TABLE 3

Conductance at a KOH Concentration of 26.37%

No.	Per cent K_2CO_3	$k_{25°}$	$k_{50°}$	$k_{97°}$
1	-	0.6753	1.0190	1.6741
2	2.55	0.6460	0.9831	1.6300
3	7.19	0.6016	0.9156	1.5398
4	13.40	0.5275	0.8199	1.4176
5	30.87	0.3291	0.5665	1.0501

TABLE 4

Conductance at a KOH Concentration of 28.58%

No.	Per cent K_2CO_3	$k_{25°}$	$k_{50°}$	$k_{97°}$
1	-	0.6694	1.0072	1.7042
2	2.41	0.6395	0.9689	1.6475
3	8.14	0.5693	0.8806	1.5176
4	14.60	0.5089	0.8013	1.3980
5	21.30	0.4115	0.6709	1.2120

TABLE 5

Conductance at a KOH Concentration of 31.45%

No.	Per cent K_2CO_3	$k_{25°}$	$k_{50°}$	$k_{97°}$
1	-	0.6660	1.0185	1.7625
2	2.81	0.6308	0.9735	1.7055
3	9.20	0.5505	0.8665	1.5473
4	11.47	0.5244	0.8340	1.4926
5	19.35	0.4294	0.7032	1.3092

TABLE 6

Conductance at a KOH Concentration of 33.72%

No.	Per cent K_2CO_3	$k_{25°}$	$k_{50°}$	$k_{97°}$
1	-	0.6449	1.0093	1.7262
2	1.05	0.6340	1.0082	1.6692
3	2.08	0.6289	0.9927	1.6198
4	2.97	0.6127	0.9604	1.5479
5	9.98	0.5113	0.8629	1.5258
6	23.5	0.3611	0.6217	1.2123

TABLE 7

Conductance at a KOH Concentration of 41.59%

No.	Per cent K_2CO_3	$k_{25°}$	$k_{50°}$	$k_{97°}$
1	-	0.5596	0.9305	1.7315
2	3.02	0.5237	0.8807	1.6601
3	7.00	0.4702	0.8023	1.5450
4	11.47	0.4164	0.7258	1.4169
5	12.50	0.3994	0.6998	1.3840

is that the conductance is lowered because of the rise in the solution's viscosity, the relative increase in the viscosity of the solution when the K_2CO_3 is added exceeding the rise in the ion concentration. To test this hypothesis we made a study of the viscosity of the same solutions at two initial KOH concentrations.

The viscosity was measured at 25 and 50°; the results are listed in Tables 8 and 9.

As we see in Tables 8 and 9, the viscosity of a KOH solution rises as the concentration of K_2CO_3 is increased. When the conductance is corrected for viscosity, the nature of the variations in conductance changes sharply.

As the concentration of K_2CO_3 is increased, the corrected conductance rises monotonously. This rise is evidence that the decrease in the conductance of KOH solutions with increasing K_2CO_3 concentration is actually due to an increase in the solution viscosity.

TABLE 8

Viscosity at a KOH Concentration of 28.58%

No.	Per cent K_2CO_3	$\eta_{25°}$	$d_{25°}$	$\eta_{50°}$	$d_{50°}$
1	-	2.0975	1.2791	1.2955	1.2644
2	2.41	2.2230	1.2947	1.3570	1.2807
3	8.14	2.5916	1.3309	1.5685	1.3177
4	14.6	3.0946	1.3689	1.8229	1.3520
5	21.3	4.1209	1.4243	2.3554	1.4112

TABLE 9

Viscosity at a KOH Concentration of 31.45%

No.	Per cent K_2CO_3	$\eta_{25°}$	$d_{25°}$	$\eta_{50°}$	$d_{50°}$
1	-	2.2786	1.3080	1.3953	1.2964
2	2.81	2.5163	1.3247	1.5254	1.3103
3	9.20	3.0707	1.3669	1.8108	1.3449
4	19.35	4.1197	1.4270	2.3506	1.4139

SUMMARY

1. The conductance of KOH solutions ranging from 18.86 to 41.59%, containing 1 to 31% potassium carbonate, has been measured. The measurements were made at 25, 50 and 97°. It has been found that the specific conductance of a KOH solution falls as K_2CO_3 is added.

2. The viscosity of two concentrations of KOH, containing varying percentages of K_2CO_3, has been measured at 25 and 50°. The viscosity of a KOH solution rises as K_2CO_3 is added. The drop in the specific conductance is due to the increase in the solution viscosity.

Received February 9, 1950.

BLANK
PAGE

THE VISCOSITY OF ESTERS OF LINOLEIC ACID AS A FUNCTION OF THEIR OXIDATION[1)]

V. G. Georgievsky and B. N. Shakheldyan

Moscow Polygraphic Institute

It is common knowledge that the oxidation of "siccative" vegetable oils entails an increase in their viscosity, causing them to harden. But notwithstanding the long time that vegetable oils have been studied and employed as film-forming substances, no work has been done on the quantitative aspect of the relationship between oxidation and the viscosity of the oils.

A large number of devices has been described in the literature for the gasometric determination of the absorption of oxygen by oils, but none of the methods cited makes it possible to follow the thickening of the oil as it oxidizes. Hence, the first objective of the present research was to develop a suitable method of following the course of oxidation together with the resulting rise in viscosity.

EXPERIMENTAL

In the apparatus of our design, the volumetric method of determing the oxygen absorption is coupled with a simultaneous determination of viscosity by the discharge method (Fig.1).

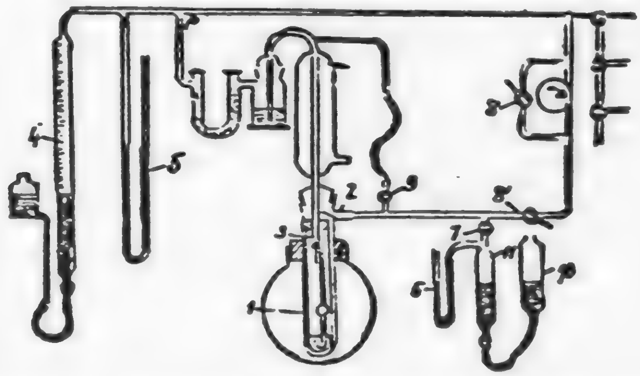

Fig.1. Diagram of apparatus for studying oxidation with parallel measurement of viscosity.

1 – Reaction vessel, 2 – air inlet, 3 – outlet for oxidation products, 4 – buret, 5 – mercury manometer, 6 – oil manometer, 7, 9 – stopcocks, 8, 8' – microstopcocks, 10 – compensating chamber.

---

1) Report I of a series on the oxidation and viscosity of film-forming oils.

The apparatus is a closed system, in which the gas filling the system is circulated by means of a special pump. The gas buret and manometer enable us to follow the course of oxidation. The amount of substance under test used was 1 ml. It was stirred by bubbling, the tube that supplied the gas having a spherical bulb and serving also as a viscosimeter.

The volatile oxidation products were collected in a system of absorbers, consisting of a vessel containing concentrated H_2SO_4, a U-shaped tube filled with solid KOH, a vessel containing a saturated solution of $CaCl_2$, and another vessel containing H_2SO_4. The rate of gas circulated was regulated by means of the two microstopcocks 8 and 8'. The rate was checked by counting the bubbles in the $CaCl_2$ vessel, the rate being about 2 liters per hour in our tests.

After a weighed sample of the substance under test had been placed in the reaction vessel, the apparatus was evacuated and kept in that state for some time to check its airtightness. Then the apparatus was filled with oxygen, an oxygen-nitrogen mixture, or nitrogen, depending upon the objective of the experiment. Before the gases entered the apparatus, they were desiccated with solid alkali and sulfuric acid. The nitrogen, taken from a cylinder, was freed of any traces of oxygen by passing it through an alkaline solution of pyrogallol and then through a tube filled with incandescent copper. When experiments were to be run in an atmosphere of pure nitrogen, the air was eliminated from the dead space behind stopcock 7, which cannot be evacuated. This was done by passing a thin rubber tube into the open end of the manometer 6, opening stopcock 7, and passing a current of nitrogen through the tube for 10-15 minutes.

The tests were run at 100°, which, together with the small quantity of substance tested, enabled us to speed up the oxidation of the oils, which is slow at room temperature. What is more, working at high temperature has the advantage of reducing to a minimum the effect upon viscosity of the physical association of the oxygen polar compounds formed during oxidation [1].

Thus the increased viscosity we observed reflected particle consolidation due to purely chemical transformations. The reaction vessel was kept at a constant temperature by immersing it in a bath of boiling water.

The volume of oxygen absorbed and the viscosity of the test substance were measured periodically during the test. The viscosity was measured by the time required for outflow from the bubbler-viscosimeter, (filled by opening stopcock 7, closing stopcocks 8' and 9, and then lowering the auxiliary compensating chamber 10.)

The small quantities of test substance used limited the size of the viscosimeter. The time required for the initial substances to flow out was about 3 seconds The error involved was negligible, however, as the viscosity changed greatly as oxidation progressed.

In view of the chemical nature of "siccative" vegetable oils, it was found advisable to make a preliminary study of the oxidation of pure esters of fatty acids and of the increase in viscosity thereby involved. To do this we synthesized the methyl and glycol esters of linoleic acid. The linoleic acid was recovered from sunflower oil and refined by recrystallizing its bromoderivative from gasoline.

The methyl ester was prepared by debrominating tetrabromostearic acid in a solution of methanol acidulated with sulfuric acid [2].

0.3844 g substance: 1.0946 g CO_2; 0.3952 g H_2O.
0.3356 g substance: 0.9765 g CO_2; 0.3692 g H_2O.
Found %: C 77.72, 77.14; H 11.42, 11.87.
$C_{19}H_{34}O_2$. Calc. %: C 77.54; H 11.56.

Iodine number: Found 171.2; Calc. 172.8; $d_4^{20} = 0.8878$.

The glycol ester of linoleic acid was prepared by the method developed for synthesizing the glyceride [3,4]. The acid chloride prepared by reacting tetrabromostearic acid with thionyl chloride was then reacted with glycol. The resultant bromo derivative of the glycol ester was isolated by crystallizing it from ether that was chilled with a mixture of acetone and dry ice, and then it was debrominated with zinc dust in a solution of absolute alcohol.

After the glycol ester of linoleic acid had been recrystallized from an ether solution three times, it was a bright liquid at room temperature.

0.3342 g substance: 0.9564 g CO_2; 0.3466 g H_2O
0.3782 g substance: 1.0706 g CO_2; 0.3788 g H_2O
Found %: C 77.98 77.28; H 11.52; 11.12.
$C_{38}H_{66}O_4$. Calc. %: C 77.82; H 11.26.

Iodine number: 172.0, 173.10; Calc. 173.4; $d_4^{20} = 0.9182$.

To protect these esters from oxidation they were kept in special containers made of dark glass, in an atmosphere of nitrogen. Preliminary tests had shown that prolonged heating of the esters to 100° in an atmosphere of nitrogen from which all traces of oxygen had been removed caused no perceptible increase in viscosity.

The progress of oxidation and of the related increase in viscosity when the esters were heated in a current of air is shown in Fig. 2.

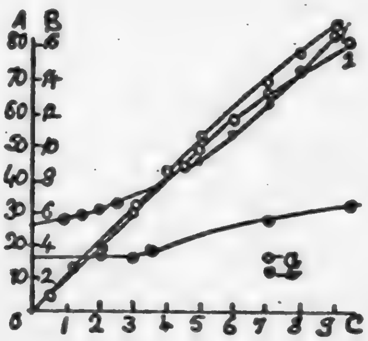

Fig.2. Oxidation and increase of viscosity of methyl linolate and glycol linolate.

A – Ml of O_2 per gram; B – outflow time, sec; C – time, hours. 1 – glycol linolate; 2 – methyl linolate. a – Oxidation; b – viscosity.

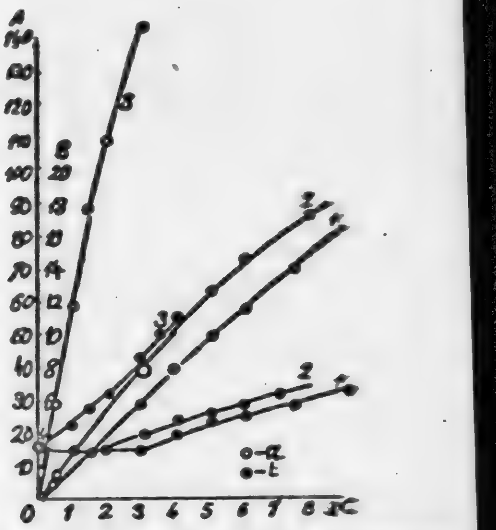

Fig.3. Comparative oxidation and viscosity rise of methyl linolate in air, in oxygen, and in air + benzoyl peroxide.

A – Ml of O_2 per g; B – outflow time sec; C – time, hours. Atmospheres: 1 – air; 2 – air + 1.7% benzoyl peroxide; 3 – oxygen. a – Oxidation; b – viscosity.

The viscosity is expressed in the outflow time required, in seconds. As we see from the graph, the oxidation of esters of lineolic acid prepared synthetically does not involve any inductión period.

There is but little difference in the rate at which oxygen is absorbed by the methyl and glycol esters. However, the glycol ester exhibits a faster rise of viscosity during oxidation than does the methyl ester, which is definitely related to the higher valency of the alcohol radical in the glycol ester [5].

An increase in the oxygen concentration greatly accelerates the oxidation and the increase in viscosity, as is seen in Fig.3 The process rate is likewise fundamentally affected by the addition of small percentages of benzoyl peroxide, which acts as an initiator in many valuable processes. It should be noted that though the benzoyl peroxide accelerates oxidation and the related increase in viscosity, it has no effect at all upon the ratio of viscosity to the amount of oxygen absorbed (Figs. 4 and 5).

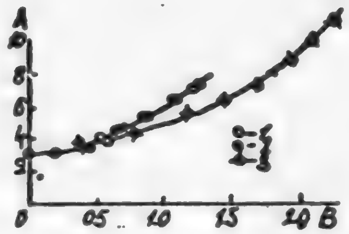

Fig.4. Viscosity of methyl linolate as a function of the extent of oxidation.

A - Outflow time, sec; B - Amount of oxygen, moles O_2 per mole methyl linolate.. Atmospheres: 1-air; 2 - air + benzoyl peroxide; 3 - oxygen.

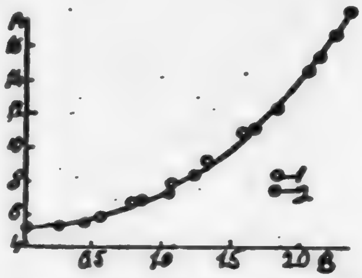

Fig.5. Viscosity of glycol linolate as a function of the extent of oxidation.

A - Outflow time, sec; B - Amount of oxygen, moles O_2 per mole glycol linolate. 1 - Pure glycol linolate ; 2 - glycol linolate + 1% benzoyl peroxide.

We may therefore assume that benzoyl peroxide does not change the processes involved in oxidation and that, therefore, the peroxide mechanism (as stated in Bach's theory) may be employed not only in oxidizing unsaturated esters, but also in their condensation, which is manifested by an increase in viscosity, usually called polymerization.

The curves in Fig. 4 exhibit still another feature, dealing with the variation of viscosity with oxidation. Increasing the oxygen concentration speeds up oxidation and the rise in viscosity, but it also affects the ratio of viscosity to the degree of oxidation, causing less viscous products to be formed.

SUMMARY

1. A method has been developed for investigating the increase of viscosity of unsaturated esters as directly affected by oxidation.

2. A study has been made of the oxidation and the related increase in viscosity of the methyl and glycol esters of linoleic acid.

3. Adding benzoyl peroxide accelerates the oxidation of the esters, but does not affect the relationship of viscosity to the extent of their oxidation.

4. Increasing the concentration of oxygen causes the relationship of viscosity to the extent of oxidation to change, resulting in a decrease in the viscosity of the end products.

LITERATURE CITED

[1] A. M. Lazarev and N. Rasshchektaev, J. Techn. Phys. 5, 1205 (1935).

[2] W. Kimura, Ber. 69, 788 (1936).

[3] D. F. Daubert, A. R. Baldwin, J. Am. Chem. Soc. 66, 997 (1944).

[4] H. C. Black, Ch. A. Overlay, J. Am. Chem. Soc. 61, 3051 (1939).

[5] A. Ya. Drinberg, J. Gen. Chem. 10, 2052 (1940).

Received July 28th, 1950.

BLANK PAGE

LOWERING THE HYDROGEN OVERVOLTAGE

M. A. Loshkarev and A. M. Ozerov

Many papers have been published on the possibility of changing the velocity constant of hydrogen discharge and, hence, the magnitude of its overvoltage during electrolysis. The most interesting of these papers, from the standpoint of application, are the researches on the effect of the material and structure of the electrode surface upon the kinetics of the electrode process. Stender and Pecherskaya [1], for example, investigated the evolution of hydrogen at industrial current densities of several metals and alloys and established the possibility of reducing the overvoltage greatly by the use of wolfram and wolfram-nickel cathodes. Other authors have likewise commented on the positive results to be obtained by the use of alloys. Kabanov and Rozentsveig [2] found that the hydrogen overvoltage depended upon the amount of oxygen bound at the surfaces of iron electrodes. Finally, the researches on hydrogen overvoltage at metallic electrodes with a greatly expanded surface (metallized ceramics and metal powders) performed by Kuzmin [3] (iron), Murtazayev [4] (cobalt), and Maitak [5] (copper) indicate the possibilities of lowering the overvoltage by employing highly disperse materials as the cathodes.

It seems to us that research along the lines of selecting a cathodematerial by means of a systematic study of the hydrogen overvoltage at disperse electrodes of various metals and alloys, prepared in various ways, ought to be of the greatest practical interest.

In our previous papers [6] we succeeded in defining the basic conditions governing the electrolytic preparation of highly disperse single and multi-component cathodic deposits of metals. These papers had as their objective the establishing of an industrial method of preparing powder metals and alloys for metallized ceramics, catalysts, and cementing materials in hydroelectrometallurgy.

The high purity, dispersion, and chemical activity of the resultant products enabled us to assume that using them as a cathode material might result in a sharp increase in the rate of hydrogen evolution. Moreover, the method we have recommended for the electrolytic deposition of thin layers of disperse metals and alloys upon dense electrodes can be readily employed in present-day apparatus, thus involving no large expenditures. In this connection we have explored the kinetics of hydrogen evolution at electroyltically prepared disperse depositis of Ag, Pt, Cu, Bi, Sn, Ni, and Fe.

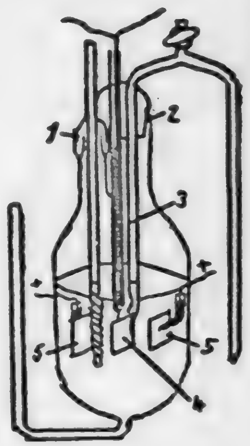

Fig. 1. Apparatus for determining polarization.

1 – hydraulic seal;
2 – ground-glass fit;
3 – contact tips;
4 – cathode;
5 – anode.

EXPERIMENTAL

Experimental method. The tested deposits were prepared by depositing the metals electrolytically upon a Pt electrode. The composition of the electrolytes and the C.D. are given in Table 1. In preparing disperse deposits on a platinum electrode, we began by depositing a layer of dense metal and then deposited a powder at C.D.'s that exceeded the limiting diffusion C.D. ($\underline{D}_{lim.}$). The value of $\underline{D}_{lim.}$ was first calculated from the equation for the maximum rate of diffusion of the ions being discharged, and then checked experimentally. When depositing disperse two-component systems, we conducted electrolysis at C.D.'s that exceeded the $\underline{D}_{lim.}$ for the deposition of the more highly electropositive metal.

TABLE 1

Conditions Governing the Deposition of Metals and Capacitance

Deposit	Composition of electrolyte	C.D., milliamp/ sq cm	Capacitance μF/ sq cm
Dense Cu	0.1 N. $CuSO_4$ + 1N H_2SO_4	D=1.5	35
Powder Cu	ditto	D_1=1.5; D_2=50	1180
Dense Ag	0.005 N. $NaAg(CN)_2$	D_1=1.5	200
Powder Ag	ditto	D_1=1.5; D_2=50	912
Dense Ni	0.1 N. $NiSO_4$ + 20 g/l $(NH_4)_2SO_4$+ +10 g/l NaCl	D_1=1.5	50
Powder Ni	ditto	D_1=1.5; D_2=50	1025
Dense Pt	Smooth commercial platinum	-	-
Powder Pt	Electrolyte platinized by the Mislovitser method	1)	1030
Dense Bi	1 N $(C_6H_3OHCH_3SO_3)_3Bi$	D_1=10	92
Powder Bi	ditto	D_1=2; D_2=150	910
Dense Fe	0.1 N. $FeSO_4$+ 20 g/l $(NH_4)_2SO_4$+ +10 g/l NaCl	D_1=4	-
Powder Fe.....	ditto	D_1=4; D_2=100	1200
Dense Sn	0.2 N. $SnSO_4$+1 N H_2SO_4+0.3 g/l diphenylamine +0.75 g/l β-naphthene	D_1=10	35
Powder Sn	0.2 N. $SnSO_4$+1 N. H_2SO_4+1g/l gelatin	D_1=10; D_2=100	577
Powder Fe + Ni	(0.1 N. $FeSO_4$+0.02 N $NiSO_4$)+ +20 g/l $(NH_4)_2SO_4$+10 g/l NaCl	D_1=4; D_2=100	1320
Powder Cu + Ag	(0.1 N. $CuSO_4$+0.02 N. Ag_2SO_4)+ 1 N. H_2SO_4	D_1=1; D_2=20	1250
Powder Fe + Cu	(0.1 N. $FeSO_4$+0.02 N $CuSO_4$)+ + 20 g/l $(NH_4)_2SO_4$+10 g/l NaCl	D_1=1.5; D_2=10	1100
Powder Sn + Cu	(0.2 N. $SnSO_4$+0.2 N $CuSO_4$) + 1N H_2SO_4	D_1=10; D_2=50	950

The amount of powder deposited was the same in every case. The time required for electrolytic deposition was determined from the equation: $\underline{D} = \underline{Q}\,\frac{Ah}{cm^2}$, which equaled 0.008 - 0.01.

1) Current was passed through from a 4-volt storage battery for 5 minutes.

Measurements were made in the electrolyzer illustrated in Fig. 1, which consisted of a glass vessel with two Pt anodes and a Pt cathode electrolytically coated, with an $S = 3$ sq cm. The hydrogen evolution potential was measured in a 1 N solution of H_2SO_4 or in 22% KOH (chemically pure). Contact tips touched both sides of the cathode, pressing rather tightly against the metal layer. The contact tips were connected via intermediate vessels to a reference calomel electrode that served as a comparison electrode.

The potential (E_k) was measured by the direct compensation method, using a Raps type potentiometer made by the Etalon factory. The electrolyzer was immersed in a thermostat, the temperature of which was kept at $30 \pm 0.5°$ C by means of an electric relay.

Electrolytic hydrogen was supplied to the electrolyzer from below. A uniform hydrogen atmosphere was maintained within the apparatus by connecting the latter to the outside air through a hydraulic seal. The overvoltage was measured at a fixed stirrer rpm. The rpm of the latter was checked against the readings of a voltmeter connected across the motor terminals.

The overvoltage measurements were paralleled by measurements of the cathode's capacitance, which was proportional to its true surface. The capacitance was measured with 0.6-0.8 volt polarization of the electrode. The method of capacitance measurement has been described before.

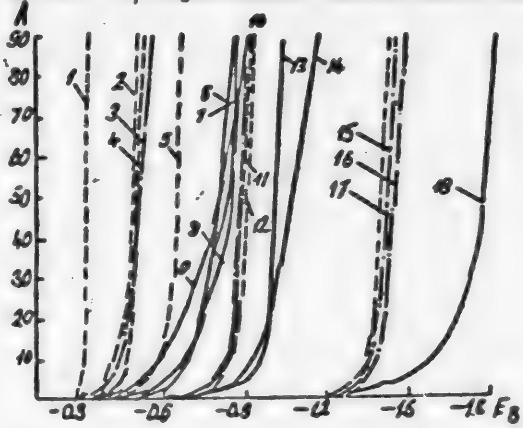

Fig. 2. H_2 evolution potentials at smooth and disperse metals in 1 N H_2SO_4 and 22% KOH (Fe). A – D, milliamps per sq cm; abscissas: E_b Metals: 1 – Pt_n; 2 – Ni_n; 3 – Ag_n; 4 – Cu_n + Ag_n; 5 – Cu_n; 6 – Pt_2; 7 – Cu_2; 8 – Ag_2; 9 – Ni_2; 10 – Sn_n + Cu_n; 11 – Sn_n; 12 – Bi_n; 13 – Bi_2; 14 – Sn_2; 15 – Fe_n; 16 – Fe_n + Cu_n; 17 – Fe_n + Ni_n; 18 – Fe_2.

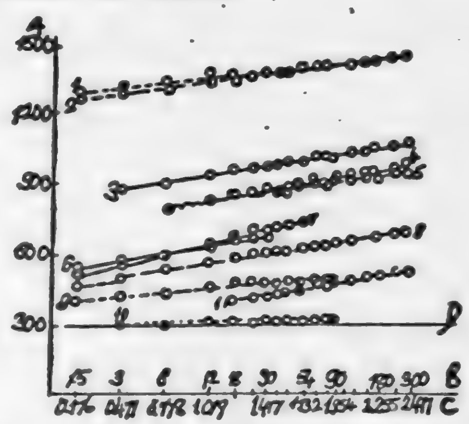

Fig. 3. E as a function of log I in the evolution of H_2. The value of $E_{equil.}$ is given for the deposition of H_2 from 1 N H_2SO_4 (0.29 volt referred to a calomel electrode). B – I, milliamps; A – E, millivolts; C – log I; D – $E_{equil.}$ Metals: 1 – Fe + Cu; 2 – Fe; 3 – Bi; 4 – Bi; 5 – Sn + Cu; 6 – Ag; 7 – Cu; 8 – Cu; 9 – Ag; 10 – Pt; 11 – Ni.

TABLE 2

Hydrogen Evolution Potentials at Dense and Disperse Metals [1)]

D, milliamps per sq cm	Electrolyte: 1N sulfuric acid					
	Cu		Ag		Ni	
	Smooth 200 μF	Powder 1180 μF	Smooth 200 μF	Powder 912 μF	Smooth 50 μF	Powder 1025 μF
0.25	0.350	–	0.342	0.232	0.313	0.377
0.50	0.479	0.453	0.523	0.380	0.356	0.378
1.00	0.545	0.490	0.558	0.406	0.410	0.379
2.00	0.590	0.531	0.580	0.433	0.473	0.381
4.00	0.643	0.565	0.621	0.448	0.526	0.389
6.00	0.667	0.585	0.639	0.459	0.562	0.397
8.00	0.682	0.585	0.657	0.466	0.583	0.413
10.0	0.691	0.590	0.676	0.470	0.600	0.418
12.0	0.701	0.596	0.682	0.474	0.623	0.428
14.0	0.711	0.601	0.690	0.478	0.640	0.439
16.0	0.723	0.610	0.706	0.481	–	0.447
18.0	0.733	0.614	0.730	0.484	0.649	0.451
20.0	0.743	0.620	0.758	0.486	0.670	0.456
22.0	0.753	0.624	0.780	0.489	0.686	0.461
24.0	0.770	0.628	0.800	0.490	0.700	0.465
26.0	0.780	0.632	0.820	0.492	0.715	0.469
28.0	0.780	0.634	0.825	0.493	0.720	0.471
30.0	0.805	0.636	0.831	0.495	0.743	0.475
40.0	0.850	0.647	0.855	0.505	0.784	0.487
50.0	0.870	0.665	0.870	0.520	0.817	0.496
60.0	0.860	0.662	0.889	0.532	0.847	0.504
70.0	0.880	0.670	0.903	0.532	0.870	0.510
80.0	0.880	0.672	0.926	0.535	0.922	0.511
90.0	0.890	0.675	0.938	0.541	0.948	0.516
100	0.900	0.679	0.950	0.544	0.974	0.522

[1)] In this table, as in Table 3, the values of E are given referred to the potential of the reference calomel electrode, taken as zero (E = +0.28).

TABLE 2

Hydrogen Evolution Potentials at Dense and Disperse Metals[1)]

Electrolyte: 1N sulfuric acid						Electrolyte: 22% KOH	
Pt		Bi		Sn		Fe	
Smooth	Powder 1030 μF	Smooth 92 μF	Powder 910 μF	Smooth 35 μF	Powder 577 μF	Smooth	Powder 1200 μF
–	0.283	–	–	0.534	0.537	1.292	1.192
–	–	0.800	0.620	0.550	0.541	1.336	1.252
0.557	0.290	0.860	0.745	0.830	0.578	1.394	1.278
0.569	0.296	0.895	0.782	0.874	0.780	1.462	1.303
0.588	0.300	0.932	0.813	0.910	0.818	1.522	1.332.
0.625	0.302	0.952	0.834	0.933	0.840	1.567	1.348
0.656	0.304	0.962	0.848	0.949	0.855	1.593	1.357
0.680	0.306	0.970	0.859	0.960	0.859	1.614	1.366
0.699	0.307	0.978	0.866	0.964	0.867	1.637	1.372
0.714	0.308	0.983	0.870	0.972	0.872	1.655	1.378
0.730	0.311	0.987	0.877	0.984	0.877	1.671	1.382
0.740	0.312	0.990	0.880	0.992	0.881	1.681	1.385
0.749	0.313	0.993	0.883	0.999	0.855	1.691	1.388
0.757	0.313	0.997	0.885	1.007	0.889	1.699	1.391
0.765	0.313	1.00	0.890	1.018	0.891	1.706	1.392
0.772	0.314	1.003	0.894	1.029	0.894	1.716	1.394
0.778	0.314	1.005	0.897	1.038	0.896	1.721	1.395
0.784	0.314	1.008	0.900	1.046	0.900	1.731	1.395
0.798	0.322	1.024	0.913	1.066	0.912	1.765	1.408
0.817	0.325	1.032	0.926	1.091	0.921	1.786	1.418
0.834	0.328	1.040	0.934	1.126	0.930	1.801	1.428
0.849	0.332	1.047	0.940	1.154	0.936	1.816	1.438
0.863	0.334	1.052	0.945	1.180	0.941	1.834	1.445
0.878	0.337	1.057	0.951	1.197	0.947	1.847	1.452
0.892	0.340	1.060	0.960	1.220	0.950	1.863	1.458

[1)] In this table, as in Table 3, the values of E are given referred to the potential of the reference calomel electrode, taken as zero (E = +0.28).

TABLE 3

Hydrogen Evolution Potentials at Disperse Two-Component Metallic Deposits.

Electrolyte: 1N H_2SO_4 and 22% KOH. Temperature: 30°

D, milliamps per sq cm	E_V				I mA	log I
	Electrolyte: 1N H_2SO_4		Electrolyte: 22% KOH			
	1250 °F	950 °F	1100 °F	1320 °F		
0.25	–	0.510	1.204	1.214	0.75	−0.125
0.50	–	0.530	1.276	1.246	1.50	+0.176
1.00	0.333	0.724	1.300	1.287	3.00	0.477
2.00	0.378	0.780	1.320	1.310	6.00	0.778
4.00	0.402	0.817	1.343	1.332	12.0	1.079
6.00	0.414	0.834	1.360	1.344	18.0	1.255
8.00	0.423	0.843	1.374	1.355	24.0	1.380
10.00	0.431	0.852	1.383	1.362	30.0	1.477
12.0	0.437	0.858	1.393	1.369	36.0	1.556
14.0	0.442	0.865	1.400	1.375	42.0	1.623
16.0	0.448	0.872	1.405	1.380	48.0	1.681
18.0	0.452	0.876	1.410	1.385	54.0	1.732
20.0	0.457	0.880	1.416	1.390	60.0	1.778
22.0	0.461	0.884	1.420	1.394	66.0	1.819
24.0	0.467	0.888	1.425	1.397	72.0	1.857
26.0	0.471	0.892	1.429	1.401	78.0	1.892
28.0	0.478	0.894	1.433	1.406	84.0	1.924
30.0	0.486	0.896	1.436	1.410	90.0	1.954
40.0	0.506	0.905	1.455	1.424	120.0	2.079
50.0	0.521	0.913	1.470	1.436	150.0	2.176
60.0	0.535	0.920	1.480	1.447	180.0	2.255
70.0	0.545	0.928	1.489	1.457	210.0	2.322
80.0	0.550	0.937	1.496	1.466	240.0	2.380
90.0	0.555	0.944	1.503	1.473	270.0	2.431
100.0	0.560	0.950	1.508	1.480	300.0	2.477

The results of our investigations of the hydrogen evolution potentials in 1N H_2SO_4 and 22% KOH at the following dense metals: Pt, Bi, Ni, Ag, Sn, Cu, and Fe and their disperse deposits and alloys are shown in Tables 2 and 3 and Figs. 2 and 3. In every case the potentials given are referred to that of a reference calomel electrode. To convert them into the hydrogen scale 0.28 volt should be deducted from the tabular values.

Inspection of the tabular data shows that the hydrogen evolution potential at disperse metals and their alloys is always lower than at dense metals and alloys. The figures below, taken from Table 2, for example, indicate that the difference between the evolution of hydrogen at dense and disperse silver at D = 100 milliamps/ sq cm is 406 millivolts, while it is 452 millivolts for nickel, etc.

Electrode material:	Pt	Fe	Cu	Ag	Ni	Bi	Sn
$\Delta E_V = E_{dense} - E_{disp.}$ at D = 100 milliamps per sq cm	0.552	0.405	0.221	0.406	0.452	0.100	0.270
Increase in area ($S_{disp.}$: $S_{dense.}$)................	-	-	35	4.5	20	10	16

Of exceptional interest is the fact that the decrease in polarization when disperse deposits are employed is always much greater than would be due to a decrease in the C.D. alone. For, let us assume that the variation of η with D is governed by the equation:

$$\eta = a + 0.116 \log D.$$

in accordance with the theory of slow discharge.

Then for the nickel cathode, say, the difference between the H_2 overvoltages at the disperse and dense electrodes should be:

$$\eta_{dense} - \eta_{disp.} = 0.116 \log 20$$

whereas the actual difference $\eta_{dense} - \eta_{disp.}$ = 0.452 volt, or about three times as great.

A similar state of affairs prevails with Ag, Pt, Sn, and the other metals. Hence, the transition from dense to disperse cathodes results in a decrease in the overvoltage largely because of the increase in the velocity constant of discharge in many instances, as well as because of the increase in the actual area of the electrodes. This agrees with the increased chemical activity of various electrolytic powders in purely chemical reactions.

When the disperse deposit includes a certain percentage of a more highly electropositive metal (a two-component system), the decrease in the overvoltage is greater still. For instance, the decrease in the potential of hydrogen evolution as we shift from dense copper to disperse copper is given by:

$$E_{dense\ Cu} - E_{powd.\ Cu} = 900 - 679 = 221 \text{ mV};$$

while when disperse Ag is included in the disperse deposit, it is:

$$E_{dense\ Cu} - E_{powd.\ Cu+Ag} = 900 - 560 = 340 \text{ mV}.$$

These potentials lie on straight lines when E vs. log I is plotted in logarithmic coordinates, the value of the coefficient b in the Tafel equation ($\eta = a - b \log D$) approaching the values given by Pecherskaya and Stender for several smooth metals, averaging 0.10-0.12. The values of the coefficient b were found to be somewhat higher for smooth (dense) Ni, Fe, and Cu (Table 4).

The value of the coefficient b is less than 0.10 for most of the disperse metals, which agrees with the findings of various authors, who held that overvoltage may also be largely due, in addition to the slow discharge, to other "stages" of the evolution of hydrogen, especially the slowing-down of the recombination of hydrogen atoms into molecules.

TABLE 4

Value of the Coefficient b for Hydrogen Overvoltage at Disperse Electrolytic Deposits

Electrode Material		Coefficient b	Electrode Material		Coefficient b
Disperse	Pt	0.015	Disperse	Fe+Cu	0.111
	Fe	0.087		Fe+Ni	0.075
	Ag	0.060		Cu+Ag	0.082
	Bi	0.096		Sn+Cu	0.0945
	Sn	0.091			
	Cu	0.150			

The experimental data set forth above indicate that the employment of electrolytic coatings of disperse metals and their alloys on cathodes opens prospects of a considerable decrease in the cathode potential (0.4 volt and more in some instances) in industrial processes, such as the electrolytic production of chlorine, the electrolysis of water, and the like, which will reduce the consumption of electric energy considerably, thus lowering the cost of the process.

SUMMARY

1. A study has been made of the hydrogen overvoltage in 1N H_2SO_4 and 22% KOH at dense and disperse electrolytic deposits of Pt, Ag, Cu, Bi, Sn, Ni, and Fe, and in the following two-component systems: Cu – Ag; Sn – Cu; Fe – Cu; and Fe – Ni.

2. It has been shown that it is possible to lower the overvoltage by more than 0.4 volt by employing certain electrolytically prepared powder electrodes.

3. It has been found that the lowering of the overvoltage is due not only to the decrease in the actual C.D. caused by the rise in the actual area of the cathode, but largely as the result of an increase in the velocity constant of the discharge of hydrogen ions.

LITERATURE CITED

[1] A. G. Pecherskaya and V. V. Stender, J. Appl. Chem 19, 1303 (1946).

[2] S. Rozentsveig and B. Kabanov, J. Appl. Chem. 22, 513 (1949

[3] L. L. Kuzmin and V. S. Poroikova, J. Appl. Chem. 22, 572 (1949).

[4] A. Murtazaev J. Phys. Chem. 23, 1247 (1949).

[5] G. P. Maitak, Proc. Inst. Chem. 6, 55 (1939); 7 (1941).

[6] M. Loshkarev, O. Gornostaleva, and A. Kryukova, J. Appl. Chem. 19, 793 (1946); M. Loshkarev, A. Ozerov, and N. Kurdryavtsev, J. Appl. Chem. 22, 294 (1949).

Received April 11, 1950.

THE FORMATION OF HYDRATES DURING THE ELECTROLYSIS OF NICKEL [1)]

A. L. Rotinyan and V. Ya. Zeldes

Institute of the Nickel, Cobalt, and Tin Industry

In our preceding papers [1,2] we investigated the conditions at which colloid hydrates of nickel, copper, and iron begin to form in the electrolyte used for the electrolytic refining of nickel.

The present paper is a report on the results of experiments testing the effect of the salt anion and of the nature of the buffer additives upon the pH at which nickel hydrates begin to form, together with a discussion of all the experimental data.

The experimental method was the same as that described in the first report. The experimental data are reproduced in Figs. 1, 2, and 3 and in Tables 1 and 2. The point at which the hydrates begin to form is marked on the titration curves by an arrow. The data for sulfate solutions have been taken from the first report.

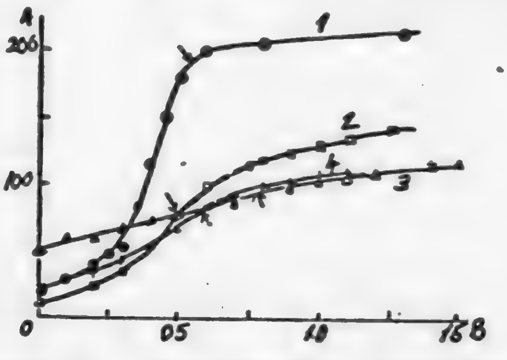

Fig. 1. Potentiometric titration curves of a pure solution of $NiCl_2$ and of buffered solutions. $\underline{t}$ = 50°.

$\underline{A}$ – Emf, millivolts; $\underline{B}$ – Ml of NaOH. Solution composition: $\underline{1}$ – 38 grams/liter of Ni; 2 – 38 grams/liter of Ni + 0.16 mole/liter of H_3BO_3; 3 – 38 grams/liter of Ni + 0.16 mole/liter of $(NH_4)_2SO_4$; 4 – 38 grams/liter of Ni + 0.16 mole/liter of NH_4Cl.

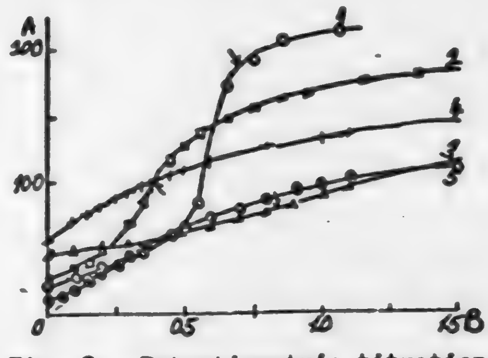

Fig. 2. Potentiometric titration curves of a pure solution of $NiNO_3$ and of buffered solutions. $\underline{t}$ = 50°.

$\underline{A}$ – Emf, millivolts; $\underline{B}$ – Ml of NaOH. Solution composition. $\underline{1}$ – 38 grams/liter of Ni; 2 – 38 grams/liter of Ni + 0.16 mole/liter of H_3BO_3; 3 – 38 grams/liter of Ni + 0.16 mole/liter of $(NH_4)_2SO_4$; 4 – 38 grams/liter of Ni + 0.16 mole/liter of NH_4Cl; 5 – 38 grams/liter of $NiNO_3$ + 0.16 mole/liter NH_4NO_3.

---

1) Report III of a series on this topic.

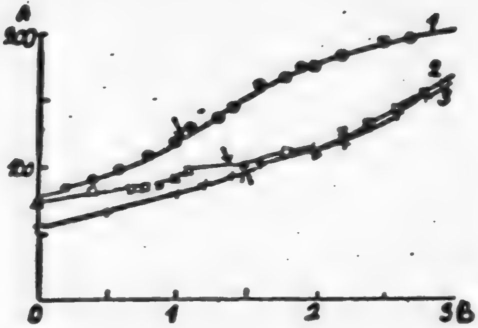

Fig. 3. Potentiometric titration curves of a nickel electrolyte to which $(NH_4)_2SO_4$ has been added as a buffer. t = 50°.

A - Emf, millivolts; B - ml of NaOH. Electrolyte: Ni (as the sulfate) - 38 grams/liter; NaCl - 5 grams/liter; Na_2SO_4 - 40 grams/liter; $(NH_4)_2SO_4$: 1 - 10 grams/liter; 2 - 20 grams/liter; 3 - 40 grams/liter.

The first line of Table 1 lists the pH at which hydrates begin to form in pure solutions of nickel sulfate, chloride, and nitrate. We see from these figures that the pH at which hydrates form is practically the same in the nitrate and chloride, while colloid hydrates begin to form in the sulfate when the medium is somewhat more alkaline. This difference is apparently due to the lower activity of the nickel ions in a sulfate solution. The difference in the pH at which nickel hydrates begin to form between the sulfate and chloride solutions is 0.4, which agrees quantitatively with the figures cited in our first report [1].

We see from Table 1 that adding boric acid to pure salt solutions decreases the pH at which nickel sulfate hydrates begin to form by 1.0, the pH for the nickel chloride and nitrate diminishing correspondingly by 1.5; in a sulfate medium, ammonium sulfate diminishes the pH nearly twice as much as does boric acid, whereas the action of the two buffers is identical in the chloride and nitrate media.

The solutions of $NiNO_3 + NH_4Cl$ and $NiNO_3 + NH_4NO_3$ are remarkable in that we were able to find neither a point of inflection in the potentiometric curves that would correspond to the appearance of the solid phase nor a diffusion section.

The effect of the concentration of ammonium sulfate upon the pH at the instant the nickel hydrates begin to form is shown in Table 2.

TABLE 1

Effect of the Addition of Buffers Upon the pH at which Nickel Hydrates Begin to Form at 50° in Solutions Containing 38 Grams of Nickel per Liter

Buffer (0.16 mole/liter)	pH at which nickel hydrates begin to form in various solutions		
	$NiSO_4$	$NiCl_2$	$Ni(NO_3)_2$
None	5.3	4.9	4.8
H_3BO_3	4.3	3.4	3.3
$(NH_4)_2SO_4$	3.5	3.5	3.3
NH_4Cl	–	3.3	?
NH_4NO_3	–	–	?

TABLE 2

Effect of the Concentration of Ammonium Sulfate Upon the pH at which Nickel Hydrates Begin to Form

$(NH_4)_2SO_4$ concentration, grams/liter	pH at which hydrates begin to form
0	5.2
10	3.9
20	3.6
40	3.4

The data of Table 2 are reproduced graphically by Curve 1 in Fig. 4. The same graph shows in Curve 2, for the sake of comparison, the pH at which hydrates begin to form in solutions buffered with boric acid [1]. Comparison of the two curves clearly indicates that ammonium sulfate lowers the pH much faster than the boric acid does. These findings are of significance in learning the mechanism involved in the formation of harder nickel deposits when ammonium sulfate is present.

Since hydrates begin to form at lower values of pH in solutions to which ammonium sulfate has been added than in solutions containing boric acid, it is obvious that more hydrates will be formed during electrolysis in the former case and the deposits will be harder than in the second case.

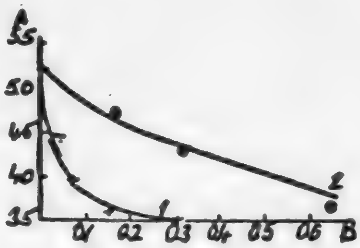

Fig. 4. Effect of the concentration of ammonium sulfate and of boric acid upon the pH at which nickel hydrates begin to form at 50°.

A – pH at the onset of hydrate formation; B – concentration of buffers, moles/liter. 1 – Ammonium sulfate added; 2 – boric acid added.

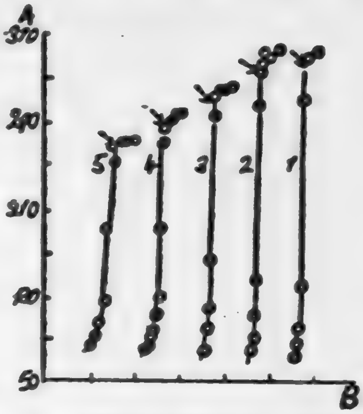

Fig. 5. Potentiometric titration curves of dilute solutions of nickel sulfate at 50°, using a glass electrode.

A – Emf, millivolts; B – ml of NaOH. Ni content, grams/liter: 1 – 0.05; 2 – 0.1; 3 – 0.5; 4 – 1.5; 5 – 5.

Our experimental data enable us to reach certain conclusions regarding the composition of the solid phase.

In essence, if we assume that the solid phase begins to form when a solubility product of the following type:

$$\alpha_{Me^{n+}} \cdot \alpha_{OH}^{n} = L_p, \tag{1}$$

is attained, i.e., the solid phase is a pure hydrate rather than a basic salt, at least at the instant of its formation, the magnitude of the solubility product should not change as the concentration of nickel sulfate is varied.

Supplementary titration tests of dilute solutions of nickel sulfate were run to get a clearer idea of this behavior pattern, the results being plotted in Fig. 5. The concrete computations of L_p from the activity coefficients will hardly be accurate enough, for the latter coefficients are known only up to 25°. A comparison of the activity coefficients at 25° [3] and at a temperature close to the freezing point of the solutions [4] indicates, to be sure, that they change

very little with temperature. The results of our calculations of L_p from all our experimental data are listed in Table 3.

TABLE 3

Data for the Computation of the Solubility Product From Experimental Findings

Nickel concentration		pH at which hydrates begin to form	Computation of L_p from the activity coefficients			Computation of L_p from the apparent degree of dissociation			
Grams/liter	Moles/liter		f	$\log a_{Ni}$	$L_p \cdot 10^{16}$	λ_v at 50°	$\alpha = \frac{\lambda_v}{\lambda_\infty}$	$\lg C_{Ni^{++}}$	$L_p \cdot 10^{15}$
0.05	0.0009	7.1	0.80	$\bar{4}.857$	3.58	158	0.84	$\bar{4}.903$	3.46
0.10	0.0017	7.0	0.70	$\bar{3}.076$	3.73	151	0.80	$\bar{3}.114$	4.28
0.5	0.0085	6.7	0.48	$\bar{3}.613$	2.03	111	0.58	$\bar{3}.778$	3.14
1.5	0.0256	6.3	0.32	$\bar{3}.914$	1.02	92	0.49	$\bar{2}.097$	1.55
5.0	0.0884	6.1	0.18	$\bar{2}.20$	0.76	71	0.38	$\bar{2}.524$	1.60
10	0.170	5.8	0.14	$\bar{2}.377$	0.30	64	0.34	$\bar{2}.762$	0.72
21	0.362	5.6	0.094	$\bar{2}.532$	0.11	55	0.29	$\bar{1}.025$	0.33
25	0.430	5.5	0.084	$\bar{2}.558$	0.07	53	0.28	$\bar{1}.100$	0.24
35	0.605	5.3	0.068	$\bar{2}.613$	0.05	51	0.27	$\bar{1}.215$	0.20
36	0.614	5.3	0.066	$\bar{2}.608$	0.05	51	0.27	$\bar{1}.215$	0.20
39	0.665	5.3	0.063	$\bar{2}.621$	0.05	50	0.27	$\bar{1}.248$	0.22
39.6	0.675	5.3	0.062	$\bar{2}.621$	0.05	50	0.27	$\bar{1}.248$	0.22
40.6	0.693	5.3	0.061	$\bar{2}.625$	0.05	49	0.26	$\bar{1}.255$	0.22
51	0.869	5.2	0.054	$\bar{2}.671$	0.04	48	0.26	$\bar{1}.364$	0.17
61	1.040	5.1	0.051	$\bar{2}.724$	0.026	46	0.24	$\bar{1}.406$	0.12

As we see in the table, the values of L_p do not remain constant, falling steadily by a factor of 137 as the nickel concentration rises from 0.05 to 61 grams per liter. We therefore also computed L_p from the values of the apparent degree of dissociation of the nickel sulfate.

In this calculation we used the following values of the required variables: $K_{W50°} = 5.6 \cdot 10^{-14}$ [5]; $\frac{1}{2} l_{Ni^{++}} = 46$; $f_{Ni} = 0.024$; $\frac{1}{2} l_{SO_4''(18°)} = 68$; $f_{SO_4''} = 0.0227$. $\lambda_{\infty 50°} = 188$, the values of $\lambda_{v50°}$ being taken from tables [6] (extrapolated in part).

Nor does the solubility product remain constant when this method of computation is used (falling by a factor of 29).

If the pH at the onset of hydrate formation is plotted against the logarithm of the ion activity, the expanded equation (1):

$$pH = -\frac{1}{2}\log a_{Ni^{++}} + \frac{1}{2}\log L_p - \log K_w \qquad (2)$$

ought to yield a straight line with the following slope:

$$-\frac{d\,pH}{d\log a_{Ni^{++}}} = \frac{1}{2}. \qquad (3)$$

The variation of the pH at which the formation of hydrates sets in is plotted in Fig. 6 as a function of the logarithm of the activity or the concentration of nickel ions. The value of slope called for by theory is obtained only in the limiting case of titration of highly dilute solutions. The slope is found to exceed the theoretical value when concentrated solutions are titrated.

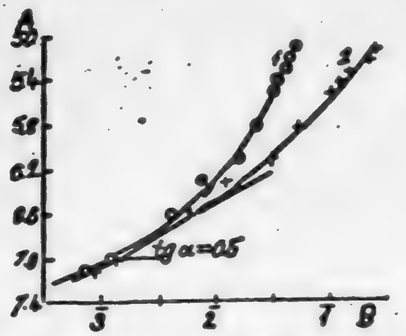

Fig. 6. Checking the correctness of Equation (2) against the data on the formation of nickel hydrates.

A – pH at which hydrates begin to form; B – logarithm of activity (concentration).
1 – pH log $a_{Ni^{++}}$; 2 – pH – log $C_{Ni^{++}}$.

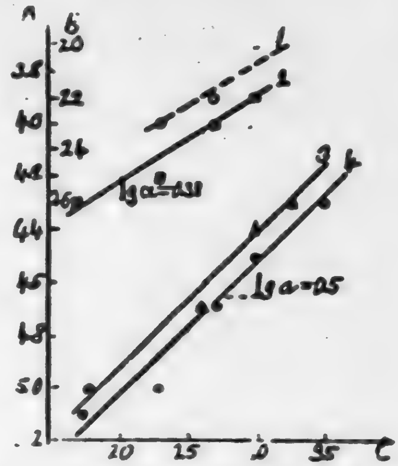

Fig. 7. Checking the correctness of Equation (4) against the data on the formation of hydrates of copper and di- and trivalent iron in a nickel electrolyte. A – pH at which hydrates begin to form (for divalent metals); B – the same for trivalent metals. 1) Fe^{++} with H_3BO_3 added; 2) Fe^{++} without H_3BO_3; 3) Fe^{+++}. 4) Cu^{++}*.

A different relationship prevails when the impurities in the nickel solution form hydrates. Applying the well-known rule that an electrolyte behaves like an ideal substance in the presence of a large (and constant) excess of another electrolyte, we can rewrite Equation (2) for the pH at the instant when hydrates of the impurities begin to form as follows:

$$pH = -\frac{1}{m}\log C_{impurity} + \frac{1}{m}\log L_p - \log K_w, \tag{4}$$

where m is the valency of the cations. We then should get straight lines with the slope of 1/2 for ferrous salts and cuprous salts and 1/3 for ferric salts in pH – log $C_{impurity}$ coordinates. As we see in Fig. 7, this theoretical requirement is satisfied.

It follows from our data, therefore, that when highly dilute solutions of nickel sulfate or impurities in the nickel electrolyte are titrated, the composition of the resulting solid phase agrees with the formula of the corresponding hydrate. It should be borne in mind that experiments involving the titration of solutions of cadmium sulfate with alkali, with parallel measurements as titration progresses, of the pH with a glass electrode, of the con-

centration of cadmium ions with a cadmium electrode, and of the concentration of sulfate ions with a lead electrode, led to a similar conclusion [7].

When more highly concentrated solutions of nickel sulfate are titrated, the composition of the resulting solid phase grows more complex, for difficultly soluble basic salts of nickel are formed instead of the pure hydrates.

In ordinary hydrolysis, the nickel ions combine suddenly in the diffusion layer at the cathode, the alkalinity increasing over the entire surface of the electrode, which favors the formation of hydrates instead of the insoluble basic salts of nickel. Hence, if we assume that the fine crystalline structure of nickel deposits is due to the formation of either colloidal hydrates or basic salts during electrolysis, the experimental material compels us to give preference to the hypothesis that hydrates are formed, rather than basic compounds.

SUMMARY

1. The pH values at which nickel hydrates begin to form in sulfate, chloride, and nitrate solutions have been determined by potentiometric titration with a glass electrode and by means of the Tyndall beam.

It has been shown that the pH values at which hydrates begin to form are the same in the chloride and nitrate solutions, while the precipitation of hydrates begins in a sulfate solution when the solution is more alkaline.

2. Adding boric acid lowers the pH at which nickel hydrates begin to form more rapidly in the chloride and nitrate solutions than it does in the sulfate solution.

3. Exploration of the effect of ammonium sulfate upon lowering the pH at which hydrates begin to form has also shown that the effect of the ammonium sulfate is greater than that of boric acid in a sulfate solution, the action of the two buffers being about alike in the chloride and nitrate solutions.

4. The greater hardness of the cathodic deposits ordinarily secured in the electrolysis of solutions to which ammonium sulfate has been added is apparently due to the large number of nickel hydrates present in the diffusion layer near the cathode.

5. Analysis of the experimental data has demonstrated that it is more probable that colloidal metal hydrates are formed than their basic compounds in the electrolysis of nickel.

LITERATURE CITED

[1] A. L. Rotinyan and V. Ya. Zeldes, J. Appl. Chem. 23, 7 (1950).1)

[2] A. L. Rotinyan and V. Ya. Zeldes, J. Appl. Chem. 23, 9 (1950).2)

[3] G. V. Akimov. Theory and research methods of metal corrosion (1945).

[4] Landolt-Bornstein Tabellen 2, 1128.

[5] Yu. Yu. Lurye. Calculation and reference tables for chemists (1947).

[6] Technical Encyclopedia Handbook, IV.

[7] M. Quittin, Comptes. rend., 226, 494 (1948). Cited in Chem. Zentr., 1, 662 (1949).

Note: The computations of the emf's used in calculating the pH in our previous papers are in error due to inaccuracy of graduation of the glass electrode. The correct pH values at which hydrates begin to form are given on page 771.

1) See Consultants Bureau Translation, p. 757.
2) See Consultants Bureau Translation, p. 991.

Received January 20, 1950

A METHOD OF ELIMINATING SULFUR FROM THE PRECIPITATING BATH IN VISCOSE MANUFACTURE

A. P. Antykov

The presence of perceptible quantities of finely disperse sulfur in the precipitating bath in viscose manufacture is, as we know, highly undesirable, since it greatly increases the spoilage of fiber ("rusty" cakes, dirtying of the thread guides and rollers, which causes a nap, etc.), interferes with the desulfuration of the rayon, and the like. All this makes the elimination of sulfur from the precipitating bath extremely necessary.

The method of eliminating the elementary finely disperse sulfur from precipitating baths (entering the settling bath via decomposition of the xanthate, the viscose formed, and the thiosulfates) now employed in viscose plants, involving the filtration of the bath through quartz filters, has several highly essential disadvantages, which reduce the efficiency of purification nearly to zero. The chief of these disadvantages are: a) the extremely rapid clogging of the quartz filters with finely disperse (sludge) elementary sulfur; b) the need to wash the sulfur out of the quartz layers at length, which requires that they be cut out of the filtration cycle for long intervals of time (8-12 hours every 2 or 3 days); c) the need for a large number of bulky and expensive lead-lined filter vats (filled with quartz); d) high losses of the precipitating bath solution in washing out the filter vats; e) inadequate rate of filtration of the settling bath through the quartz layer, which drops off steadily (as the filter becomes increasingly clogged); f) losses of elementary sulfur in washing out the filter vats; g) large amount of labor and bulk involved in repairs to the filter vats.

All these deficiencies render the method of filtering the precipitating bath through quartz filter vats highly inefficient.

We have worked out a continuous, rapid, and efficient method of eliminating finely disperse sulfur from the precipitating bath, involving the extraction of the finely disperse sulfur with carbon tetrachloride totalling 1% by volume of the bath.

EXPERIMENTAL

Periodic extraction of sulfur from a precipitating bath. 25 ml of pure carbon tetrachloride were placed in a one-liter separatory funnel, and 500 ml of the viscose precipitating bath of ordinary composition (see table) were added.

After the precipitating bath had been added, the funnel was agitated either by hand (shaking) or by means of a stirrer (80-90 rpm) for one minute at 20-35°. After stirring, the mixture stood for one minute, and the bottom layer of carbon tetrachloride (which contains the dissolved sulfur) was allowed to flow out through the bottom stopcock into a 100-ml beaker, while the upper layer of the completely transparent bath was decanted into a receiver for the purified (clarified) bath. The clarified bath may be re-used for the spinning process after first being heated to 45-47°.

The carbon tetrachloride in the beaker was recharged into the same one-liter separatory funnel, another 500 ml of the precipitating bath were added, and the foregoing purifying operation was repeated. The third, fourth, and fifth purifying operations were performed in exactly the same manner, with the same quantity of carbon tetrachloride (always returned to the separatory funnel).

After the fifth operation, the 24-24.8 ml of carbon tetrachloride separated from the precipitating bath were distilled into a distilling tower to free it of the sulfur, all of the carbon tetrachloride being distilled into a condenser and collected in a pure state in the receiver, from which it was taken for the subsequent purifying operations of the precipitating bath. The column consisted of an Erlenmeyer flask, connected via adapters to a straight, water-cooled (12-15°), condenser. The distilled carbon tetrachloride was collected in a 100-ml beaker. The heat for distilling the carbon tetrachloride was supplied by a boiling water bath in which the flask containing the carbon tetrachloride was immersed (and connected to the condenser). The water bath may be heated, in turn, either by steam (via a coil) or by a Bunsen burner.

The distilled carbon tetrachloride was re-used as indicated above in the removal of sulfur from the precipitating bath.

The mechanical losses of carbon tetrachloride after five purification cycles as outlined above was 1.5 to 2% (<u>cf</u> table).

The sulfur left in the carbon tetrachloride was driven off was mixed with three to four times its quantity of water (3-4 ml), poured into a funnel (with a suction filter using one thickness of cloth) and re-used as such after it had been freed of its water.

The precipitating bath, freed of its sulfur as described above, was a transparent colorless liquid with a transparency of 24-28 cm before purification There was no change in the composition of the precipitating bath (<u>cf</u> table).

<u>Continuous sulfur removal from the precipitating bath</u>. In our elaboration of this method of eliminating sulfur from a precipitating bath under laboratory conditions we developed the continuous-cycle purification shown in the figure.

The purification process is as follows. (See Plate, page 773.)

Two half-liter precipitating flasks <u>1</u> and <u>2</u> (in the factory these would be lead-lined tanks with a capacity of 12-20 cu m) are connected together by the rubber tubing <u>3</u>, and 140 ml of pure carbon tetrachloride are poured into each flask. A glass bubbler 170 mm long, with a dilated bottom end pierced by numerous holes, is placed in each flask, passing through the stopper, the bubblers being connected to the rubber tubing <u>4</u>, through which compressed air reaches them from the air line <u>5</u>. Industrially, we could either use lead bubblers

of lead-sheathed high-speed stirrers (80-90 rpm). Compressed air at 0.3-0.5 atm is passed through the bubblers during the purification process to stir up the mixture of the precipitating bath plus the carbon tetrachloride vigorously. The second precipitating flask 2 is connected through the overflow tube 6 to the 300 ml separatory flask 7. The separator, in turn, is fitted with an outlet 8 for the purified precipitating bath that leads to the receiver (collecting tank) for the purified bath (beaker 9). After the apparatus described has been assembled, compressed air at 0.3-0.5 atm is passed through the bubblers in flasks 1 and 2, and a continuous flow of the impure bath enters flask 1 through the unpurified bath entrance tube 10.

The impure bath first fills flask 1 as high as the overflow tube 3, being vigorously stirred by the bubbled air with the carbon tetrachloride which absorbs its finely disperse sulfur.

When flask 1 is full, the bath liquor flows through tube 3 to the second flask 2, where the same process of stirring and extraction takes place as in flask 1. When flask 2 is full, the purified bath overflowsthrough tube 6 into the separator 7, where part of the entrained carbon tetrachloride settles to the bottom, the purified bath overflowing through tube 8 after the separator is full, passing to the purified bath receiver 9. The unpurified bath continously enters flask 1 under pressure (siphoned through tube 11) from the supply flask 12, while the air is discharged, after bubbling, through tube 13 and a condenser.

The impure bath is passed through the apparatus and mixed with the carbon tetrachloride (by the compressed air) until 28-30 liters of impure bath liquor (99 times the volume of the carbon tetrachloride charged into the flask) has been passed through (and stirred intensively by the compressed air). Then the carbon tetrachloride is discharged from the flasks 1 and 2 (via special bottom valves under industrial conditions) into a receiver (a 500-ml flask) for the contaminated carbon tetrachloride, from which it is transferred to a distilling column for distillation as described previously.

After distillation, the pure carbon tetrachloride is re-used to purify the precipitating bath. After the carbon tetrachloride contaminated with extracted sulfur has been drained from flasks 1 and 2, 140 ml of pure carbon tetrachloride are again poured into each flask, and the purifying of the precipitating bath is resumed (the bath being siphoned through tube 11) as before. The purified bath, collected in the receiver 9, has a transparency of 24-28 cm and the usual composition (cf table). In a large-scale installation, when two 18-cu m lead-lined precipitator tanks are used, as much as 5 cu m of carbon tetrachloride must be charged into each tank. No less than 500 cu m of dirty bath liquor should be passed through the precipitator tanks (in series) with intensive stirring before this quantity of carbon tetrachloride is replaced by a new batch. Then the contaminated carbon tetrachloride must be replaced by a new batch and fractionated (regenerated) in a distilling column or filtered.

The sulfur remaining in the distillation tank may be used as such (as much as 200 kg of sulfur may accumulate in the tank during a single operational cycle).

Parallel with our removing the sulfur from the precipitating bath by use of carbon tetrachloride we tested other solvents, keeping the same proportions to the amount of bath to be purified (the ultimate figure being 1%), viz.: carbon disulfide, pyridine, chloroethane, and tetrachloroethane.

Results of Using Carbon Tetrachloride to Eliminate

Used in the test							
		Composition and transparency of the precipitating bath					
Grams/liter of 100% CCl_4	Ml of precipitating bath	Ml of Sulfuric acid	Grams/liter of zinc sulfate	Grams/liter ammonium sulfate	Grams/liter of sodium sulfate	Suspended sulfur, %	Trans-parency cm
25	500	131.1	18.3	24.6	250.4	0.0308	3
-	500	131.1	18.3	24.6	250.4	0.0308	3
-	500	131.1	18.3	24.6	250.4	0.0308	3
-	500	131.1	18.3	24.6	250.4	0.0308	3
-	500	131.1	18.3	24.6	250.4	0.0308	3
25	500	129.2	17.8	25.2	249.1	0.032	2
-	500	129.2	17.8	25.2	249.1	0.032	2
-	500	129.2	17.8	25.2	249.1	0.032	2
-	500	129.2	17.8	25.2	249.1	0.032	2
-	500	129.2	17.8	25.2	249.1	0.032	2
25	500	130.4	17.1	28.7	248.3	0.0316	2
-	500	130.4	17.1	23.7	248.3	0.0316	2
-	500	130.4	17.1	23.7	248.3	0.0316	2
-	500	130.4	17.1	23.7	248.3	0.0316	2
-	500	130.4	17.1	23.7	248.3	0.0316	2
25	500	129.7	19.4	24.9	247.5	0.0312	3
-	500	129.7	19.4	24.9	247.5	0.0312	3
-	500	129.7	19.4	24.9	247.6	0.0313	3
-	500	129.7	19.4	24.9	247.6	0.0312	3
-	500	129.7	19.4	24.9	247.6	0.0312	3

The purification results obtained with these solvents resemble those secured with the carbon tetrachloride but are much inferior to the latter; moreover, they are either inflammable or poisonous. Thus they are inferior to carbon tetrachloride in several respects, so that using the latter for purification is most practicable and preferable.

SUMMARY

1. A new, simple and effective method has been found for continously eliminating finely disperse sulfur from a viscose precipitating bath, involving the extraction of the sulfur with carbon tetrachloride, which is added as 1% by volume to the contaminated bath, with vigorous stirring. The carbon tetrachloride losses may be eliminated by installing a condenser in the purification system.

Ml of precipitating bath	Secured in the test: Composition and transparency of the precipitating bath — Ml of sulfuric acid	Grams/liter of zinc sulfate	Grams/liter of ammonium sulfate	Grams/liter of sodium sulfate	Suspended sulfur, %	Transparency, cm	Refractionated CCl_4, Ml	Elementary sulfur (after fractionation, g	Remarks
496	131.1	18.3	24.6	250.4	None	26	-	-	First test Series
500	131.1	18.3	24.6	250.4	None	26	-	-	
500	131.1	18.3	24.6	250.4	None	26	-	-	
500	131.1	18.3	24.6	250.4	None	26	-	-	
500	131.1	18.3	24.6	250.4	None	25	24.8	0.980	
495	129.2	17.8	25.2	249.1	None	26	-	-	Second test Series
500	129.2	17.8	25.2	249.1	None	26	-	-	
500	129.2	17.8	25.2	249.1	None	27	-	-	
500	129.2	17.8	25.2	249.1	None	26	-	-	
500	129.2	17.8	25.2	249.1	None	25	24.7	1.020	
496	130.4	17.1	23.7	248.3	None	26	-	-	Third test Series
500	130.4	17.1	23.7	248.3	None	26	-	-	
500	130.4	17.1	23.7	248.3	None	26	-	-	
500	130.4	17.1	23.7	248.3	None	25	-	-	
500	130.4	17.1	23.7	248.3	None	25	24.65	1.010	
496	129.7	19.4	24.9	247.6	None	28	-	-	Fourth test Series
500	129.7	19.4	24.9	247.6	None	26	-	-	
500	129.7	19.4	24.9	247.6	None	26	-	-	
500	129.7	19.4	24.9	247.6	None	25	-	-	
500	129.7	19.4	24.9	247.6	None	25	24.6	1.080	

2. This method makes possible the complete utilization of the sulfur contained in the precipitating bath and lost up to now in the wash waters of the quartz filters

3. The transparency of the purified bath is increased from 2-3 cm to 24-28 cm (cf table).

4. The method is free from fire or explosion hazard.

5. The losses of carbon tetrachloride during purification total 1.5-2% of the amount charged. There actually is a gain in material during purification, owing to the complete sulfur recovery.

6. The method makes it possible to do away with the costly, bulky, and labor-consuming lead lined quartz filtering vats. What is more, it lightens the labor process involved in purifying the precipitating bath.

7. Other organic substances may be employed to purify the precipitating bath, such as: carbon disulfide, dichloroethane, pyridine, and the like, but they all suffer from fundamental disadvantages, compared to carbon tetrachloride (fire hazard, explosion hazard, toxicity, etc.) so that carbon tetrachloride is preferred.

Received November 15, 1949.

BLANK PAGE

THE EFFECT OF DEFORMATION UPON METAL POTENTIALS [1)]

E. M. Zaretsky

The preceding paper discussed the factors linking deformation and corrosion behavior. Data were cited on the effect of deformation upon the corrosion rate of some rolled technical metals [1].

The present report deals with the effect of deformation upon the electrochemical characteristics of these metals. The changes in the electrode potentials of magnesium, the magnesium alloys MA_1 and MA_3, aluminum, steel, copper, and zinc due to deformation have been explcred. Some experiments were made with a model microcell made of magnesium alloys.

Investigation of electrode potentials may yield valuable information on the corrosion behavior of strained metals. Their magnitudes provide an idea of the distribution of poles when a strained metal is in contact with an unstrained one, and sometimes indicate the hazard involved in such contact and the protective properties of the oxide films formed on the surfaces of deformed metals.

The change in the electrode potential of metals due to deformation has been known for some time [2,3]. In most cases deformation makes the potentials less noble. Nevertheless, the nature of this phenomenon is still not definitely known.

There are two points of view concerning the reason for this change in potential. Akimov asserts that the potential is made less noble principally by a diminution in the work involved in the exit of the ion-atom from the strained metal. The breaking of the oxide film during deformation has an analogous effect upon the magnitude of the electrode potential [4].

According to another view, the potential is made less noble by the increase in the accumulated potential energy due to deformation [5]. Evans [6] shares this view, though he points out the important part played by the oxide film in the corrosion behavior of strain metals.

The amount of change of electrode potential as the result of deformation varies with the nature and state of the metal, the kind and magnitude of deformation, and the nature of the corrosion medium. The change in potential due to deformation does not exceed a few hundredths of a volt as a rule [4,7,8].

---

1) Report II of a series on this topic.

If the change in electrode potential due to deformation is governed by the increase in the stored potential energy, this change ought to equal the work of deformation.

Let us imagine a metallic electrode Me immersed in an electroylte MeAn and subjected to deformation.

As we know, whenever a process arises within any system as the result of outside work, the change in energy involved may be expressed by the following equation:

$$U = A + q, \tag{1}$$

where $\underline{U}$ is the work performed; $\underline{A}$ is the increase in the system's free energy; and $\underline{q}$ is the heat evolved in the process.

We recall that the elementary work $\underline{du}$ of deformation will be:

$$du = \lambda dP, \tag{2}$$

where $\underline{P}$ is the load, and λ is the elongation of the metallic electrode.

But

$$\lambda = \frac{Pl}{ES}, \tag{3}$$

where $\underline{l}$ is the length of the electrode, $\underline{E}$ is the modulus of elasticity, and $\underline{S}$ is the cross-section area of the electrode.

Hence,

$$-du = \frac{PdPl}{ES} \tag{4}$$

Integrating from $\underline{P} = 0$ to $\underline{P} = \underline{P}$, we get:

$$U = \int_0^P \frac{PdPl}{ES} = \frac{P^2l}{2ES}. \tag{5}$$

Since $\underline{lS} = \underline{V}$, and $\underline{P}/\underline{S} = \underline{p}$, (6)

Expressing the work expended in increasing the free energy of the system in terms of the potential, we get:

$$A = nFe, \tag{7}$$

where $\underline{n}$ is the valency of the metal; $\underline{F}$ is the value of the faraday and $\underline{e}$ is the potential of the metal.

Since the free energy is related to the work done by the equation:

$$-U = A + T\frac{dA}{dT}, \tag{8}$$

and

$$\frac{dA}{dT} = nF\frac{de}{dT}. \tag{9}$$

substituting the values of $\underline{U}$, $\underline{A}$, and $\underline{dA}/\underline{dT}$ from (6), (7), and (8) in (9), we get:

$$e = -\frac{p^2V}{2EnF} + T\frac{de}{dT}. \tag{10}$$

The last equation indicates that the potential varies as the square of the stress, the potential shift being independent of the concentration of the metal's ions in the electrolyte. Inasmuch as the heat evolved is negligibly small compared to the total work of deformation [9], the term $T\frac{de}{dT}$ in Equation (10) may be disregarded in calculations.

Let us calculate the reversible potential of a magnesium electrode under strain. We shall take the stress as equal to the ultimate strength (17 kg/mm^2). We express the work of deformation in joules referred to one gram equivalent of magnesium. Since $E = 4260\ kg/mm^2$; $P = 17\ kg/mm^2$; $F = 96{,}500$; $n = 2$, and $V = \frac{24.32}{2\cdot 1.74}$, we get $e = 2.5$ millivolt.

Magnesium alloys. Now let us consider the results of measuring the potential of deformed magnesium alloys.

The distribution of poles between the strained and unstrained areas was shown clearly by means of a color indicator. A steel ball was used to make small depressions in samples made of magnesium and of the alloys MA1 and MA_3,[1] the depressions filled with a 0.1 molar solution of NaCl + 0.1% neutral red. The dark-raspberry color of the indicator changes to yellow when OH' ions formed at a cathode are present. This color change was observed within 5-6 seconds in that part of the drop next to the undeformed surface. When no deformation had taken place the drop began to turn yellow after 25-30 seconds.

We explored the changes in the electrode potentials of magnesium alloys as deformation was increased gradually by bending samples in a device made of hard rubber (Fig.1,a).

The device consisted of two blocks 1, turning freely on shafts passing through the holes 2, and a base board 3, that passed through U-shaped slots in the blocks.

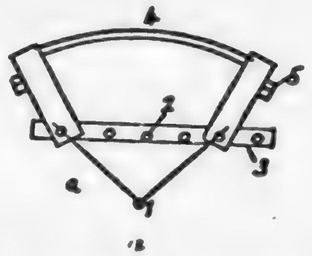

Fig. 1. Device for bending samples.
a – Diagram of the device: 1 – blocks; 2 – openings; 3 – baseboard; 4 – sample being deformed; 5 – wedges.
b – Weighting the device (see Plate, page 773).

A sample 4, 160 x 15 x 1 mm, was fastened to the blocks by means of the T-shaped wedges 5. The sample was deformed by moving block A with respect to the other block, after which the blocks were clamped to the baseboard. The outer surface of the bent sample was under tension, and the inner surface under compression. The device for determining how the stress varied with the position of the block on the baseboard 3 is shown in Fig. 1,b. The force was transmitted to the block 1 by a cord passing over a pulley. The action of the weight 2 caused the block 1 to turn in ball bearings past a polished steel plate. The shaft was also mounted in ball bearings to reduce

[1] Alloy MA1 contains about 1.7% Mn, while alloy MA_3 contains about 6% Al, 0.3% Mn, 0.5% Zn, the remainder being magnesium.

friction. The stress was calculated from the bending moment. During these tests the sample was completely immersed in a solution of 0.1 molar NaCl. The baseboard was fastened above the level of the electrolyte by clamps to a stand. The active surface of the sample totaled 12 sq cm. Special care was taken to insulate the nonoperating surfaces of the sample and the lead-in wire connected to the end of the sample from the electrolyte. This was effected by treating one of the surfaces of the sample with selenic acid and then coating it with a layer of hot drying lacquer and paraffin. The potential grew steady, some two or three hours after the sample had been immersed in the stirred electrolyte, becoming constant within 30 minutes or so. Then the device's block was moved to the next hole, one minute later the potential was read, after another minute the sample was again strained, and so forth. Despite the differences in the initial potentials, there was satisfactory agreement between the changes of potential caused by deformation in parallel tests. The electrode potentials were shifted slightly toward the negative, in tension as well as in compression. The most typical values of the electrode potentials in the unstrained state and at maximum bending strain are listed in the table.

TABLE

Effect of Bending Strain (Elastic + Residual) Upon the Electrode Potentials of Magnesium Alloys in a 0.1 Molar Solution of NaCl

Alloy	Kind of strain	Load, kg/sq mm	Electrode potential, on the hydrogen scale [1]
Commercial magnesium	Tension	5.7	-1388 -1405
	Compression	5.7	-1404 -1419
MA1	Tension	7.8	-1434 -1440
MA3	Tension	8.7	-1234 -1249
	Compression	8.7	-1234 -1249

These figures indicate that the electrode potentials of magnesium alloys are some 20 millivolts less noble after residual strain, which is about ten times as much as the value calculated above. Hence, the change in electrode potential must largely be due to the rupturing of the oxide film during deformation, rather than to any increase in the stored potential energy. In every test the potential did not vary by more than 1-2 millivolts in elastic deformation, however.

We were interested in learning whether this difference between the electrode potentials of strained and unstrained metals persisted with time.

---

[1] The figures on the upper lines are the metal potentials in the undeformed state; those on the lower lines are the potentials at maximum bending strain.

With this as our objective, samples shaped like an F [1] were stretched in an Amsler testing machine under loads that were 90% of σ_v [1]. The processing of the sample's surfaces has been described in our first report [1]. The potentials were measured in solutions at rest, used for corrosion tests. One liter of electrolyte was used. All parallel tests were run simultaneously in the same vessel. The active surface of the samples totaled 6 sq cm. The mean results of five measurements are reproduced in Figs. 2,3,4,5,6,7, and 8.

Fig.2. Effect of residual tensile strain upon the electrode potential of magnesium in a 0.1 molar solution of NaCl.
A – E_N millivolts; B – log t. 1 – After deformation; 2 – before deformation.

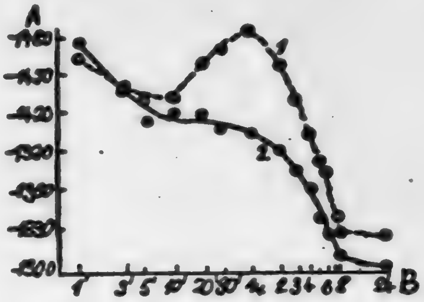

Fig.3. Electrode potentials of the alloy MA1 in 0.1 molar NaCl.
A – E_N millivolts; B – log t. 1 – After deformation; 2 – before deformation.

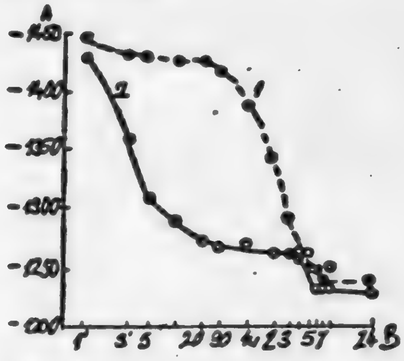

Fig.4. Electrode potentials of alloy MA3 in a 0.1 molar solution of NaCl.
A – E_N millivolts; B – log t. 1 – After deformation; 2 – before deformation.

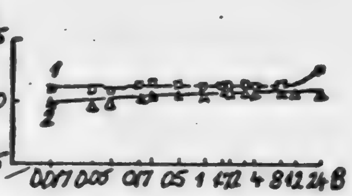

Fig.5. Electrode potentials of aluminum in a 0.3 molar solution of HCl.
A – E_N millivolts; B – log t. 1 – After deformation; 2 – before deformation.

---

1) σ_v is the ultimate strength.

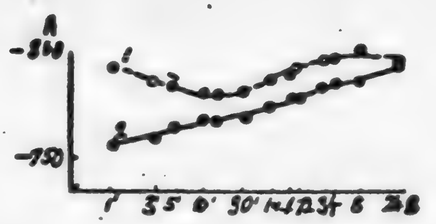

Fig.6. Electrode potentials of zinc in a 0.0125 molar solution of H_2SO_4. A – E_N millivolts; B – log t. 1 – After deformation; 2 – before deformation.

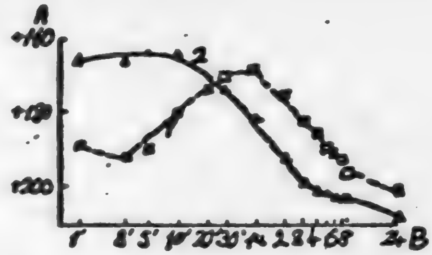

Fig.7. Electrode potentials of copper in a 0.5 molar solution of H_2SO_4. A – E_N millivolts; B – log t. 1 – After deformation; 2 – before deformation.

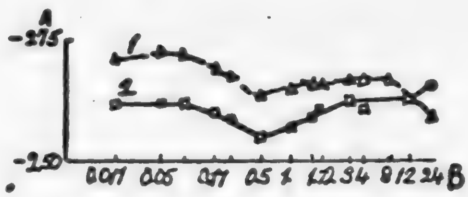

Fig.8. Electrode potentials of steel in a 1.5 molar solution of H_2SO_4. A – E_N millivolts; B – log t. 1 – After deformation; 2 – before deformation.

These results show that tensile strain corresponding to a load of 90% τ_v. causes the potential of magnesium to become 30-50 millivolts less noble, though the potential differences diminish with time. Four hours after deformation the strained magnesium has a more positive potential than the unstrained one.

The electrode potential of magnesium is ennobled with time, both before and after deformation, probably as the result of the formation of a sparingly soluble film of magnesium hydroxide. After 24 hours had elapsed the potential of the strained magnesium was 17 millivolts more positive than that of the unstrained metal. The shift in the relative positions of the electrode potentials is evidence that under these conditions the contact between the unstrained and strained magnesium cannot produce intensive corrosion of the latter. The alloy MA1 is more positive for a few minutes after deformation, but then the potential ratio is reversed. Little change occurs in the potential of unstrained samples in the interval of time between 10 minutes and 1 hour, whereas the potential of the strained samples is noticeably ennobled and then grows less noble. Here, too, the change of potential may be explained as due to the diminution in the protective properties of the film over the strained surface. As time passes, the difference between the potentials of the strained and unstrained state diminishes, totaling 25 millivolts after 24 hours.

What characterizes the alloy MA3 is the rapid ennobling of the electrode potentials of strained samples of this alloy. The potential values of the two curves are practically identical after 24 hours have elapsed.

Aluminum. The electrode potentials of strained and unstrained aluminum in a 0.3 molar solution of HCl are shown in the curves of Fig 5. The electrode

potential of aluminum is lowered approximately 5 millivolts by deformation. The extent of the potential shift and the electrode potentials of aluminum suffer practically no change with change. The difference between the potential values obtained in parallel tests did not exceed 1-2 millivolts. The slight extent to which the potential of aluminum becomes less noble may also be explained by the rupturing of the oxide film during deformation.

Zinc. The effect of deformation upon the electrode potentials of zinc in a 0.0125 molar solution of H_2SO_4 is shown in Fig.6. At the beginning of the test the decrease in potential due to deformation is about -35 millivolts. As time passes, the difference diminishes, falling to 5 millivolts when 24 hours have elapsed. The potential of unstrained zinc becomes progressively less noble, probably due to dissolution of the oxide film. The potential of the strained zinc is somewhat ennobled at the start, but then also grows less noble.

Copper. The electrode potentials of copper were measured in a 0.5 molar solution of H_2SO_4.

As we see in Fig.7, the potential of strained copper is more positive than that of the unstrained metal for the first 25 minutes after immersion. The potentials approach each other rapidly, however, and after one hour has elapsed the strained copper's potential is some 20 millivolts more negative. Thereafter the two potential curves move in parallel toward higher positive potentials.

The scattering of results in parallel measurements was 20 millivolts at the start of the test, dropping to 14 millivolts after one hour had elapsed. The anomalous position of the curves at the left-hand side of the graph is probably related to the properties of the oxide films produced during the deformation of the copper. The ennobling of the copper potential with time may be explained by the accumulation of copper ions in the solution.

Steel. Deformation lowers the potential of 10 - 20 steel by about 0.01 volt (Fig.8.). The curves of change of potential with time are parallel to each other. The difference between the potentials of strained and unstrained steel slowly diminishes with time. After 24 hours have elapsed, the strained steel's potential was more negative than that of the unstrained steel.

Thus, deformation makes the electrode potential more or less pronouncedly less noble in all the metals tested. The lowering of the potential did not exceed a few hundredths of a volt in most cases. The relative position of the potential before and after deformation was not steady sometimes varying at the start of the test or after some time had elapsed, due, most likely, to the formation of corrosion products.

Polarization characteristics and operation of a model microcell. Curves of the anodic and cathodic polarization of magnesium and of the alloy MA3 in a 0.1 molar solution of NaCl were plotted to reveal the effect of deformation upon the anodic and cathodic processes. Deformation was produced by stretching the samples under a load of 90% σ_v, as when we measured the electrode potentials.

The potential values were read off for every C.D. value, the C.D. being gradually raised to its maximum value.

The mean results of our measurements of the cathodic and anodic polarization of magnesium are plotted as curves in Fig.9.

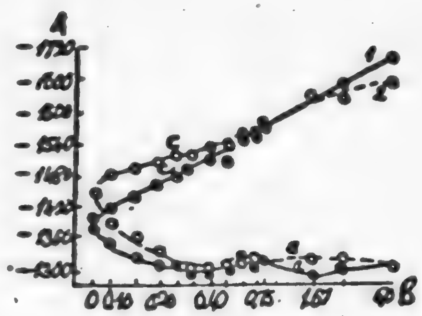

Fig.9. Cathodic and anodic polarization of magnesium in a 0.1 molar solution of NaCl.
A - E_H millivolts; B - log i, milliamps/sq cm. 1 - Before deformation; 2 - after deformation. c - Cathodic polarization; a - anodic polarization.

Notwithstanding the comparatively high scattering of the potential values in the several tests, the following facts stand out:

1) Anodic control is somewhat more effective than cathodic control in the range from zero to 0.4 milliamp/sq cm.

2) The cathodic and anodic processes occur at more highly negative potentials in strained electrode at C.D's below 1 milliamp/sq cm; as the C.D. is raised, the difference between the potentials of the strained and unstrained magnesium grows smaller.

3) At C.D.'s higher than about 0.9 milliamp/sq cm, the curve of cathodic polarization of the strained magnesium is higher than that of the unstrained magnesium.

4) The curves of anodic polarization are superposed on each other in the C.D. range from 0.4 to 0.8 milliamp/sq cm.

The polarization curves have the same shape for the alloy MA3.

The fact that the curves of cathodic polarization come closer together as the C.D. is raised may be related to the slighter mechanical rupturing of the oxide film over the strained surface as the result of the evolution of bubbles of hydrogen. That is why the strained magnesium is polarized somewhat less than the unstrained metal at C.D.'s above approximately 1 milliamp/sq cm.

The oxide film is ruptured more pronouncedly at the strained surface as the anodic C.D. is increased. This is probably responsible for the super-position of the anodic polarization curves at high C.D.'s.

The observed change in the polarization characteristics when electrodes are strained has been confirmed by tests made with a model microcell.

Two of the devices described above (Fig. 1,a) were clamped to a stand and immersed in a 0.1 molar solution of NaCl. The baseboards of the devices were above the level of the electrolyte. The solution was stirred and a current began to flow in the cell's circuit owing to a certain heterogeneity of the electrodes and of the layer of electrolyte surrounding them. After the current was stabilized, the sample was strained exactly as during our measurements of electrode potentials. The current was read for each position of the block. In all the tests one of the electrodes was bent.

At loads less than 3 kg/sq mm, the current of the Mg_1/0.1 molar NaCl/Mg_2 couple hardly changed at all when the cathode or the anode was strained (Fig.10). It is probable that the oxide film had not been ruptured as yet at this load. A change in the current was also opposed by the fact that the operation of the cell is largely governed by the processes taking place at the unstrained electrode.

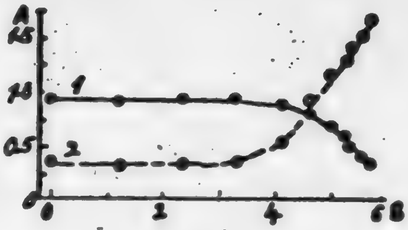

Fig.10. Variation of current with deformation in a Mg_1/0.1 molar NaCl/Mg_2 cell.
A – Current, milliamps; B – load, kg/sq mm. 1 – Compression of the cathode; 2 – compression of the anode.

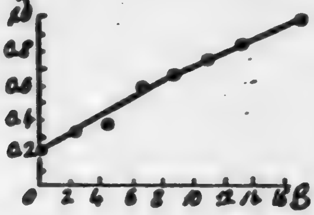

Fig.11. Variation of current with deformation in a Mg_1/0.1 molar NaCl/Mg_2 cell.
A – Current, milliamps; B – Tensile load on anode, Kg/sq mm.

As might have been expected, further increases in the deformation of the anode resulted in a rise in current. Deformation of the cathode caused the current of the cell to fall, owing to the cathode becoming less noble.

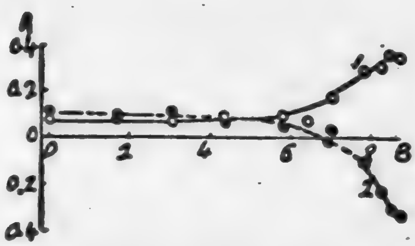

Fig.12. Variation of current deformation in an Alloy $Ma3_1$/0.1 molar NaCl/Alloy $MA3_2$ cell.
A – Current, milliamps; B – load, kg/sq mm. 1 – Compression of the cathode; 2 – compression of the anode.

These behavior patterns persisted at higher deformations. In these tests the end of the tensile-test sample was placed between the two halves of a cork stopper, which was placed in a glass tube filled with the electrolyte. The cork was coated with Mendeleev cement inside and outside the tube to prevent the exuding of the solution. The other electrode was immersed in the same tube. The sample was gradually stretched in an Amsler testing machine. As we see in Fig.11, increasing the deformation of the anode up to the breaking point has practically no effect upon the shape of the curve, entailing an increase in the cell current. The fact that the potential of the cathode grows less noble as it is strained may cause an interchange of polarity between the electrodes. In the Alloy $Ma3_1$/0.1 molar NaCl/Alloy $MA3_2$ cell (Fig.12), deformation caused the cathode potential to shift to the anode potential at the point where the curve crossed the axis of abscissas, and the flow of current stopped. Further increase in deformation reversed the current. The electrode that had been the cathode acquired a more highly negative potential than that of the undeformed electrode, and became the anode. Resuming the deformation of this electrode caused the current to rise.

Anologous behavior patterns were observed in the elastic deformation of the anode and cathode, though the changes in current covered a narrower range.

These tests explored the separate effects of deformation of the anode and of the cathode upon the current of the model microcell. In actual microcells the anodes and cathodes are deformed together. In the ensuing test of an Alloy $MA1_1$/0.005 molar H_2SO_4/Alloy $MA1_2$ cell, both electrodes were strained alternately, the deformation being raised gradually.

As we see in Fig.13, deformation produces similar changes in a medium that attacks the oxide film more vigorously than the sodium chloride solution does.

It is worthy of note that each increment of load in the range of 2-6 kg/sq mm changed the direction of current flow, though the magnitude of the current hardly varied from the initial value, provided the strains were equal. A further increase in deformation resulted in a gradual rise in the current. The latter phenomenon was also observed in electrodes of magnesium and the MA3 alloy, strained in a 0.1 molar solution of NaCl.

The rise of the cell current during equal deformation of the anode and the cathode agrees with the shape of the polarization curves reproduced in Fig.9. The steeper slope of the curve of anodic polarization indicates that the operation of the model microcell is predominantly controlled by the anodic phenomena.

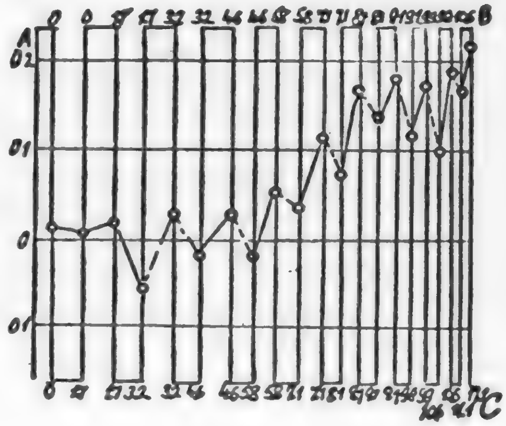

Fig.13. Variation of current with deformation in an Alloy $MA1_1$/0 005 molar H_2SO_4/Alloy $MA1_2$ cell with alternate deformation of both electrodes.
A – Current, milliamps; B and C – tensile load, kg/sq mm.

SUMMARY

1. With the work of deformation as a basis, an endeavor has been made to calculate the change in electrode potential due to deformation. It has been shown that the calculated value is several times smaller than the experimental one

2. Tensile and compression strain of magnesium and of the magnesium alloys MA1 and MA3 in a 0.1 molar NaCl solution makes their electrode potentials 6-17 millivolts less noble.

3. The residual tensile strain corresponding to a load of 90% σ_v makes the electrode potential of aluminum in 0.3 molar HCl, zinc in 0.0125 molar H_2SO_4, steel in 1.5 molar H_2SO_4, and copper in 0.5 molar H_2SO_4 less noble by about 35 millivolts.

4. The difference between the potentials of the strained and unstrained metals diminishes with time.

5. Strained magnesium suffers greater cathodic polarization and less anodic polarization in a 0.1 molar solution of NaCl than unstrained magnesium does. As the C.D is raised to about 0.6 milliamps/sq cm, the difference between the courses of the curves of strained and unstrained magnesium diminishes.

6. A model microcell made of magnesium alloys has been utilized to show that anode deformation increases and cathode deformation decreases the cell current. Deformation of both the anode and the cathode increases the corrosion current.

LITERATURE CITED

[1] E. M. Zaretsky, J. Applied Chem. 24, 477 (1951)[1].

[2] Wiedeman, Lehre von Elektrizitat, 9, 723 (1893).

[3] C. F. Burgess, Trans. Am. Electrochem. Soc. 13, 17 (1908).

[4] G. V. Akimov. Principles of corrosion theory and metal protection, 145. (1946).

[5] G. Tamman, C. Wilson, Z. anorg. allgem. Chem. 2, 156 (1928).

[6] U. R. Evans. Metallic corrosion, passivity, and protection (trans. from the English), 587 (1941).

[7] G. V. Akimov and Z. A. Vrutsevich, Trans. VIAM 39, 37 (1936).

[8] L. B. Nikitin, J. Gen. Chem. 9, 9, 975 (1939).

[9] W. Rosenhain, V. H. Scott Proc. Royal. Soc. A. 140, 9, 890 (1933).

Received August 6, 1949.

1) See Consultants Bureau Translation, p. 521.

BLANK
PAGE

THE HYDRODYNAMICS OF PACKED EXTRACTION COLUMNS

V. V. Kafarov and M. A. Planovskaya

The simplicity of design and operation of packed extraction columns has gained them wide acceptance in industry.

But absolutely no research has yet been done on the rational operation of packed extraction columns. This is due, first of all, to the absence of research on the hydrodynamics of liquid flow through a packing, which chiefly governs the rate of mass transfer of the dissolved substance from one liquid phase to the other.

In extraction in packed columns, the heavier liquid is fed in at the top of the column, and the lighter liquid at the bottom. As a rule, the extractor is completely filled with one liquid, which constitutes the dispersion medium, the other liquid – the disperse phase – being continuously distributed throughout it as it penetrates the dispersion medium.

The difference between the specific gravities of the two liquids is the motive force giving rise to the relative motion of the two phases in the column.

The phase velocities in the column can be varied only within rigidly defined limits. Raising or lowering the velocity of the dispersion medium or the disperse phase beyond a certain limit establishes a reverse phase motion in which one liquid is entrained by the other, thus disrupting the operation of the column.

Planovsky and Kafarov [1] made a survey of the experimental data [2,3] on the extraction of acetic acid from water with benzene and methyl isobutyl ketone and demonstrated that there is a definite velocity of the dispersion medium at which reversal of phase motion or the so-called choking of the extractor takes place.

The few experimental figures, however, did not allow of shedding light on the various factors affecting the nature of the phase flows in packed extraction columns.

It was the objective of the present research to explore the hydrodynamics of packed extraction columns in order to establish the limiting loads of the columns' dispersion medium and disperse phase.

EXPERIMENTAL

Our tests were run in a model installation, working up the test results by the scale-effect method, which enables the application of the research results

to other sizes of extraction columns.

The following systems were investigated: benzene - water, acetic acid - water, and chlorobenzene - phenol dissolved in hydrochloric acid.

In working up our test results, we also made use of the experimental data cited by Colburn [4] for the xylene - water, toluene - water, and isopropyl ether - water systems, and of the experimental data of Sherwood and others [2] for the benzene - acetic acid - water system.

The benzene was frozen, freed of its sulfuric acid, and double-distilled; its boiling point was 80°; density 0.878. The chlorobenzene was double-distilled; its boiling point was 131°; density 1.107. The acetic acid was chemically pure, the acetic acid concentration at the inlet being about 6%.

The packing tested consisted of glass tubes 6.62 X 6.70 X 0.6 mm in size (the mean of 50 determinations). These tube dimensions enabled us to consider the packing as approaching the form of Raschig rings. The packing surface S = 810 sq m/ cu m, the free packing volume F = 0.78 sq m/cu m, and the number of rings per cu m was 2,930,000.

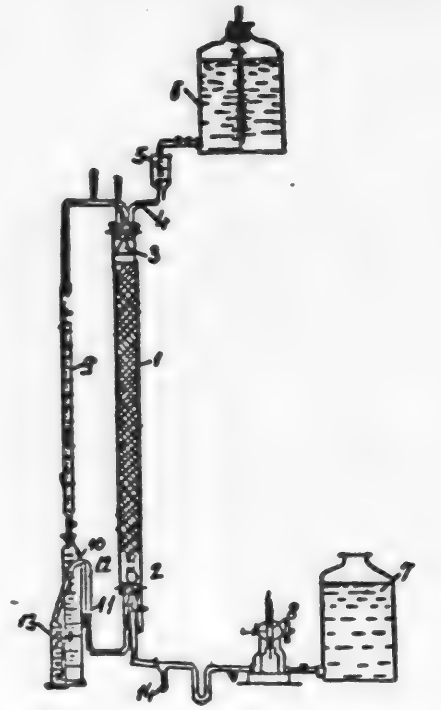

Fig.1. Diagram of the experimental installation.
1 - Glass column; 2 - nozzles; 3 - funnel; 4 - tube; 5 - indicator, pressure regulator; 6 - pressure tank; 7 - benzene tank; 8 - feeder pump; 9 - buret; 10 - receiver; 11 - stopcock; 12 - syphon. 13 - receiver; 14 - drain pipe.

The tests were run in the installation shown diagrammatically in Fig.1.

The installation consisted of a column (1), the pressure tanks (6) and (7), and the receivers (10) and (13). The glass column, with a diameter of 42 mm, had internal hollows in its lower section, in which there were placed coils to support the packing. The free cross section of the coils was made equal to that of the packing. The ratio of the column diameter to the packing diameter was greater than 6, thus satisfying the condition for geometrical similarity in packed columns [5]. The height of the packing layer within the packing layer within the column was 1130 mm, the overall height of the column being 1300 mm. The zone beneath the packing contained 4 distributing nozzles, 1.2 mm in diameter and 60 mm long, joined into a single collector. When a phase with a higher specific gravity was to be dispersed, the nozzles were placed in the upper part of the column, in the zone above the packing.

When a lighter liquid entered at the bottom of the column, a glass funnel (3) fitting the inner diameter of the column was placed in the zone above the packing at the top of the column, thus making it possible to collect and draw

off the light fluid and separate it from the heavy liquid entering the column. When a heavy liquid was to be dispersed, the funnel was placed at the bottom of the column.

Fig.1 shows the installation as set up for the introduction of a light liquid (benzene) into the bottom of the column via the nozzles (2). The heavy liquid (water) was fed in at the top of the column via the indicator and pressure regulator (5) and the tube (4). Before starting up, the column was two-thirds filled with water or benzene, depending upon which liquid was to serve as the dispersion medium. Then water was let into the column from the pressure tank at constant level (6), while benzene was fed in from the tank(7) via the feeder pump (8). The benzene rose counter to the flowing water and was drawn off to the receiver (10) through the funnel (3) and the measuring buret (9). The water was drawn off from the bottom of the column to the receiver (13) via the stopcock (11) and the U-shaped tube (syphon) (12). The position of the U-shaped tube (12) determined the level of the phase boundary, for the tube is connected to flexible tubing, making it possible to vary this level and thus change the phase. To ensure the mutual saturation of one phase by the other, water was poured on the bottom of the tank (7), while a thin layer of benzene was placed above the water in the tank (6). All the tests were run at 18-24° C.

The velocities of phase flow were measured during the tests and the phases were varied.

The rate of flow was measured at the inlet by means of the feeder pump (8), via the drain pipe (14), and by the indicator (5). The readings of the measuring buret (9) and of the collecting cylinder (13) served as a further check.

When visual observation of flow was employed, the column was filled with 8 X 8 X 2 mm porcelain rings, with the equivalent diameter $\underline{d} = \frac{4F}{S} = 0.00328$ meter; the liquids were colored with a dye that was soluble in one phase and insoluble in the other.

Visual observations. Visual observations of a colored liquid were used to study the nature of liquid flow through packed extraction columns.

At low flow velocities, the dispersed liquid travels either as individual drops or spreads out as a jet, depending on its properties. We have observed, for example, that when benzene was dispersed in water, it moved in drop form, whereas when water was dispersed in benzene, the water spread in the form of a jet. Fig. 2 is a photograph of the flow during the dispersion of colored water in benzene. (See Plate, page 773).

The volumetric rate of flow of the benzene, which was the continuous phase, was $\underline{v}_c$ = 6 cu m/ sq m/hour, while the flow rate of the dispersed water was $\underline{v}_d$ = 2 cu m/sq m/hour. The blackened rings in Fig. 2 show the striated nature of the motion of the disperse phase, it being evident that not all the surface of the packing acts as a phase contact surface, only a minute portion of the surface being so used.

Contact between the phases takes place at the individual elements of the packing, with no perceptible turbulent flow at the surface of the liquid film. We have defined this kind of operation as film operation.

When the rate of flow of the continuous phase was kept constant at $\underline{v}$ = 6 cu m/ sq m/hour, and the flow rate of the disperse phase was increased to

V_d = 2.50 cu m/ sq m/hour (Fig.3), a marked change was observed in the pattern of phase motion. The free volume of the packing was filled with drops and globules, the jets broke off, the continuous phase was penetrated by the disperse phase, all the rings were covered with the liquid being dispersed, and the surface of contact rose sharply. Considerable turbulence of flow was observed, and the column operation became turbulent.

A further increase in the rate of flow led to even higher turbulence of flow, an increase in the degree of dispersion, and the formation of an infinite number of minute eddies. The entire packing is penetrated by tiny eddies, the liquid being emulsified as it were (Fig. 4). It might be expected that this type of operation of a packed extractor would be the most efficient, since the surface and time of contact are at a maximum. We have defined this type of operation as eddy-emulsified operation and called the flow rates characteristic of this type of operation the "optimum" velocities. In this type of operation the zone above the packing is likewise filled with emulsified phases.

The volumetric rate of flow of the continuous phase in this type of operation, as shown in Fig. 4 (see Plate, page 773) was 6 cu m/sq m/hour, that of the disperse phase being 3.0 cu m/sq m/hour.

It is worthy of note that in this type of operation the properties of the dispersed liquid have no effect upon the nature of the flow: dispersing water in benzene exhibits the same visual pattern as the dispersing of benzene in water.

Raising the phase velocities above the optimum values results in flooding[1] the column and the entrainment of one phase by the other. Flooding usually sets in by the zones preceding the packing being filled with liquid, consisting either of the disperse or the continuous phase, depending on the phase whose velocity change caused the reversal of motion. Figures 5 and 6 (see Plate, page 773) show the instant at which the column began to flood, when the flow rate of the disperse phase was raised to 3.5 cu m/sq m/hour, and the flow rate of the continuous phase was 6 cu m/sq m/hour.

The formation of liquid seals directly above and below the packing upsets the normal phase flow. The fusing together of the individual drops rapidly increases the height of the liquid columns, diminishes the turbulence of flow, and causes the phases to flow in the same direction, one carrying the other along. Flooded operation of a column is close to operation at optimum flow rates, so that the search for the quantitative ratio governing the onset of flooded column operation becomes particularly important. We have found that the flow rates ordinarily employed in packed columns lie much below the optimum rates, so that packed extraction columns operate very inefficiently at the present time.

<u>Effect of various factors upon the load limits of packed extraction columns.</u> The quantitative data secured in our investigations of the load limits of packed extraction columns are given in the table.

---

[1]) The previously introduced [1] definition of this type of operation as choking is, in our opinion, a less accurate description of what happens here.

Effect of Various Factors Upon the Load Limits of Packed Extraction Columns

Volumetric rate of phase flow, cu m/sq m/hour: Continuous phase, v_c	Volumetric rate of phase flow, cu m/sq m/hour: Disperse phase v_d	Velocity of the continuous phase when flooded, W_c meters/sec	Difference between the phase spec. gravities, $(\Delta\gamma)$ (kg/m^3)	Spec. grav. of the continuous phase, γ_c, kg/cu m	Difference between the viscosities of the liquid phases, $\Delta\mu$, centipoises	Surface tension, (σ), dynes/cm
Packing: glass rings, 6.62 X 6.70 X 0.6 mm; S = 810 sq m/cu m; F = 0.78 cu m/cu m						
Benzene	Water					
8.68	2.17	0.00241				
5.20	3.26	0.00145	123[8]	877	0.322	35[7]
3.26	4.35	0.00091				
Chlorobenzene	Phenol dissolved in hydrochloric acid					
1.65	1.12	0.00048	20	1060	0.590	73.56
Benzene	Aqueous acetic acid					
8.00	3.98	0.00223	123[2]	877	0.322	35[2]
8.00	4.96	0.00223				
Aqueous acetic acid	Benzene					
6.08	3.04	0.00169	123	1000	0.322	35[2]
6.08	5.05	0.00169				
Packing: Raschig rings, 12.7 X 12.7 mm; S = 374 sq m/cu m; F = 0.74 [2,4]						
Xylene	Water					
4.52	23.8	0.00126				
5.90	20.8	0.00164				
11.6	16.55	0.00323	151[4]	849	0.372[7]	37.7[7]
26.4	12.0	0.00732				
29.2	3.6	0.00810				
Water	Xylene					
3.74	34.2	0.00104				
8.32	23.0	0.00231	151	1000	0.372	37.7
16.0	13.3	0.00445				
24.1	8.31	0.00668				
30.6	1.61	0.00850				
Water	Toluene					
4.57	14.2	0.00127	138[4]	1000	0.417[7]	36.1[7]
12.90	9.25	0.00360				

Effect of Various Factors Upon the Load Limits of Packed Extraction Columns.Contd.

Volumetric rate of phase flow, cu m/sq m/hour		Velocity of the continuous phase when flooded, W_c meters/sec	Difference between the phase spec. gravities, $(\Delta\gamma)$ in kg/cu m	Spec. grav. of the continuous phase, γ_c, kg/cu m	Difference between the viscosities of the liquid phases, $\Delta\mu$, centipoises	Surface tension, (σ), dynes/cm
Continuous phase, V_c	Disperse phase, V_d					
Aqueous acetic acid	Benzene					
12.20	4.03	0.00340	123	1000	0.353[7]	35[2]
9.15	6.73	0.00254				
6.11	11.80	0.00170				
Water	Isopropyl ether					
5.32	48.5	0.00148				
12.6	42.0	0.00350				
26.8	26.8	0.00745	275[4]	1000	0.687[7]	4.44
45.1	15.1	0.01255				
50.0	5.0	0.01395				

Effect of nozzle size. It has been found [3] that the nozzle size affects the drop size only in the zones preceding the packing, the size of the drops changing continuously as they pass through the packing, assuming some mean size that is independent of the nozzle dimensions. As flooded operation is approached, the whole of the packing is penetrated by fine jets, which are emulsified independent of nozzle size.

The cross section of the support underneath the packing may substantially affect the drop size and the onset of flooding. The column begins to flood at lower phase velocities whenever this cross section is smaller than the free cross section area of the packing. We made the cross section of the support beneath the packing (a glass spiral) the same as the free cross sectional area of the packing to eliminate this factor as an influence in our investigations of the prevailing quantitative relationships.

Effect of the packing. The packing promotes the disintegration of the drops of the disperse phase or the development of eddies as flooded operation is approached. The limiting flow rates, at which flooding occurs, are raised when the free volume of the packing is increased. When we compare the results of our investigation of the limits at which the packing is flooded in the water – benzene – acetic acid system, for example, we find that the same rate of flow of the continuous phase, corresponding to flooding, $W_c = 0.0017$ meter/sec, is attained at a volumetric flow rate ratio of $\frac{V_c}{V_d} = 1.22$ when the free volume $F = 0.78$, and at $\frac{V_c}{V_d} = 0.52$ when the free volume $F = 0.74$.

Therefore, the load limit of columns rises with an increase in the packing free volume.

Effect of the physical properties of the liquids. The relative motion of the

phases in extraction columns is produced by the difference in the specific gravities of the liquids. We must expect, therefore, that increasing this difference in specific gravity will increase a column's load limit. The smaller this difference, the lower the flow rate at which one phase will be entrained by the other. Plotting the ratio of the volumetric rates of flow of the continuous and the disperse phase, $\frac{v_c}{v_d}$ along the axis of abscissas, and the values of the volumetric rate of flow of the continuous phase, v_c, in cu m/sq m/hour, for the full column cross section and corresponding to the flooding limit along the axis of ordinates, we get the set of curves reproduced in Fig. 7 for systems with varying specific-gravity differences.

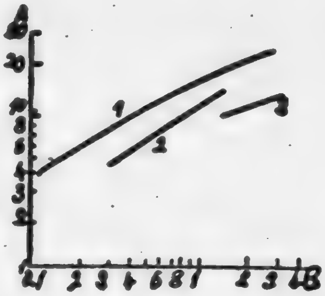

Fig. 7. Effect of differences between the specific gravities of liquids upon the flooding rate of flow.

A - volumetric rate of flow of the continuous phase, v_c, cu m/sq m/hour; B - ratio of the continuous-phase of the volumetric rate of flow to that of the disperse phase, $\frac{v_c}{v_d}$. 1 - Xylene - water, $\Delta\gamma$ = 151; 2 - toluene - water, $\Delta\gamma$ = 138; 3 - benzene - water, $\Delta\gamma$ = 123.

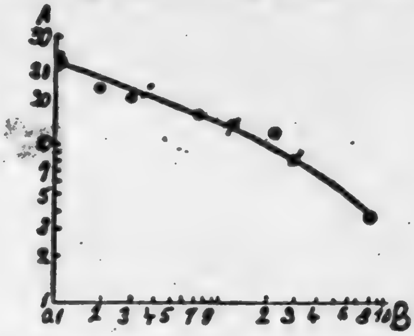

Fig. 8. Effect of the volumetric rates of flow of the phases and of phase interchange upon the column of flooding limits.

A - volumetric rate of flow of the disperse phase, v_d, cu m/sq m/hour; B - ratio of the volumetric rate of flow of the continuous phase to that of the disperse phase, $\frac{v_c}{v_d}$. • - disperse phase water - continuous phase: xylene; ɛ - disperse phase: xylene - continuous phase: water.

Curve 1 was plotted for the system xylene - water, with a specific-gravity difference of $\Delta\gamma$ = 151 kg/cu m; Curve 2 for the system toluene - water, with $\Delta\gamma$ = 138 kg/cu m; and Curve 3 for the system water - benzene, with $\Delta\gamma$ = 123 kg/cu m. The surface tension and the specific-gravity difference were fairly close in the systems compared.

It follows from Fig. 7 that the curves for systems with a greater difference in specific gravities lie higher than do those for systems in which the specific-gravity difference is smaller. Hence, an increase in the specific-gravity difference between the liquids causes flooding to occur at a higher level, thus raising the load limit of the columns in question.

Besides the effect of the specific-gravity difference, the motion of the liquid phases is also complicated by the parallel effect of the liquid viscosities and the surface tension at the boundary between the liquid phases. This made it difficult to explore the separate effect of the latter factors, with all other influences excluded. It may be assumed that an increase in the viscosity of one

liquid with respect to the other will affect the flooding rate of flow.

The surface tension largely governs the dimensions of the drops of the disperse phase, which change continuously as they pass through the packing and, of course, affects the flooding rate of flow at which the drop dimensions are increased.

By working up our experimental data on generalized coordinates we were able to plot the influence of liquid viscosity and surface tension in definitive form.

Effect of phase velocities and phase alternation. Flooding of the column may be caused by an increase of the column load beyond some optimum for the continuous or the disperse phase. The phenomenon of flooding is the same in either case – one phase hinders the passage of the other and then entrains it with it.

Figure 8 illustrates the effect of the phase rates of flow upon the flooding limit, together with the effect of interchange of the phases. This graph is based upon our experimental data for the xylene – water system, with the water dispersed in xylene, and with the xylene dispersed in water. As the graph shows, the attainment of the flooding stage as the load on the continuous phase is raised causes a corresponding decrease in the disperse-phase load on the column.

Interchanging the phases has no perceptible effect upon the changes in the column's limiting load due to flooding, which agrees with our visual observations described earlier.

Evaluation of Results

In an earlier paper [1], analysis of the dimensionality of the variables that govern the flooding of extractors yielded a functional relationship that made it possible to determine the rates of phase flow at which flooding occurs.

The accumulation of further experimental material now enables us, however, to refine the equation advanced previously and to make it more generally applicable to various liquid systems.

Consideration of the individual factors affecting the load limits of packed extraction columns enables us to chart the path for generalizing our research results.

The ratio of the volumetric rate of flow of the continuous phase (v_c) to that of the disperse phase (v_d) will depend upon the magnitude of the interacting forces in the two streams. These forces will be the gravity pull of one liquid and the corresponding upward thrust, determined by the difference between the specific gravities of the phases, the frictional forces, and the surface tension.

The effect of the gravity pull is given by the Froude criterion (Fr), the upward thrust by the Archimedes simplex (Ar), the frictional force by the Reynolds criterion (Re), and the surface tension by the Weber criterion (We).

Hence, in the most general state, we get the following function:

$$\frac{v_c}{v_d} = f\,(Fr_d, Fr_c, Ar, Re_d, Re_c, We_d, We_c \ldots).$$

But if we introduce the differences between the physical variables for the

liquids constituting the phases instead of the absolute values of these physical variables, and express the linear phase velocity by the linear velocity of the continuous phase, as is usually done in determining the cross section of an extraction column, the function given above may be simplified considerably. Moreover, combining the individual criteria results in further simplification of the appearance of this function.

The Froude criterion is given by the expression: $Fr = \frac{W_c^2}{gd}$, where W_c is the linear of the continuous phase in meters/sec, $\underline{d}$ is the equivalent diameter of the packing in meters, equal to $\frac{4F}{S}$, in which $\underline{F}$ is the free volume of the packing in cu m/cu m, and $\underline{S}$ is the packing surface in sq m/cu m.

The Archimedes simplex has this form: $\frac{\gamma_c}{\Delta\gamma}$, where γ_c is the specific gravity of the continuous phase in kg per cu m, and $\Delta\gamma$ is the difference between the specific gravities of the continuous and disperse phases, in kg per cu m. The Reynolds criterion $\underline{Re} = \frac{W_c \cdot d\rho_c}{\Delta\mu}$, combined with the Weber criterion $\underline{We} = \frac{W_c^2 d\rho_c}{\sigma}$, yields the criterion $\frac{\Delta\mu W_c}{\sigma}$, which expresses the effect of the liquid viscosity $\Delta\mu$ and the system's surface tension σ at a velocity of the continuous phase given by W_c.

Inasmuch as the linear velocity of the continuous phase W_c enters into both the Froude criterion and the criterion $\frac{\Delta\mu W_c}{\sigma}$, dividing the Froude criterion by the latter yields the new criterion $\frac{W_c\sigma}{gd \cdot \Delta\mu}$.

Thus, the final form of the hydrodynamical equation for packed extraction columns is:

$$\frac{V_c}{V_d} = f\left(\frac{W_c\sigma}{g \cdot d \cdot \Delta\mu} \cdot \frac{\gamma_c}{\Delta\gamma}\right).$$

We have established the shape of this function experimentally.

Plotting the ratio of the volumetric rate of flow of the continuous phase to that of the disperse phase, $\frac{V_c}{V_d}$, at the column's load limit along the axis of abscissas in a logarithmic anamorphosis, and the expression $\underline{N} = \frac{W_c}{g \cdot d}\left(\frac{\gamma_c}{\Delta\gamma}\right)^{0.5}\left(\frac{\sigma}{\Delta\mu}\right)^{0.2}$ along the axis of ordinates for various systems of liquids and packings, we get Fig. 9, in which we see that the experimental points are grouped about a single curve.

In the complex expression given above, $\underline{W_c}$ is the linear velocity of the continuous phase at the flooding stage, referred to the complete cross section of the column; its dimensions are meters per second.

This generalized expression may be regarded as fairly reliable, when it is realized that the ratio of the volumetric rates of flow was measured over a range extending from 0.1 to 20, i.e., a ratio of 200 to 1, the surface tension being measured from 4.44 to 73.5, or 16.6 to 1, the difference in viscosity from 0.322 to 0.687, or 2.15 to 1, and the difference in specific gravities from 20 to 275, or 14 to 1; and that, in addition, the phases were interchanged. It should also be noted that in this generalization we employed not only experimental data on

systems consisting of two pure liquids, but also data on systems consisting of two liquids with a substance distributed between them. On the basis of the foregoing, the load limits of packed extraction columns — the velocities of the continuous phase at the flooding stage — are calculated as follows. Given the extractor output and the concentration, the ratio of the rates of phase flow are calculated from the material balance:

$$\frac{v_c}{v_d} = \frac{C_{1d} - C_{fd}}{C_{1c}\ C_{fc}},$$

where v_c and v_d are the volumetric rates of flow of the continuous and disperse phases, respectively, in cu m/sq m/hour; C_{1c}, C_{fc}, C_{1d}, and C_{fd} are the initial and final concentrations of the dissolved substance in the continuous and disperse phases in kg/cu m.

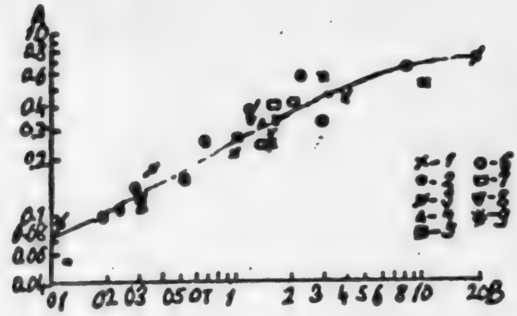

Fig. 9. Generalized curve for calculating the load limits of extraction columns.

A — the complex expression $N = \frac{W_c}{g \cdot d_3}\left(\frac{\gamma_c}{\Delta\gamma}\right)^{0.5}\left(\frac{\sigma}{\xi\mu}\right)^{0.2}$.

B — ratio of the volumetric rate of flow of the continuous phase to that of the disperse phase, $\frac{v_c}{v_d}$.

Notation for the disperse and continuous phase, respectively: 1 — water — benzene; 2 — xylene — water; 3 — water — xylene; 4 — toluene — water; 5 — isopropyl ether — water; 6 — aqueous acetic acid — benzene; 7 — benzene — aqueous acetic acid; 8 — aqueous acetic acid — benzene; 9 — chlorobenzene — phenol dissolved in hydrochloric acid.[1]

Once the ratio $\frac{v_c}{v_d}$ has been found, the value of the complex expression N is found from Figure 9. The value of N is used to calculate the limiting velocity of the continuous phase:

$$W_c = \frac{N \cdot g \cdot d \cdot \Delta\gamma^{0.5} \cdot (\xi\mu)^{0.2}}{\gamma_c^{0.5} \cdot \sigma^{0.2}} \text{ meters/sec.}$$

The diameter of the extractor column, dimensioned for the limiting velocity, is found from the equation: $d_k = \sqrt{\frac{4G_c}{3600 \cdot 3.14 \cdot W_c \cdot \gamma_c}}$ meters,

where G_c is the gravimetric rate of flow of the continuous phase, in kg per hour.

When fixing the diameter of the extractor, the velocity of the continuous phase W_c — should be taken some 20-25% below the velocity as given by Fig.9 in order to avoid flooding of the packing.

---

1) 1,2,3,4,5,6, figures in the literature [2,4]; 7,8,9, author's figures.

LITERATURE CITED

[1] A. N. Planovsky and V. V. Kafarov, J. Chem. Ind. 1945, 6.

[2] T. K. Sherwood, J. E. Evans, I. V. A. Longcor, Ind. Eng. Chem. 31, 1144 (1939).

[3] I. H. Perry, Chem. Eng. Handbook, N. I. 1268 (1941).

[4] A. P. Colburn, Tr. Am. Inst. Chem. Eng. 38, 336 (1942).

[5] N. M. Zhavoronkov, J. Chem. Ind. 1948, 9.

[6] A. N. Planovsky and V. V. Kafarov, J. Chem. Ind. 1946, 4.

[7] Technical Encyclopedia Handbook, Vols. V, X (1949).

Received December 15, 1949.

BLANK
PAGE

REMOVING SERICIN FROM RAW SILK BY MEANS OF SOLUTIONS CONTAINING THE PRODUCTS OF SERICIN HYDROLYSIS

V. N. Krestinskaya and M. B. Aimukhamedova

Laboratory of Colloid Chemistry, Chemical Institute of the Kirghiz Branch of the USSR Academy of Sciences

The research set forth below was undertaken in response to the demands of the textile industry, which required a cheaper method of removing sericin from silk fabric than the soap-and-soda used at the present time. Most of the attempts to find a substitute for soap involved a search for a salt whose solution, like the soap solution, would have a weakly alkaline reaction and buffer properties (soda, sodium silicate, sodium phosphate, etc.). Other methods, using a solution of caustic soda [1,2], a soda – sulfite solution [3], and a sulfide solution [4,5], have been proposed instead of the method employing a soap-and-soda solution. Efforts to employ proteolytic ferments did not yield any worthwhile results [6,7].

Research undertaken by one of the authors of the present paper [8] on the fractional composition of a sericin solution revealed the ability of the A and B fractions to turn into B and A fractions interchangeably, depending upon the experimental conditions. It was shown that it was possible to convert the more soluble fraction B into the less soluble fraction A. Since this conversion took place during the dialysis of the sericin solution, it was inferred that the different fractions were interrelated by the amount of stabilizer present at the surface of the micelles, rather than by the degree of their dispersion. In dialysis, part of the stabilizer, which possesses true solubility, removes the fraction B from the micelles, thus increasing the percentage of the fraction A.

The stabilizer is transferred to the dialyzate waters, and as it must exhibit a peptizing effect upon sericin, its presence may be disclosed by comparing the action of the dialyzate waters upon raw silk with that of distilled water. As a matter of fact, under otherwise identical conditions the dialyzate waters removed 3% more seracin than the water did.

The objective of the present section of our research has been to learn whether there was any possibility of practically utilizating the foregoing observations.

EXPERIMENTAL

The solutions containing the products of sericin hydrolysis were prepared in two ways. 1) a weighed sample of "vests" or damaged cocoons was placed in distilled

water (8 or 16 grams per 1000 ml of water) and allowed to stand for 5 days at room temperature, after which the solution was filtered through a paper filter; 2) a colloid solution of sericin was prepared by boiling a weighed sample of damaged cocoons in distilled water (8 or 16 grams per 1000 ml of water) for 3 to 5 hours filtering the solution, and then reboiling the solution for 2-5 hours.

The solutions prepared by both methods were cloudy. Dialysis tests showed that these solutions contained a colloid. Analysis disclosed the presence of sericin in the solutions (precipitation with alcohol, positive biuret reaction) plus various products of its hydrolysis (determination of the total nitrogen, the nonprecipitating nitrogen and the amino-acid nitrogen). The pH of all solutions for which it was determined was close to 7 (6, 5, 7, and 7.5).

The solutions obtained by steeping the silk in water at room temperature had a much lower concentration of nitorgenous substances (sericin, in particular) than the solutions prepared by boiling: the former contained 0.5 to 1 mg total nitrogen per 50 ml of solution, while the latter had 10 to 20 mg of nitrogen; 50 ml of the former solutions contained no more than 0.45 mg of sericin, while the latter often contained more than 14 mg of sericin.

The action of the solutions was tested with raw crepe de chine. A sample of the fabric was weighed on the analytical balance in the air-dried state. The moisture content of the raw silk was determined periodically in order to be able to find the weight of the absolutely dry fabric. The weighed sample of silk was refluxed with the test solution for 2-3 hours. Then the silk sample was washed in hot distilled water, dried at 105-110°, and weighed in a small box. No constant bath factor (ratio of the weight of the fabric to the weight of the solution) was maintained in the first tests.

TABLE 1

Results of Tests of the Removal of Sericin From Raw Silk

Date of preparation of solution	Absolute dry weight of raw silk, g	Weight of fabric after treatment, g	Ml of solution	Hours of boiling	Sericin removal			
					By solution		By water	
					g	per cent	g	per cent
31 V 1945	0.5082	0.3694	200	3	0.1388	27.31		
Water	0.4741	0.4084	200	3			0.0657	15.27
31 V 1945	0.4200	0.3212	100	2	0.0988	23.52		
Water	0.3204	0.2852	100	2			0.0352	10.98
28 V 1945	0.4057	0.3146	200	3	0.0911	22.45		
Water	0.4087	0.3666	200	3			0.0421	10.3
7 IX 1945	0.3172	0.2370	100	3	0.0802	25.28		

The results of tests of solutions prepared from "vests" at room temperature are given in Table 1. The moisture content of the raw silk was 5.79%. The data of preparation of the solution refers to the date when its preparation was completed and usually indicates the time the test was run.

As we see from Table 1, the solutions prepared by steeping the "vests" removed sericin efficiently. The percentage of sericin in the fabric, as determined by boiling the raw silk for many hours, was 26%. The fabric from which 26% of sericin had been removed was dyed lemon-yellow by picrocarmine.

Parallel tests in which the fabric was boiled in water yielded a much lower percentage of sericin removal. The difference between the action of the solution and that of water was 11 to 12%.

The solution cited on the last line of Table 1 was used in an experiment aimed at determining whether the boiled-out bath could be re-used. Four weighed samples of silk were placed successively in the same solution. The bath was not strengthened in any way, as is done in industry. The results are listed in Table 2.

TABLE 2

Results of Experiments on the Repeated Utilization of "Vest" Solutions

No. of Fabric sample	Absolute dry weight of raw silk, g	Weight of fabric after treatment, g	Ml of solution	Hours of boiling	Sericin removal	
					g	per cent
1	0.2747	0.2054	200	3	0.0693	25.59
2	0.2714	0.2300	200	3	0.0447	16.57
3	0.3454	0.2978	200	3	0.0476	13.78
4	0.2579	0.2252	200	3	0.0327	12.67

The figures in Table 2 indicate that the solution cannot be re-used; after the processing of the first sample, from which practically all the sericin was removed, the activity of the solution falls off, continuing to fall, as we see in Runs 3 and 4.

The results of tests using a solution prepared by steeping damaged cocoons for 5 days at room temperature are given in Table 3.

TABLE 3

Results of Tests Using a Solution of Damaged Cocoons

Absolute dry weight of the raw fabric, g	Weight of fabric after treatment, g	Bath factor	Hours of boiling	Sericin removed	
				g	Per cent
0.1877	0.1476	1:50	3	0.0401	21.40
0.1926	0.1466	1:100	3	0.0459	23.80
0.1964	0.1482	1:150	3	0.0482	24.5
0.1876	0.1450	1:200	3	0.0426	23.0

The solution prepared from damaged cocoons yields about the same percentage of sericin removal as the solutions made from "vests" .

The tests listed in Table 3 were made at four different bath factors and showed that a bath factor of 1:100 could be employed henceforth, since any further increase in the amount of solution used causes no perceptible increase in the percentage of sericin removed. We usually retained this bath factor in our subsequent research.

The experiments using sericin solutions prepared by boiling damaged cocoons in water are listed in Table 4.

The figures in Table 4 indicate that freshly prepared colloidal solutions of sericin either possess slight activity (Solutions 5 and 8) or possess an activity equal to that of distilled water (Solutions 2 and 4). Additional boiling increased

TABLE 4

Results of Tests Using Solutions Prepared by Boiling Damaged Cocoons in Water

Solution No.	g of cocoons per liter	Hours of boiling	Per cent sericin removed		Additional boiling, Hours
			Fresh Solution	Boiled Solution	
2	16	3	12.3	26.6	4
4	16	3	12.0	19.1	3
5	16	3	16.5	21.6	2
8	8	5	16	20.2	2

the activity of the solution. Boiling the solution accelerates its hydrolysis, increases the percentage of hydrolysis products, and ought to increase the peptizing action of the solution. But as we see in Table 4, the increase in activity does not always parallel the additional boiling.

We see from the tests cited in Tables 1, 2, 3, and 4 that solutions prepared in various ways, but all containing products of sericin hydrolysis, remove practically all the sericin from raw silk. It was a great temptation to utilize these solutions in the baths of the finishing shop of a silk plant. The silk would then be degummed without the consumption of any expensive soap or of any other chemical reagent. Preparation of the solution would require nothing but the raw materials of production ("vests" and cocoons) and water. We proposed to use nothing but production waste: scrapped cocoons and "vests", in preparing our solution. After the solution had been prepared and filtered, the used waste silk could be shipped off for silk waste utilization so that even this raw material was not lost.

Preparing the solutions by steeping silk wastes at room temperature proved to be more economical than preparing the solutions by boiling. We had to learn how to fortify the bath and find out whether enough "vests" and scrap cocoons were obtainable in production. It was suggested that composition of the basin water of the silk-reeling room ought to approximate that of the solutions we had prepared. Since this research was performed in Kirghiz, we got in touch with a silk plant in 1947.

The inadequate equipment of the plant's laboratory gave rise to considerable difficulty in carrying out our research, so that only three experiments were run, their results being listed in Table 5.

TABLE 5

Results of Tests Employing Various Solutions

Solution	Absolute dry weight of raw fabric, g	Weight of Fabric after treatment, g	Bath Factor	Hours of Boiling	Sericin removed	
					g	Per cent
Of cocoons	0.8935	0.6876	1.100	3	0.2059	23.05
Of vests	0.9112	0.7068	1:100	3	0.2049	22.19
Waste waters of the reeling room	0.8464	0.6266	1:100	3	0.2198	25.97

As we see from Table 5, the best results – complete removal of the sericin – were obtained when the raw silk fabric was treated with the waste waters of the reeling room. It is found, therefore, that the solution we have investigated in the laboratory is continuously prepared in the normal process of production in a silk plant. We were unable to make tests on a semi-plant scale, since the finishing shop was not yet in operation at the silk plant at the time.[1] In making our laboratory tests with solutions prepared by steeping cocoons in water at room temperature we ran into the following difficulty: though all the experimental conditions were kept constant, we secured satisfactory solutions in some instances, and inactive ones in others (Table 6).

TABLE 6

Results of Tests With Solutions Secured by Steeping Cocoons

Date of preparing the solution	Absolute dry weight of the raw fabric, g	Weight of fabric after treatment, g	Bath Factor	Ml of Solution	Sericin removed from the fabric		Per cent moisture in the raw fabric
					g	Per cent	
10 XI 1945	0.3101	0.2658	1:100	–	0.0443	14.2	7.95
9 I 1946	0.2957	0.2438	1:100	–	0.0519	17.5	
4 II 1946	0.2291	0.1932	1:100	–	0.0359	15.7	8.4
9 II 1946	0.2548	0.2182	1:100	–	0.0366	14.3	
10 VI 1946	0.2703	0.2049	–	100	0.0654	24.19	
22 V 1946	0.2209	0.1608	–		0.0511	23.13	6.7
10 VII 1946	0.2142	0.1640	–		0.0502	20.4	
1 X 1946	0.1755	0.1304	–		0.0451	25.79	
X 1946	0.1759	0.1308	–	50	0.0451	26.68	
19 XI 1946	0.2012	0.1594	–		0.0418	20.77	8.54
28 XI 1946	0.1935	0.1490	–		0.0445	23.0	
8 I 1946	0.2405	0.1942	–		0.0463	19.3	

The wide fluctuations in the per cent of sericin removed observed in the tests recorded in Table 6 may be due to a much greater effect of an increase in the bath factor than would follow from the data in Table 3. In the tests of Table 6, the highest percentage of sericin was removed at bath factors that were higher than 1:200. It may be that this rising effect of the bath factor is present only in solutions of low activity, containing an insufficient percentage of the peptizer. This observation compelled us to undertake further investigations to ascertain the chemical nature of the active substance and to determine its percentage in the solution.

SUMMARY

1. It has been found that all solutions that contain the products of the hydrolysis of sericin, though prepared in different ways, remove practically all the sericin from raw silk when the latter is boiled in these solutions for a few hours, provided the solution contains enough of the sericin hydrolysis products

1) Tests were made on a semi-plant scale (using 50 meters of crepe de Chine) in the summer of 1949; the waters of the reeling room degummed the silk completely.

to impart active properties to the solution.

2. All active solutions are distinguished from the solutions customarily employed to degum raw silk by being neutral (their pH ranging from 6.5 to 7.5).

3. The mechanism involved in the removal of sericin from silk may be regarded as a process of peptizing the sericin in the fabric by the products of its own hydrolysis, present in solution and acting as a stabilizer of the colloidal solution of sericin. It may be that even in the degumming of silk with soap, the sericin is removed in the same way, the alkaline medium being required solely to create the necessary percentage of stabilizer.

LITERATURE CITED

[1] M. Korchagin and A. Karpov, Silk,1939, 3, 12.

[2] M. Vasilyeva, Archives of the Uzbek Silk Research Institute (1943).

[3] K. Markuze and V. Maleev, Textile Industry 1941, 3, 36.

[4] V. Krestinskaya and P. Karpova, Kirghiz Branch, USSR Acad. Sci. Trans. Chem. Inst. 1, 52 (1946).

[5] V. Krestinskaya and M. Aimukhamedova, loc. cit. 1, 53 (1946).

[6] H. Mosher, Amer. Silk. J. 50 (1931).

[7] V. Krestinskaya and M. Aimukhamedova, loc. cit. 1, 43 (1946).

[8] V. Krestinskaya and T. Ivanova, Colloid J. 8, 135 (1946).

Received September 14, 1949.

ACTIVATING HYDROLYSIS LIGNIN BY PROCESSING IT IN VARIOUS WAYS

N. G. Mendlina

The raw material used to secure sulfite cellulose extracts is sulfite cellulose liquor, which contains many deleterious substances in addition to the basic tanning constituent: lignosulfonic acid (5-7%). This has made it necessary to search for other raw materials superior to sulfite cellulose liquors.

The lignin left undissolved in the hydrolysis of wood by mineral acids under pressure may serve as a new kind of raw material. The efficient utilization of hydrolysis lignin is of practical interest, for this raw material is more homogeneous, more concentrated, and not in short supply - all of which make it utilizable in the leather and other industries.

Hydrolysis lignin is secured after it is separated from wood by weak mineral acids under pressure at high temperature, all the carbohydrates dissolving and the lignin remaining as the insoluble residue. The lignin isolated by various researche [1] is more or less greatly changed and is much more inert than natural lignin. This is explained by Freudenberg as follows: in the isolated lignin the units are not connected together by an ether linkage, as in natural lignite, but by condensation and polymerization, giving rise to high-molecular substances that react with difficulty with various chemical reagents [2].

In the recovery of lignin from wood, condensation takes place within the molecule in some instances, while in others the hydroxyl and carboxyl groups responsible for its solubility are either greatly changed or disappear completely. We know that lignin is partially sulfonated by strong sulfuric acid, a difficultly soluble sulfonic acid being produced.

When acted upon by concentrated hydrochloric acid for a long time, lignin loses its ability to be methylated, which may be due to the partial ring-closure of the hydroxyl groups. According to Hegglund, lignin hydrochloride remains insoluble when heated with bisulfite in the digestion process. When lignin is treated with alkali, only 12-14% dissolves, the phenolic hydroxyl groups of the lignin forming phenolates. Processing isolated lignin with phenols and chlorine yields a high percentage of lignin derivatives that are water-insoluble but are soluble in organic solvents.

It should be added that research methods in which the hydrolysis lignin is substantially changed, such as sulfonation, sulfitization, processing with phenols and chlorine, may entail many difficulties in experimental procedure and can merely roughly outline the path to be followed in converting it into the soluble state.

Our research had as its objective the activation of hydrolysis lignin and its conversion into the soluble state by the methods of sulfonation, sulfitization, chlorination, and phenol treatment. At the same time we investigated the chemical-technological and tanning properties of the soluble lignin products thus produced and of the condensation products of the lignin.

EXPERIMENTAL

Before we started, the hydrolysis lignin (which contained 71.2% moisture, was strongly acid, and was dark-brown in color) was washed to free it of its acid and then air-dried until its moisture content was 17.8%. The washed lignin was lighter in color, contained 0.7% ash, and was insoluble in water or in organic solvents. Dissolving it in 1% alkali by refluxing it on a water bath for 2 hours yielded 23% of solubles. The alkaline extract of lignin was brown, exhibited a reaction with aniline, had a pH of 4.5, precipitated gelatin, and was unstable when acidified.

Sulfonation. The method of sulfonating humic acids was employed in sulfonating the hydrolysis lignin, owing to its resemblance to these acids in some respects.

The lignin was sulfonated with 10% oleum (Tests 1-6), 20% oleum (Test 7), and strong sulfuric acid (Test 8), the amount of acid used being 1000% of the lignin by weight. The reaction temperatures were 10,20, and 40°, the reaction lasting 2 to 5 hours. The sulfo product was secured as a thick, dark mass. The excess oleum or sulfuric acid was removed by washing the sulfo product with a small amount of water. The washed sulfo product was again dissolved in cold and hot water until the resultant slightly colored solutions exhibited no reactions with gelatine. All the solutions were filtered very slowly. The aqueous extract of the sulfo products was dark-brown, strongly acid (pH 1.7 and 2.7), and of low concentration; it reacted with aniline and precipitated gelatine. The resultant solutions were alkalinized with soda to the required pH, and then their tanning properties were tested. The water-insoluble portion of the sulfo product was quantitatively collected as a black powder and dried to constant weight.

The results of analysis are given in Table 1.

TABLE 1
Results of Analysis of Lignin Sulfo Products

Test No.	Length of reaction, hours	Fraction temperature, °C	Insoluble residue, % of initial lignin	Tannide yield, % of the soluble lignin	Quality %
1	2	10	46.9	6.4	1.8
2	5	10	46.7	19.3	2.5
3	2	20-25	34.1	44.0	5.0
4	5	20-25	32.0	67.1	8.2
5	2	40	45.2	15.1	3.1
6	5	40	34.2	41.3	5.8
7	2	20-25	24.1	18.2	3.9
8	5	20-25	50.7	17.0	5.1
9	2	20-25	24.1	–	42.7
10	5	20-25	32.0	–	50.0
11	2-5	20-40	–	–	55.7
12	5	20-25	37.7	50.1	53.4

These figures indicate that increasing the time of sulfonation with 10% oleum at 10° from 2 hours to 5 hours produces hardly any change in the percentage of insolubles, but does increase the yield of tannides (Tests 1 and 2).

At 20-25°, prolonging the sulfonation time by the same amount (from 2 to 5 hours) diminishes the percentage of insolubles, but increases the yield of tannides and the quality, as compared to the figures for the 10° test (Tests 3 and 4). Sulfonation at 40° does not increase the tannide yield or the quality of the soluble portion of the lignin. The lignin is evidently partially carbonized at this temperature.

Sulfonation with 20% oleum (Test 7) at the same time and temperature conditions yields the lowest percentage of insolubles, though the quality of the solubles is not improved. Evidently, all that happens is that a larger proportion of nontanning substances enters solution. Processing the lignin with strong sulfuric acid under the same conditions (Test 8) yields more of the insoluble product, while the quality of the soluble product remains unchanged.

The product was dialyzed through parchment paper to remove its ash content. The quality of the product was improved considerably by dialysis, up to 55.7%, or 8 to 10 times as high as in the tests in which dialysis was not employed (Tests 9-11). Neutralization of the sulfuric acid with calcium carbonate until the pH was the value required for analysis improved the quality to 53.4% and increased the tannide yield to 50.1% (Test 12). The cooking temperature of the tanned leather is 68.4°.

These figures indicate that the optimum conditions for sulfonating hydrolysis lignin are a temperature of 20-25° and a reaction time of 5 hours. The soluble portion of the sulfonated lignin (50-65%) is not a high-grade tanning agent as such, as its yield and quality are low unless dialysis is used. The high ash content of the product interferes with diffusion of the tannides. Only dialysis or processing with calcium carbonate improves the quality of the tanning agent substantially. These tests indicate that the hydrolysis lignin has lost some of its hydroxyl and carboxyl groups, which are responsible for its solubility and its better tanning properties.

Sulfitization. The processing of wood with sodium sulfite and bisulfite instead of calcium bisulfite is fairly widely employed in industry by now. The same method is utilized to secure tanning extracts from the humic acids of peat. Hegglund [3] asserts that this method of digesting the wood yields a lighter liquor with fewer condensed substances and less ash. He also states that lignin hydrochloride behaves like natural lignin when treated with sodium sulfite and bisulfite. Eliashberg [4] states that digesting wood with sulfuric acid delignifies it much better than when the acid contains a base. The process takes half the time required when 0.9% of calcium oxide is present.

We used the same initial washed lignin. It was treated with sulfite, a 38% solution of bisulfite, and a mixture of the two, totaling 50 to 100% of the lignin by weight. The processing involved refluxing at 115-120° on an oil bath for 40 hours and in an autoclave at 140° for 12-49 hours. Despite the rather severe processing conditions, equivalent to the conditions used in digestion, hardly any of the lignin dissolved.

The residual insoluble lignin was the practically unchanged original

lignin, merely finely divided and yellow-brown in color. The lignin treated with sulfite and bisulfite was condensed with formalin and furfural, totaling 50 and 100% of the lignin by weight. Condensation was effected by heating to 25-30° in an alkaline medium on a water bath for 7 hours, to 115-120° on an oil bath for 20 hours, and to 140° in an autoclave for 15 hours. Condensation with formalin was unsuccessful. Condensation with furfural under exactly the same conditions in an alkaline medium produced partial dissolution of the lignin – 17 to 33% dissolving. The solution was brown, precipitated gelatin, and reacted with aniline.

The quality of the product ranged from 17 to 20%.

The hydrolysis lignin was processed with 7%, 9%, and 3.5% sulfuric acid in a bronze autoclave at 125-145° for 24 hours, with 10 ml of 25% ammonia as a catalyst, but no soluble product was obtained.

These experiments show that hydrolysis lignin, as a greatly changed product, is unaffected by chemical reagents, even under rather severe conditions: autoclaving at 145°. Evidently, no complete sulfonation takes place, causing the product to be soluble. Under these conditions no bisulfite compound of the lignin is formed, as the result of a reaction between the sodium bisulfite and the lignin's aldehyde group, which either disappeared completely in the tested lignin or was so greatly changed as not to react under these conditions. The absence of a condensation reaction likewise is proof of the disappearance of the groups responsible for condensation in the molecule of the tested lignin. All these data bear out the assertions in the literature to the effect that some groups, such as the acetyls and formyls, disappear from the lignin during its separation from wood and that the reactivity of this lignin is lowered appreciably.

It is obvious that sulfitization of hydrolysis lignin cannot be utilized to recover tanning extracts from it.

Chlorination. We know from the literature that chlorination of wood is one of the methods used to separate the lignin from the cellulose; it is even a method of quantitatively determining the lignin. This method has recently been employed on an industrial scale to produce cellulose from straw and aspenwood [5]. Strong [6] found that when wood is chlorinated, only 4 of 12 atoms of chlorine combine with the lignin, the other 8 atoms, that is, 67%, forming HCl. These figures indicate that chlorination of wood involves not only a substitution reaction, but the following oxidation reaction as well:

$$RH + Cl_2 + H_2O \longrightarrow ROH + 2HCl.$$

When Holmberg [7] chlorinated isolated lignin, he secured a non-homogeneous product.

When sulfate lignin is chlorinated at various temperatures, about 90% of the methoxy groups are split off.

It is much harder to react chlorine chemically with pine. This difficulty of chlorination must be even greater with the isolated lignin. The chlorination reaction depends upon many factors: temperature, moisture content, the method employed in the preliminary processing of the material, and the chlorination time.

The experiments were run at 20-40° for 2-20 hours after the preliminary processing of the sawdust. The sawdust was steamed by heating it with water for 2 hours or else processed with 1% alkali in the cold for 12 hours and boiled on a water bath at 95° for 2 hours. After the lignin had been processed with alkali, the reagent was washed out of it with water, and the lignin was suction-filtered until it contained 10, 20, and 30% of the dry substance, and then chlorinated in a chlorinator. The chlorine entered the chlorinator at the bottom, thus ensuring the uniform chlorination of the entire mass.

The lignin was suspended in water and chlorinated in a round-bottomed flask fitted with an inlet and an outlet tube. In some of the experiments the chloro product was washed during chlorination with water to remove the hydrochloric acid formed, as well as the water-soluble oxidation products of lignin, which hinder the deeper penetration of the chlorine into the lignin molecule. After the colored lignin had been washed, chlorination was resumed. After chlorination was complete, the free chlorine was washed out of the chlorolignin.

The chloro product weighed 8.3-50.0% of the initial lignin, depending on the chlorination time; this agrees with the figures in the literature.

The washed moist chlorolignin was readily rubbed to a homogeneous, bright-red mass, which did not look like the original lignin at all. It was insoluble in hot or cold water or in a 2% or stronger solution of sulfite; it dissolved in 1% caustic alkali, soda, and alcohol, though the solution was unstable when acidified. To secure soluble chlorolignin, it was extracted with a 1% solution of caustic alkali and a 5% solution of soda in the cold and then refluxed at 100° for 2-3 hours. The resultant alkaline solutions of chlorolignin were dark-brown, of low concentration (1.5-2.8° Be), and strongly alkaline, their pH ranging from 6.5 to 10. They were unaffected by acidulation with acetic acid to a low pH, though a precipitate was thrown down when they were acidulated to a pH below 3.5 with 6% sulfuric acid.

All these solutions exhibited a reaction with aniline and precipitated gelatin. We see from our test results (Table 2) that the consumption of alkali in the preliminary treatment of the lignin totaled 12%, the consumption of alkali in the subsequent extraction likewise being rather high, varying with the chlorination conditions.

The yield of soluble products was as high as 70%, fluctuating with the preliminary treatment employed and the chlorination conditions. Increasing the chlorination time from 2 hours to 12 improved the quality from 7.7% to 20.7% and increased the tannide yield from 12.5% to 47.4% (Tests 1-5). Under these conditions chlorination with $FeCl_3$ as a catalyst (Test 6) did little to improve the process. Chlorination of the lignin in an aqueous-alkaline medium (Test 6) yielded a quality of 35.1% and a tannide yield of 57.3%.

TABLE 2

Results of the Analysis of Chlorolignin After It Had Been Treated With Alkali

Test No.	Chlorination time, hours	Alkali consumption, % of lignin		Per cent yield of soluble chlorolignin	Yield of tannides, % of the solubles	Quality, %
		In preliminary processing	In extracting the chlorolignin			
1	2	11.8	25.0	72.2	12.5	7.7
2	2	11.8	23.2	65.3	13.7	12.4
3	12	–	38.0	72.0	20.0	16.2
4	12	11.8	40.0	42.0	47.4	17.9
5 [1]	12	11.8	80.0	78.7	21.5	20.7
6 [2]	20	23.0	52.0	62.6	57.3	35.1

There is reason to believe that oxidation is more vigorous under these conditions, yielding more soluble products that possess better tanning properties, even though the ash content is higher.

These figures indicate that no matter what conditions are used for the chlorination of hydrolysis lignin and the ensuing extraction of the chlorolignin, tanning extracts that possess satisfactory tanning properties cannot be secured by the chlorination method. The cooking temperature of the tanned hide was 65.8°, which is not high enough for a good tanning agent. The ash content of the chlorolignin and its quality were about the same as those of chlorinated sulfite cellulose liquor. Moreover, the method of chlorination followed by extraction is very laborious and tedious in production.

Processing with phenol. This is one of the basic methods of separating lignin from cellulose. By this method we can directly obtain a condensation product that resembles synthetic tanning agents. The carboxyl group of the lignin reacts with the para hydrogen atom of the phenol. The reaction rate depends upon the substituent groups in the phenol, the reaction temperature, and the catalysts employed.

For this condensation we used anhydrous phenol, as a reagent not in such short supply, and the same initial lignin. The lignin was treated with the phenol on a water bath at 100° for 6-12 hours, the phenol – lignin ratios used being 1:5 and 1:12. 0.07% to 5% of hydrochloric acid was used as a catalyst. Treatment on an oil bath lasted 4 hours at 120-130°, 8 parts of phenol being used per part of lignin, with 0.1% of sulfuric acid as the catalyst. Under these conditions the reaction product was a homogeneous violet-brown liquid mass. Processing the reaction mass in an autoclave at 140° for 3 hours turned it into a thick, black, tarry liquid. Driving off the excess phenol yielded a dark-brown powder with a violet tinge, which was nonhygroscopic, insoluble in water, and soluble in weak alkali, its solution decomposing when acidulated. The very appearance of the resultant substance indicated that the lignin molecule had been greatly changed due the condensation process. Phenol totaling 8.3% by weight of the lignin entered into the reaction.

[1]) Chlorinated in an aqueous medium.
[2]) Chlorinated in an aqueous-alkaline medium.

The water-insoluble phenollignin powder was treated with sulfite, bisulfite, and a mixture of these two reagents at atmospheric pressure and at 110°, as well as in an autoclave at 140° for 5 to 28 hours. In all these tests we used 100% of the reagents by weight of the phenollignin. Water-insoluble substances were secured in all these tests. Only when the phenollignin was processed for 28 hours in an autoclave at 140° did we get 33% of soluble substances, with a quality of 39.3%. Condensing the phenollignin with acetaldehyde in an acid medium likewise yielded insoluble products. Then the phenollignin powder was subject to more severe treatment: sulfonation. It was sulfonated with 10% oleum (Tests 1-3 and 5-6) and with strong sulfuric acid (Test 4), the acid used totaling 100% to 200% by weight of the air-dry powder and of the weight of the liquid product, and the sulfonation lasting 3-5.5 hours, with stirring, on a water bath at 25 to 100°. The reaction was fairly smooth and very much faster than with the original lignin.

In all these tests the sulfo product was secured as a thick dark-red liquid that was fully soluble in water. The solutions of the sulfo products were red-brown and strongly acid (pH 1.5-3), precipitated gelatin, and exhibited a reaction with aniline.

For analysis, the solutions of the sulfo products were neutralised to the requisite pH with calcium carbonate. The results of analysis (Table 3) showed that the best results were obtained when we sulfonated with 200% of oleum at 25 to 80° for 5 hours. the quality was 55.0%, the tannide yield 70.4%, and the cooking temperature of tanned samples of leather 73.1° (Tests 2 and 3).

TABLE 3

Results of Analysis of Phenollignin Sulfonated Under Various Conditions

Test No.	Substance analyzed	Amount of reagent, as % of the phenollignin	Reaction temperature, ° C	Tannide yield, %	Quality %	Cocking temperature of tanned leather samples, ° C
1	Phenollignin powder	200	30-35	66.3	–	63.1
2		200	25-80	70.4	55.0	73.1
3		200	25-80	68.5	47.0	69.2
4		100	25-80	34.5	32.0	67.3
5	Phenollignin-phenol mixture	100	30	16.0	14.9	62.5
6		200	100	37.7	17.0	63.6
7	Free phenol	200	25-80	10.4	4.4	–

When the liquid phenollignin product mixed with free phenol was sulfonated (Tests 5 and 6), the sulfo product was of poor quality and the tannide yield was low. Hence, free phenol impairs the tanning properties of the phenollignin sulfo product, as was borne out by a blank test in which phenol itself was sulfonated under the same conditions (Test 7).

Hence, an extract whose quality ranges from 47.0 to 55.0%, possessing tanning properties, may be secured by employing a simple method of treating hydrolysis lignin with a small amount of phenol for 5-6 hours on a water bath with HCl or H_2SO_4 used as a catalyst, and then sulfonating the condensation product with oleum. The cooking temperature of the tanned leather samples is 73.1° (that of samples tanned with a sulfite cellulose extract being 60°).

Leather tanned with these extracts is somewhat better than leather tanned with the usual sulfite cellulose extracts. The phenollignin condensation product is unaffected by sulfite or bisulfite, which is not the case with the condensation products of hydroxy derivatives of organic substances with the aldehydes. This is further evidence that the hydrolysis lignin either lacks the aldehyde complex required for the formation of a water-soluble aldehyde-bisulfite compound or else the original lignin is already so condensed and changed as to be unaffected by a simpler chemical treatment.

SUMMARY

1. Hydrolysis lignin is a greatly changed substance, almost completely insoluble and containing few hydroxyl groups, which is one of the reasons why it is chemically inert.

2. Processing hydrolysis lignin with sulfite, bisulfite, free sulfuric acid, or chlorine under varying conditions cannot be used to secure soluble tanning agents.

3. Sulfonating hydrolysis lignin with 10% oleum yields about 50% of soluble products that possess tanning properties after suitable processing with calcium carbonate. The quality is 42.7-55.7%, and the cooking temperature of the tanned leather samples 68.4°.

4. Processing hydrolysis lignin with phenol yields a water-insoluble condensation product.

5. Subsequent sulfonation of the condensation product yields a fully soluble tanning agent. Its quality is 47-55%, and the cooking time of tanned leather samples ranged from 69.2 to 73.16°. The method of preparing this tanning agent is fairly simple, and its quality is higher than that of the sulfite cellulose extract.

LITERATURE CITED

[1] Fuchs, Cellulosechemie, 7, 66 (1935); Ender, Papier-Fabrikant, 26, 301 (1934).

[2] Komarov, Paper Ind. 1934, 12, 32.

[3] Hegglund, Paper Ind. 1934, 8, 69.

[4] Eliashberg, Paper Ind. 1948, 2, 20.

[5] Rozenberg, Mater. Paper Ind. Inst. 12, 14 (1933); 13 (1934).

[6] Strong, Papier-Fabrikant, 30, 91 (1931).

[7] Howley and Wythe. The chemistry of wood (Russ. ed.), 55 (1933).

Received June 6, 1950.

THE PENTAERYTHRITIDE OF TALL OIL FATTY ACIDS

V. D. Khudovikov

Central Institute of Wood Chemistry Research

Crude tall oil, consisting of resin acids, fatty acids, neutral substances, and oxidation products, is produced by the action of acid reagents upon crude sulfate soap – a by-product of sulfate cellulose plants. Crude tall oil is widely employed as such in various industries (soap, dyes and lacquers, etc.); in addition products of higher grade may be made from it by appropriate processing.

In the most widespread distillation method of treatment [1], for instance, fractionating crude tall oil in vacuo with superheated steam yields rosin, tall oil, fatty acids, and pitch. Tall oil fatty acids (a technical term) are a mixture of, for the most part, fatty acids (linoleic, oleic, and linolenic acids) with some resin acids and neutral substances; they are used principally in the manufacture of laundry soap. By now, as the result of research on the composition of the fatty constituents of crude tall oil [2], it is certain that the predominating acid in the oil is not oleic acid, but rather linoleic acid, and that the composition of the fatty constituents of tall oil is closest to that of the drying and semidrying oils (linseed and perilla oils), used, as we know, as film-forming materials. Thus the tall oil fatty acids may be another source of high-grade raw material for the manufacture of these latter materials [3]. Appropriate processing of the tall oil fatty acids yields constituents for any type of lacquer: reacting them with metallic oxides yields esters of the tall oil fatty acids, used as paint vehicles and siccatives; reacting them with polyhydric alcohols (glycol, glycerol, pentaerythritol) yields alkyd resins that may be used as the major constituents of lacquers.

The domestic literature contains several papers demonstrating the merits of film-forming materials made from tall oil and tall oil fatty acids via the glycerides [4]. To produce a glyceride, the tall oil fatty acids are usually heated to 250-270° C for 5-8 hours with 11% of glycerol, followed by a short period of heating to 300° C. The resultant glyceride has an acid number of 10-15. It has been found that the glycerides of the tall oil fatty acids are a satisfactory substitute for linseed oil. It was then learned that atomicity of the alcohol employed in esterification has a profound effect upon such properties of the lacquer film as its hardness, lustre, and drying quality. It was stated in the literature [3,5] that the production of alkyd resin by esterifying pentaerythritol yielded resins with better properties than by esterifying glycerol. Dipentaerythritol, tripentaerythritol, and mixtures of the two, are also employed.

We[1] set as our objective establishing the optimum conditions for producing the pentaerythritide of tall oil fatty acids and testing its suitability as a film-forming material.

We investigated the variation of the rate of esterification of the tall oil fatty acids with the alcohol employed in esterification, the temperature and time of the process, and the resin acid content. Other factors affecting the rate of esterification (percentage of esterified acids and alcohol, and the stirring rate) were eliminated to focus the experiments on the variables desired.

EXPERIMENTAL

Tall oil fatty acids containing 15.4, 22.1, and 39.6% of resin acids were used in preparing the esters. The pentaerythritide, the test results of which are given below, was prepared from the tall oil fatty acids that contained 15.4% of resin acids. The constants and composition of these tall oil fatty acids were determined by the existing method [6]; they are listed in Table 1.

TABLE 1

Constants and Composition of Tall Oil Fatty Acids

Chemical indexes of the acids	Numerical value
Acid number	163.2
Saponification number ...	170.0
Iodine number	201.1
Thiocyanogen number	91.0
% Composition:	
Neutral substances	16.7
Resin acids	15.4
Fatty Acids	67.9
Fatty Acid Composition %:	
Saturated acids	5.4
Oleic acid	31.79
Linoleic acid	58.72
Linolenic acid	4.09

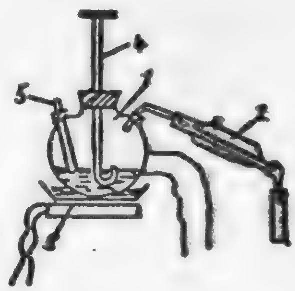

Esterification apparatus.

1 - glass flask; 2 - condenser with measuring cylinder; 3 - electric plate with rheostat, 4 - stirrer fitted with seal, 5 - thermometer.

The figures in Table 1 are evidence of the rather high quality of the tall oil fatty acids as raw material for the production of film-forming materials.

The esterifying alcohols employed were glycol, glycerol, and, most of all, pentaerythritol. The published papers contain sufficient proof that the percentage of esterifying alcohol should not exceed 11%. We always employed 11% of the alcohol.

The esterification conditions employed when pentaerythritol was used were as follows: 50 g of the tall oil fatty acids (200 g were taken in subsequent

[1]) M. V. Kartseva and R. D. Strtsova took part in this research.

samples) were placed in an electrically heated wide-necked glass flask, the stirrer was started, and after the contents had been heated to 130-140° C, 11% of pentaerythritol was added in powder form. Then the temperature of the reaction mass was raised to the desired value in no more than 1 hour. This instant was taken as the time the reaction started. The acid number of the mixture was about 140. The temperature was maintained at the desired level by means of a rheostat, and one hour later samples were taken to determine the acid number, the change in the number serving as an index to the process rate. The esterification apparatus is illustrated in the figure.

When glycerol or glycol was used in esterification, a reflux condenser was bathed in steam. The water containing a minute quantity of oil that formed in every run was collected in a receiver. After the reaction was over, the overall ester yield was determined as well as the ester's constants. The esters of the tall oil fatty acids were a thick, crimson resin.

The yield of esters was about the same as the weight of the tall oil fatty acids placed in the reaction.

Comparison of the esterification rates of tall oil fatty acids (containing 22.1% of resin acids) with glycol, glycerol, and pentaerythritol. The rate of esterification of the tall oil fatty acids may be estimated by the change in the acid number of the esterified product, shown in Table 2.

TABLE 2

Change in the Acid Number During the Esterification of Tall Oil Fatty Acids With Glycol, Glycerol, and Pentaerythritol at 290° C

Time, hours	Ester Acid Number		
	Of glycol	of glycerol	Of pentaerythritol
1	47.3	48.6	39.8
2	37.2	28.0	24.7
3	25.0	20.2	18.0
4	23.1	17.9	13.3
5	23.0	17.0	11.0
6	21.4	16.6	10.1

As we see in Table 2, pentaerythritol esterifies tall oil fatty acids faster, all conditions being the same, than glycol or glycerol, yielding a product with an acid number of 10-11 after 6 hours at 290° C.

Rate of esterification at various temperatures of tall oil fatty acids containing various percentages of resin acids. The only alcohol used in this esterification of the tall oil fatty acids was pentaerythritiol. We ascertained the esterification rate as a function of the percentage of resin acids in the tall oil fatty acids, of temperature, and of time. Our results are listed in Table 3.

We see from the figures in Table 3 that raising the reaction temperature speeds up esterification considerably. It is best to use a temperature of 280-290° C. to secure an ester with the lowest acid number. At these temperatures the esterification process is concluded within 6-7 hours. It was later discovered, however, that the heating time had to be prolonged to 15-17 hours if the esters were to be used as film-forming materials. This did not affect the acid number of the product, but it did increase the ester's viscosity. The resin acids contained in the tall oil fatty acids reduce the esterification rate, but the difference in acid numbers grows smaller at 290° C, with a longer heating time.

TABLE 3

Change in the Acid Number During the Esterification of Tall Oil Fatty Acids with Various Percentages of Resin Acids at Various Temperatures

Time, hours	Change in the Acid Number at following percentages of resin acids.				
	22.1			39.6	
	Temperature, ° C				
	220	230	290	230	290
1	101.2	67.4	39.0	71.2	62.7
2	60.0	40.6	17.5	52.7	36.3
3	41.0	33.2	15.7	40.8	28.1
4	36.9	30.5	14.5	36.8	17.6
5	32.0	26.9	11.9	35.0	15.8
6	26.5	24.5	10.1	31.3	14.3
7	28.0	24.4	10.4	29.4	12.2
8	26.7	24.0	8.6	-	10.2
9	-	-	8.2	-	-
10	-	-	8.1	-	-
11	-	-	8.2	-	-

TABLE 4

Results of Tests of the Technical Paint Qualities of a Lacquer Made From the Pentaerythritol Ester

Index	Test Results
Drying at 18-20° C	24 hours - peels; 48 hours - nearly completely dry
Hardness	Satisfactory
Elasticity	1 mm
Impact Strength	15 kg/cm
Water resistance	1 hour - no change

A sample of the pentaerythritol ester of tall oil fatty acids was produced under the following conditions, therefore: 11% pentaerythritol used, reaction temperature 280°, reaction time 17 hours. The sample was tested for its serviceability as a film-forming material.

Results of testing the pentaerythritol ester of tall oil fatty acids[1]. The pentaerythritol ester was dissolved in the cold in white spirit (100:40 ratio), and 10% of Siccative No. 7640 (lead-manganese-cobalt). Its technical paint properties, as required for oil varnishes, and its suitability as a binder in the manufacture of enamels were determined. The test used was the OST 10086-39 (All-Union Standard) "Methods of testing paint and lacquer materials and coatings."

The results of our tests of the technical paint qualities are listed in Table 4.

As we see in Table 4, the technical painting qualities of the lacquer are satisfactory.

Paints were prepared with red ocher and zinc white, by grinding them in equal proportions with the lacquer, to establish the feasibility of preparing lacquers for interior painting.

The principal technical paint qualities were tested by applying a single layer of the resultant paints by brush to tinplate sheets and allowing them to dry at 18-20° C.

The test results are listed in Table 5.

[1] The tests were made by the Moscow branch of Lacquer and Paint Coatings.

TABLE 5

Test Results of the Technical Paint Qualities of Paints Using Pentaerythritol Lacquer as a Base

Index	Results	
	Zinc white	Red Ocher
Drying at 18-20° C	24 hours - considerable peeling; 48 hours - dried	24 hours - considerable peeling; 48 hours - dried
Hardness	Hard	Hard
Elasticity	1 mm	1 mm
Impact Strength	45 kg/cm	50 kg/cm
Water resistance	1 hour - no change	1 hour - no change

As we see in Table 5, zinc white and red ocher on a pentaerythritol lacquer base yield satisfactory technical paint qualities that meet the requirements for enamel paints for general consumption.

Thus, the lacquer based on the pentaerythritol ester may be employed as a binder in the preparation of enamels for interior work.

It should be noted that the results of our tests of the pentaerythritol esters of tall oil fatty acids that contained a higher percentage (22.1%) of resin acids indicated somewhat poorer drying properties and hardness.

SUMMARY

1. Data have been obtained on the esterification of tall oil fatty acids with pentaerythritol.

2. The optimum conditions for the preparation of the pentaerythritol ester of tall oil fatty acids have been established.

3. Satisfactory results have been obtained in testing the pentaerythritol ester of tall oil fatty acids as a lacquer and as a binder for paints.

LITERATURE CITED

[1] N. N. Nepenin. The manufacture of cellulose, 881 (1940).

[2] M. Hess. Paint Technolog. 294-304 (1946).

[3] V. G. Kiselev. Lacquers and varnishes. State Chemical Press (1940).

[4] P. M. Romanova and A. I. Kotlyar, Ind. Org. Chem. 1939, 6, 257-258.

[5] Paint, Oil and Chemical Rev., 107, 84-86 (1944).

[6] A. L. Zinovyev. The chemistry of fats, 224 ff (1939).

Received May 29, 1950.

BLANK
PAGE

THE KINETICS OF CATALYTIC OXIDATION OF CYCLANES IN THE LIQUID PHASE WITH ALKANES PRESENT

V. K. Tsykovsky and P. V. Likhamanova

In discussing the rate of oxidation of hydrocarbons belonging to various groups (but having molecules of the same size), the hypothesis has been advanced [1,2] that open-chain hydrocarbons, such as the alkanes and alkenes are oxidized fastest, followed by the cyclanes and the aromatic hydrocarbons. It should be said that this hypothesis has been deduced from investigations of oxidation processes, most of which take place without a catalyst (such as the burning of hydrocarbons).

It has been learned from a study of the catalysis phenomena occurring in the liquid-phase oxidation of hydrocarbons that the kinetics of this reaction are quite singular, differing very markedly from noncatalytic processes.

Though the initial research in this field [3] did not discuss the behavior during catalytic oxidation of individual hydrocarbons possessing molecules of the same size, but rather studied the behavior in this process of all the hydrocarbons belonging to various groups (possessing approximately the same physical constants), it did introduce certain corrections into the hypotheses advanced previously. This research demonstrates, more particularly, that of all the hydrocarbons oxidized under these conditions, it is not the alkanes, but rather the polymethylene hydrocarbons that exhibit the highest reaction rate.

This observation shows that there is a substantial difference between the catalytic and autocatalytic oxidation process. It is highly probable that the excitation of the molecules of polymethylene hydrocarbons during autocatalytic oxidation will be altogether different, thus making the velocity of the reaction of these hydrocarbons with atmospheric oxygen higher. This is borne out by the fact that the alkanes are oxidized at faster rates in the liquid phase when the temperature is raised, even without any catalyst present, which is not the case when, say, cyclanes are oxidized. Hence, the concept of the oxidation rate of hydrocarbons is, in general, a highly relative one, applicable only to certain reaction conditions.

We have explored the joint catalytic oxidation of only such hydrocarbons as the cyclanes and the alkanes, in order to make a more thorough study of this phenomenon.

EXPERIMENTAL

The experimental materials were narrow fractions of kerosene, consisting

of the hydrocarbons specified above, possessing approximately the same overall physical properties, but having different structures. The latter was due to the fact that these narrow fractions were secured from broad kerosene fractions of petroleums from different fields.

The narrow fractions, with different kerosene compositions, the boiling points of which were 200-220, 220-240, and 240-260° C, were secured by distilling broad kerosene fractions in a laboratory rectifying column under rigidly identical conditions.

The aromatic hydrocarbons were separated from the narrow fractions in the usual manner; the completeness of their removal was established by means of a formolite reaction. The properties of the collected narrow fractions and their group composition are listed in Table 1.

TABLE 1

Physico-Chemical Properties of Kerosene Fractions Used in Oxidation

No.	Group composition of the fraction, per cent by weight		Specific gravity d_{20}	Molecular weight	Refractive index n_D^{20}
	Cylanes	Alkanes			
		200-220° C Fraction			
1	18.0	82.0	0.786	189.0	1.436
2	24.0	76.0	0.7862	187.0	1.437
3	35.0	65.0	0.7874	184.0	1.438
4	40.5	59.5	0.7876	182.0	1.438
5	47.5	52.5	0.7877	180.0	1.439
6	56.5	43.5	0.7879	177.4	1.440
7	62.5	37.5	0.7882	175.1	1.442
8	69.0	31.0	0.7884	173.3	1.442
		220-240° C Fraction			
9	3.0	97.0	0.7964	190.8	1.437
10	30.0	70.0	0.7992	186.0	1.442
11	34.0	66.0	0.7998	184.0	1.449
12	45.5	54.5	0.8016	181.7	1.452
13	57.5	42.5	0.8022	179.1	1.454
		240-260° C Fraction			
14	2.5	97.5	0.7984	192.0	1.442
15	9.5	90.5	0.8009	190.0	1.443
16	11.08	88.92	0.8010	189.6	1.445
17	15.5	84.5	0.8016	188.0	1.446
18	39.0	61.0	0.8102	182.6	1.447
19	40.0	60.0	0.8111	181.7	1.449
20	50.5	49.5	0.8121	182.0	1.452

All the fractions were oxidized in the liquid phase with atmospheric oxygen at constant parameters (rate of air flow across the reactor cross section, weight of the substrate, temperature, reaction time, catalyst concentration, and the like).

Oxidation was effected in a glass reactor of the type described in the literature previously [4].

The oxidation products were carefully collected in special traps filled with an alkaline solution and the appropriate solid adsorbents. The amount of oxidation products absorbed by the absorbents and adsorbents was determined gravimetrically.

The oxidation products were analyzed as follows.

The oxidized product taken from the reactor after the latter had cooled was neutralized in the cold with a 5% aqueous solution of sodium hydroxide (corresponding to its acid equivalent). Sodium salts of hydroxy acids, of complex ether acids, and of the simplest carboxylic acids were formed during neutralization.

After the sodium salts had all been thoroughly eliminated, the dissolved oxidized fraction still contained esters and ethers that were hard to saponify. The esters were extracted by prolonged saponification with a normal alcoholic solution of potassium hydroxide, the ester yield being determined by the difference in weight between the product before saponification and that of the hydrocarbons that did not enter into the oxidation reaction. These esters were not investigated further.

All our attention was focussed upon the simplest carboxylic acids, prepared from their sodium salts. The sodium salts of the carboxylic and hydroxy acids were decomposed with a weak solution of sulfuric acid. The resultant mixture of acids was dissolved in ten times its volume of petroleum ether (b.p. 35-55° C). The hydroxy acids settled out of the solution, their total being allowed for. What remained dissolved in the petroleum ether were the carboxylic acids and part of the complex ether acids. After all the SO_4' ion had been thoroughly washed out of the solution of carboxylic acids in petroleum ether, the solution was evaporated, and the carboxylic and ether acids analyzed qualitatively and quantitatively after they had been brought to constant weight.

The following terminology is used henceforth for the sake of simplicity.

Carboxylic acids: a mixture of the simple carboxylic acids with ether acids, soluble in any volume of petroleum ether.

Hydroxy acids: The total of various hydroxy acids and their esters, precipitated when the petroleum ether is diluted.

Ethers: a mixture of ethers and esters that are hard to saponify but are wholly soluble (in low concentrations) in petroleum ether.

The unreacted hydrocarbons in each fraction were freed of all their saponifiable constituents and then were added to the hydrocarbons entrained by the current of air and collected in the traps. After the entire mass of unreacted hydrocarbons had been thoroughly refined to free them of the residual oxidation products, their weight and group composition were determined. The collected volatile oxidation products were not analyzed, but allowance was

made for them quantitatively, as stated above.

This method of analysis enabled us to draw up a precise material balance for the oxidation of each fraction, differentiated according to the basic derivative of this process.

The results of oxidation are given in Table 2. In the oxidation of all three of the tested fractions, the end result refers only to the total percentage of cyclanes in the fractions.

TABLE 2

Results of Oxidizing Kerosene Fractions

No.	Overall yield of oxidation products, per cent by weight of the oxidized fraction	Reacted hydrocarbons as per cent by weight of these carbons in the original fraction		Resulting oxidation products as per cent by weight of the original fraction					
					Including				
		Cyclanes	Alkanes	Total	Carboxylic acids	Hydroxy acids	Ethers	Volatile oxidation products	Molecules of water
				200-220° C Fraction					
1	109.5	33.8	36.6	47.5	22.5	3.5	7.5	14.0	8.0
2	111.8	45.0	37.2	54.8	20.8	10.5	5.5	18.0	10.0
3	114.6	59.0	46.4	66.6	19.6	17.0	7.4	22.6	15.2
4	115.8	60.7	46.9	69.5	18.6	18.4	9.0	23.3	15.6
5	116.0	62.5	47.0	70.5	16.5	19.4	10.6	24.0	15.9
6	116.4	63.2	47.8	72.9	14.0	19.6	12.8	26.5	15.95
7	117.3	64.5	46.5	75.0	12.2	19.9	15.0	24.9	15.1
8	117.9	71.5	44.6	77.9	10.3	20.2	16.6	30.8	16.8
				220-240° C Fraction					
9	111.4	52.0	42.9	57.4	24.2	–	6.4	26.8	8.8
10	113.4	56.4	50.9	67.9	17.0	11.8	10.5	28.6	10.6
11	117.7	64.1	51.4	73.1	14.9	12.5	11.9	33.8	12.8
12	119.4	69.1	53.2	79.9	13.2	14.3	12.7	39.7	14.6
13	120.9	75.0	53.1	84.4	11.4	18.4	16.8	37.6	17.4
				240-260° C Fraction					
14	113.5	61.4	38.1	53.5	26.0	–	14.1	13.5	8.5
15	119.4	65.7	39.4	62.4	21.0	9.2	12.9	19.5	10.0
16	119.2	69.2	39.8	63.2	17.4	12.2	13.5	21.1	12.8
17	124.3	76.3	–	70.3	17.2	12.3	14.0	26.8	14.8
18	128.7	84.2	39.9	77.7	16.1	15.0	18.0	28.7	16.4
19	128.9	86.4	40.1	78.9	15.2	16.8	20.5	26.4	16.8
20	129.8	89.7	40.3	81.9	14.0	17.3	25.2	24.48	17.6

The absence of any marked discrepancies in this experiment justify the assertion that the structure of the cyclanes (including those oxidized together with the alkanes) has no substantial effect upon the nature of the experiment. No matter what the cyclane structure, the rate of oxidation increases proportionally to their normal concentration in each fraction tested. The fact that the

rate of oxidation rises in that very group of hydrocarbons is likewise evidenced by such indexes as the percentage of reacted cyclanes, the total oxygen absorbed in this process, and the continuously increasing quantity of the total oxidation products.

The percentage of the cyclanes entering into the oxidation reaction is found to be higher in the fractions that contained more of the cyclanes. One highly curious factor is the circumstance that the percentage of reacted cyclanes is generally little affected by their initial concentration or by the boiling ranges of the fractions tested. This is further proof that cyclanes react with atmospheric oxygen in this process much faster than do the alkanes.

When we consider how the composition of the saponifiable constituents varies (Table 2), it is easy to see that these changes are likewise directly related to the concentration of the cyclanes in the original fraction and to the percentage of cyclanes entering into the reaction. We first notice that as the concentration of cyclanes in the fractions (no matter what their boiling range) increases, the yield of carboxylic acids continues to fall, while the yield of hydroxy acids, esters, and other oxidation products begins to rise. It may be assumed that the cyclanes are oxidized more rapidly in all stages, owing to their higher reactivity. Thus, the carboxylic acids formed in any stage of the process, according to Bonet's theory of hydroxylation, are rapidly converted into the respective hydroxy acids, etc. This is the only possible explanation of the falling yield of carboxylic acids and the increasing percentage of various secondary oxidation products in the saponifiable constituents.

The increase in the rate at which secondary oxidation products are formed is paralleled by the continuously increasing yield of molecular water. In the given case, we may assume that water is formed as follows:

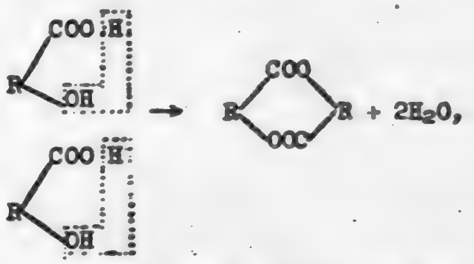

i.e., the condensation of two molecules of the hydroxy acid yielding one molecule of the ether and two molecules of water.

Returning to Table 2, we see that the ether yield actually is proportional to the percentage of molecular water in the observed stabilization of the formation of hydroxy acids. This hypothesis is in good agreement with the continuously falling yield of the carboxylic acids.

In contrast to the alkanes, therefore, the cyclanes react with atmospheric oxygen much faster, irrespective of molecular weight or structure, being rapidly converted from simple acids into various ethers.

Significant evidence of secondary changes is observed in the composition of the carboxylic acids (Table 3). As the concentration of the cyclanes entering into the reaction rises, the hydroxyl and ester numbers of the carboxylic

acids increase. This agrees very satisfactorily with the kinetics of the change in composition of the saponifiable constituents as a function of the concentration of cyclanes in the original fraction.

When we consider what happens when we pass from the oxidizable fraction with one boiling range to another, we readily see that the behavior pattern set forth above still holds good, though the ratios of the yields of carboxylic acids, hydroxy acids, and ethers change as the reaction rate continues to rise. Even a negligibly small increase in the molecular weight of the fractions is enough to prove that the higher the molecular weight, the more carboxylic acids and ethers will be formed, with less of the hydroxy acids (for the same cyclane concentration).

TABLE 3

Properties of Gasoline-Soluble Carboxylic Acids Secured in the Oxidation of Kerosene Fraction

No.	Acid number, mg of KOH per g	Saponification number	Ester Number	Hydroxyl Number	Molecular weight	Specific gravity d^4_{20}	Refractive index n_D^{20}
			200-220° C Fraction				
1	129.0	180.0	51.0	102.0	305.5	0.9284	1.440
2	127.0	187.0	60.0	106.5	299.5	0.9409	1.443
3	126.0	183.5	56.5	110.0	289.5	0.9664	1.445
4	128.0	187.0	59.0	108.0	284.5	0.9783	1.448
5	128.0	201.0	73.0	109.5	278.5	0.9816	1.449
6	129.0	207.0	78.0	114.0	270.5	0.9879	1.454
7	135.0	202.0	67.0	130.0	265.5	0.9915	1.455
8	131.5	215.0	84.5	124.0	260.0	0.9961	1.456
			220-240° C Fraction				
9	128.4	187	58.6	108.5	316.0	0.9284	1.440
10	129.0	192.4	63.4	109.3	301.0	0.9417	1.445
11	131.7	205	73.3	113.0	291.0	0.9501	1.446
12	130.0	207	77.0	118.0	281.5	0.9674	1.447
13	133.0	210.5	77.5	119.5	277.0	0.9742	1.452
			240-260° C Fraction				
14	135	187.8	52.8	101.5	318.0	0.9454	1.457
15	129	182.4	53.4	106.5	307.0	0.9489	1.458
16	131.8	185.0	54.0	109.0	306.0	0.9496	1.458
17	130.7	186.3	55.6	111.3	300.5	0.9510	1.459
18	132.5	203.3	70.8	115.8	295.6	0.9582	1.464
19	133.5	208.6	75.1	116.5	291.3	0.9602	1.465
20	135.5	212.6	77.1	117.5	283.5	0.9615	1.461

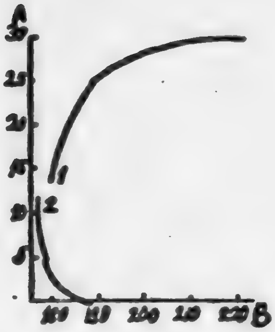

Variation of the yields of ethers and hydroxy acids with the molecular weight of the fraction.

A – Yield, % by weight; B – molecular weight of the mixture to be oxidized (33% alkanes; 67% cyclanes). 1 – Ether yield; 2 – yield of hydroxy acids.

To emphasize the influence of the fraction's molecular weight, we oxidized different kerosene fractions under identical conditions, containing approximately the same percentages of cyclanes (67%) and alkanes (33%). We found (see figure) that the yield of hydroxy acids dropped to zero at certain values of the molecular weight, whereas the percentage of ethers formed rose uninterruptedly.

Here we find an experimentally corroborated increase in the reaction rate of cyclanes as their mean molecular weight increases.

At a certain value of the molecular weight the reaction rate becomes so high that the hydroxy acids are apparently converted into ethers at the instant they are formed. More particularly, we attribute to this circumstance the fact that no hydroxy acids are found when some high-boiling kerosene fractions are oxidized, although high yields of carboxylic acids with high hydroxyl numbers and ethers that are hard to saponify are observed.

In conclusion we wish to thank K. D. Tammik and V. P. Zaginaiko, who did the experimental work for this research.

SUMMARY

1. It has been found that when a complex mixture of cyclanes and alkanes is oxidized, the former react with atmospheric oxygen at a higher rate.

2. The rate of oxidation of the cyclanes is linearly proportional to their initial concentration in the mixture to be oxidized.

3. Owing to the higher oxidation rate of cyclanes, a high percentage of secondary reaction products is always formed when they are oxidized.

4. The evolution of molecular water, observed when large masses of cyclanes are oxidized, may be due, principally, to condensation of the hydroxy acids and the formation of ethers.

5. At a certain value of the cyclanes' molecular weight, the yield of hydroxy acids may drop to zero during their oxidation, the formation of difficultly saponifiable ethers being a maximum.

LITERATURE CITED

[1] V. S. Varlamov. The oxidation of petroleum hydrocarbons. (1937).
[2] B. N. Dolgov. Catalysis in organic chemistry (1949).
[3] V. K. Tsyskovsky, Azerb. Petrol. Chem. 1949, 4.
[4] V.K.Tsyskovsky, J.Appl. Chem., 4, 1949.

Received February 28, 1950.

BLANK PAGE

BRIEF COMMUNICATIONS

THE THERMAL AND VISCOSIMETRIC ANALYSIS OF THE SELENIC ACID - WATER SYSTEM

A. F. Kapustinsky and A. N. Zhdanova

The D. I. Mendeleev Institute of Chemical Engineering, Moscow

The method of physico-chemical analysis is founded upon the theory of the structural unity of the composition - property diagram, elaborated by Kurnakov [1]. No final conclusions can be drawn regarding the nature of the interaction between a system's constituents from a study of only one property, that is why the present research is a natural extension of the preceding one. It deals with the thermal analysis and the viscosimetry of the system: $H_2SeO_4 - H_2O$.

Though the $H_2SO_4 - H_2O$ system has been explored thoroughly and repeatedly [2,3,4,5,6,7,8], little research has been done on the properties of aqueous solutions of the analog of sulfuric acid, selenic acid.

Cameron and Macallan [9] isolated selenic acid monohydrate, $H_2SeO_4 \cdot H_2O$, and determined its melting point (25° C). Metzner [10] states that this point is 15°C. Meyer and Aulich [11] later established that the melting point of this hydrate is 26° C.

The fusibility diagram of the $H_2SeO_4 - H_2O$ system was plotted by Kremann and Hofmeier [12]. These authors noted the formation of two selenic acid hydrates, namely, $K_2SeO_4 \cdot H_2O$, fusing at 26° C according to the findings of Cameron and Macallan and Meyer and Aulich, and selenic acid tetrahydrate, $H_2SeO_4 \cdot 4H_2O$, with a melting point of 51.7° C. Inasmuch as the research of all these authors, with the exception of Meyer and Aulich, was done nearly half a century ago, we resolved to make a new study of the fusibility diagram of the $H_2SeO_4 - H_2O$ system, using an improved method, and to investigate the system's viscosity.

EXPERIMENTAL

We have described the preparation of the selenic acid in our previous paper. The concentration of the original solutions of selenic acid was determined analytically by a volumetric method, involving titration with a 0.1 N solution of sodium hydroxide, using methyl orange as an indicator. The concentration of dilute solutions was determined from the weight of the added water. Repeatedly redistilled water and chemically pure Kahlbaum sodium hydroxide were used in making up the sodium-hydroxide solution.

In our exploration of the fusibility curve we employed the method described by Kapustinsky and Drakin [13]. The viscosity of aqueous solutions of selenic acid was measured with an Ostwald viscosimeter. The measurements were made at the standard temperature of 25° C, which was kept constant in a

thermostat to within 0.005°. The viscosimeter was calibrated with repeatedly redistilled water, the viscosity being expressed in relative units (the viscosity of water being taken as unity).

The results of our determination of the melting points of aqueous solutions of selenic acid are given in Table 1.

TABLE 1

Experimental Data for the Fusibility Curve of the H_2SeO_4 – H_2O System

H_2SeO_4 concentration, % by weight	Melting point, °C.	H_2SeO_4 concentration, % by weight	Melting point, °C.
2.96	-1.5	62.15	-54.1
4.65	-1.9	64.13	-52.9
7.12	-2.1	66.23	-51.5
8.09	-2.6	68.23	-51.9
9.79	-3.7	69.95	-53.7
10.86	-4.2	70.39	-55.5
14.36	-6.2	74.08	-48.5
16.58	-6.9	74.31	-44.3
18.80	-9.2	75.43	-42.6
21.63	-9.9	76.61	-29.8
23.27	-10.9	77.75	-19.5
25.19	-12.4	78.75	-20.0
28.44	-16.6	79.52	-14.2
30.88	-19.2	80.05	- 8.6
31.23	-20.5	80.45	- 6.6
33.11	-25.2	81.03	- 0.5
34.78	-25.8	82.38	7.4
40.17	-35.7	84.80	19.8
41.75	-45.5	86.85	24.7
42.44	-54.1	87.79	25.4
46.71	-70.5	88.97	23.8
47.76	-74.1	89.96	21.9
54.26	-71.6	90.39	13.9
55.60	-63.2	91.96	28.9
59.04	-58.0	97.60	50.8
59.89	-55.7		

Fig. 1. Fusibility curve of the selenic acid – water system.

A – Temperature, °C; B – concentration, per cent by weight. 1 – $H_2SeO_4 \cdot 4H_2O$; 2 – $H_2SeO_4 \cdot 2H_2O$; 3 – $H_2SeO_4 \cdot H_2O$.

Our fusibility curve for the H_2SeO_4 – H_2O system, plotted from these data, is reproduced in Fig. 1.

The melting point of anhydrous selenic acid, as established by Cameron and Macallan, agrees with our findings (Fig. 1). The liquidus curve coincides with the curve plotted by Kremann and Hofmeier for all concentrations, with the exception of the section for 70-78% selenic acid. In this section we have found, in contrast to the findings of Kremann and Hofmeier, a concealed maximum, close to the composition of the hydrate $H_2SeO_4 \cdot 2H_2O$, which has not been mentioned before in the literature.

Mixtures of selenic acid and water exhibit an extraordinarily great tendency to supercooling and the formation of a hyaline mass. Like Kremann and Hofmeier, we induced the crystallization of a mixture of selenic acid and water by introducing seed crystals of the respective selenic acid hydrate. Crystallization can sometimes be brought about by introducing the analogous hydrate of sulfuric acid into the chilled mixture. It was particularly difficult to bring about crystallization in the concentration range of 70-78% H_2SeO_4. Kremann and Hofmeier [12] have this to say about it: "Once the solution has reached the strength of 78.4% selenic acid, crystallization cannot be brought about even by introducing crystals of $H_2SeO_4 \cdot H_2O$, when more water is added." A similar phenomenon is observed when we explore the fusibility curve of the sulfuric acid – water system. Hulsman and Biltz [6] also noted that it was very hard to induce crystallization in the region approximating 65-75%, equivalent to the bihydrate ($H_2SO_4 \cdot 2H_2O$), the mass remaining semi-transparent and "opalescent". Although Hulsman and Biltz encountered crystallization difficulties at other concentrations, the difficulty of crystallization was particularly striking in this range. Gable, Betz, and Maron have made similar observations [8].

In some of our tests we have succeeded, though with great difficulty, in crystallizing a mixture of selenic acid and water in the specified concentration range, as may be seen from the shape of the heating curve, with the pronounced bend corresponding to the fusion of the mixture. These findings were used to plot the section of the curve extending from 70 to 78% H_2SeO_4, in which the peritectic point is clearly visible at 78.75% selenic acid and a temperature of -20°.

It should be noted that we apparently do not have a fully established equilibrium here, owing to the very high viscosity of these mixtures. It may be that the hidden maximum would be more pronounced in this part of the curve if equilibrium were attained. This type of phenomenon is common to high-viscosity systems [14]; Kurnakov [1] notes that the ability to crystallize diminishes at high solution viscosities, such as are typical of mixtures whose composition approaches that of a compound.

Hulsman and Biltz [6], in their study of the structural diagrams of the sulfuric acid – water system also observed the exceptionally high viscosity of strong solutions of sulfuric acid at low temperatures.

The present research has therefore established the existence of the following hydrate of selenic acid, $H_2SeO_4 \cdot 2H_2O$, in agreement with our preceding investigation.

The viscosity isotherm of the H_2SeO_4 – H_2O system is an S-shaped curve, such as is typical of a system with pronounced chemical interaction, resulting in the formation of several dissociated compounds [15,16].

The results of our determinations of the viscosity of aqueous solutions of selenic acid and the calculated derivatives of viscosity with respect to composition are listed in Table 2.

The viscosity isotherm is an example of an irrational diagram. Breaks are seen in the isotherm diagram, corresponding to the following hydrates:

$$H_2SeO_4 \cdot H_2O; \quad H_2SeO_4 \cdot 2H_2O \text{ and } H_2SeO_4 \cdot 4H_2O.$$

TABLE 2

Viscosity and Derivative of Viscosity With Respect to Composition of Aqueous Solutions of Selenic Acid

H_2SeO_4 concentration, % by weight	Viscosity, η	$\left(\frac{\partial\eta}{\partial p}\right)_t$
97.27	37.22	
94.33	37.07	0.051
92.36	37.08	0.004
90.31	36.16	0.447
89.25	35.29	0.816
88.25	33.83	1.472
87.23	32.11	1.676
83.37	24.27	2.033
81.38	19.82	2.230
80.34	17.92	1.838
79.34	16.40	1.514
77.33	13.49	1.399
74.14	11.21	1.028
71.00	7.92	0.730
68.95	6.89	0.500
67.45	6.15	0.408
65.99	5.60	0.378
64.92	5.40	0.186
63.92	5.03	0.369
63.02	4.75	0.324
60.98	4.26	0.242
57.88	3.72	0.173
52.90	3.07	0.129
46.97	2.53	0.091
41.81	2.21	0.062
36.70	1.92	0.055
30.77	1.68	0.041
25.36	1.51	0.031
20.71	1.39	0.024
14.11	1.23	0.024
9.12	1.13	0.020
4.23	1.06	0.015

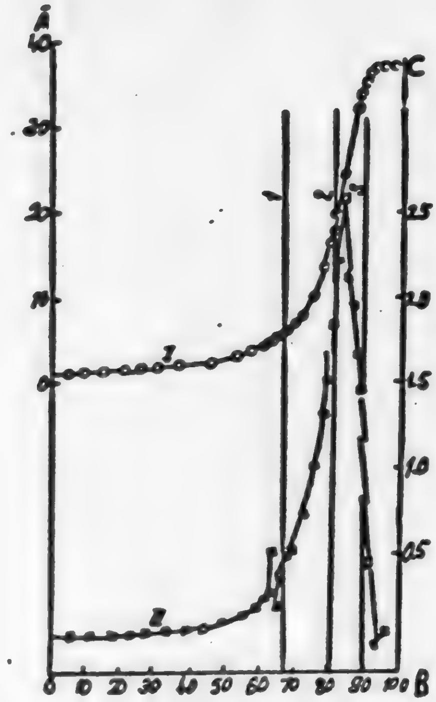

Fig. 2. Viscosity and derivative with respect to composition of aqueous solutions of selenic acid at 25° C.

A – Viscosity; B – H_2SeO_4 concentration, % by weight; C – the derivative $\left(\frac{\partial\eta}{\partial p}\right)_t$

I – Viscosity curve, II – curve of the derivative of viscosity with respect to composition.

1 – $H_2SeO_4 \cdot 4H_2O$; 2 – $H_2SeO_4 \cdot 2H_2O$, 3 – $H_2SeO_4 \cdot H_2O$.

The derivation of viscosity with respect to composition (in per cent by weight) $\left(\frac{\partial\eta}{\partial p}\right)_t$ exhibits the breaks at points corresponding to the stoichiometrical composition of these hydrates. Hence, the viscosity isotherm of the H_2SeO_4 – H_2O at 25° C, like the fusibility curve, indicates the formation of the following hydrates $H_2SeO_4 \cdot H_2O$ and $H_2SeO_4 \cdot 4H_2O$, and corroborates the existence of the hydrate $H_2SeO_4 \cdot 2H_2O$. Several isotherms would have had to be explored to determine the nature of these compounds. This was not done because of the specific experimental difficulties described in this paper.

SUMMARY

1. An investigation of the fusibility curve of the selenic acid – water system has disclosed that it coincides with the curve plotted by Kremann and Hofmeier except in the concentration interval of 70-78% H_2SeO_4, in which a concealed maximum, corresponding to the hydrate $H_2SeO_4 \cdot 2H_2O$, has been found.

2. An investigation of the viscosity isotherm of the H_2SeO_4 – H_2O system has borne out the data of the fusibility curve on the formation of the selenic acid hydrates H_2SeO_4 H_2O and $H_2SeO_4 \cdot 4H_2O$ and of the previously unknown hydrate $H_2SeO_4 \cdot 2H_2O$.

3. The findings we obtained in our previous investigation of aqueous solutions of selenic acid by the method of specific gravities of selenic acid solutions have been corroborated by the methods of thermal analysis and viscosimetry.

LITERATURE CITED

[1] N. S. Kurnakov. Introduction to physico-chemical analysis. USSR Acad. Sci. Press (1940).

[2] M. A. Pickering, J. Chem. Soc., 57, 331 (1890).

[3] E. V. Biron, Jour. Russ. Phys. Chem. Soc. 31, 517 (1898).

[4] Knietsch, Ber., 34, 4100 (1901).

[5] N. I. Podkopaev, Ibid. 44, 481, 1005 (1912).

[6] O. Hulsman and Biltz, Z. anorg. Chem., 218, 369-378 (1934).

[7] Bright, Hutchison and Smith, J. Soc. Chem. Ind., 65, 385-388 (1946).

[8] C. Gable, H. Betz, S. Maron, J. A. C. S., 72, 1445 (1950).

[9] C. A. Cameron and J. Macallan, Chem. N., 59, 232 (1889).

[10] R. Metzner, Comptes rend., 127, 52 (1898).

[11] J. Meyer and W. Aulich, Z. anorg. Chem. 172, 321 (1928).

[12] R. Kreman, F. Hofmeier, Sitzber. Akad. Wien, 117, 735 (1908).

[13] A. F. Kapustinsky and S. I. Drakin, Izv. Sect. Physicochem. Anal. 19, 256 (1949).

[14] G. B. Ravich, V. A. Volnova, and G. G. Tsurinov, Ibid. 19, 220 (1949).

[15] M. I. Usanovich, JGC 5, 701, 996 (1935).

[16] N. A. Trifonov. Bull. D. I. Mendeleev All-Union Chem. Soc. 1939, 9, 10.

Received July 21, 1950.

BLANK
PAGE

A CHROMATOGRAPHIC METHOD OF FINDING ADSORPTION ISOTHERMS, ISOBARS, AND ISOSTERES

M. I. Yanovsky

The fundamental chromatography equation makes it possible to calculate the adsoprtion isotherms from the desorption curve customarily recorded in chromatographic practice [1]:

$$\frac{V}{x} = M\frac{df(C)}{dc}, \qquad (1)$$

whence

$$f(C) = \frac{1}{Mx}\int_0^{C_0} V dc \qquad (2)$$

Here $\underline{V}$ is the volume of the solvent put through; $\underline{x}$ is the distance from the beginning of the column, in the direction of flow; $\underline{C} = \underline{C}\ (V, x)$ is the concentration of the sorbed substance in solution; $\underline{f}\ (\underline{C})$ is the adsorption isotherm, and $\underline{M}$ is the weight of a unit length of the layer.

When the relationship between the concentration of the substance $\underline{C}$ in the solution flowing out of the column and the volume of the solution put through is given as an experimental curve $\underline{C} = \underline{C}\ (\underline{V})$, the integral (2) becomes an area bounded by the curve $\underline{C} = \underline{C}\ (\underline{V})$, the concentration axis, and the ordinates $V_{C=C_0}$ and $V_{C=0}$. Using the expression (2) as it stands often involves considerable difficulty because of the great elongation of the chromatographic "tail" for well-sorbing substances. It is simpler to use graphic integration which consists, as we know in plotting a curve whose ordinates are proportional to the values of the given integral at the appropriate points. The essence of the method is evident from Fig. 1.

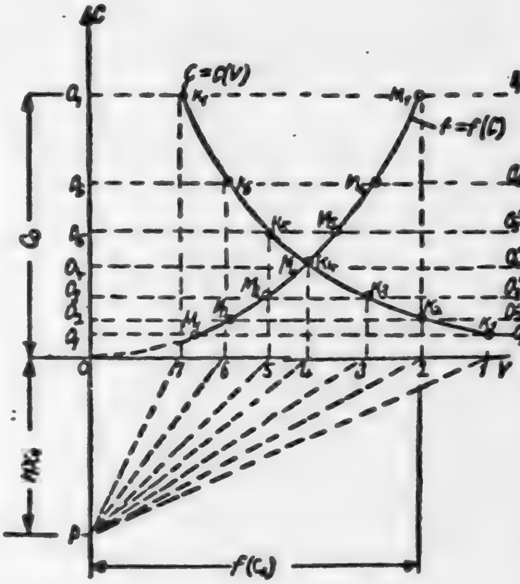

Fig. 1. Plotting the absorption isotherm from the experimental desorption curve.

Let us assume the desorption curve $C = C(V)$ has been recorded. We lay off on this curve a series of points $k_1, k_2, \ldots k_7$, the projections of which on the axes of ordinates and abscissas are $O_1, O_2, \ldots O_7$ and 1, 2, 3, ... 7, respectively. We lay off the length $OP = Mx_0$, equaling the column length in this case, below the point O. We call the length OP the "pole distance." From the point P we draw the rays $P - 1$, $P - 2$, $P - 3$, etc. Before starting our plot we have to pick some point through which the desired isotherm is to pass, say, the point with the ordinate $C = C_0$, where C_0 is the concentration of the substance at the formation of the adsorption ring, and the abscissa $f(C) = f(C_0)$ (the point M_7 in Fig. 1). We now begin the approximate plot of the isotherm. From the point M_7 we draw the straight line M_7M_6 parallel to $P - 7$ and thus having the slope $\frac{df(C_0)}{dC} = \frac{V_0}{Mx_0}$. The straight line interesects the horizontal O_6O_6 at the point M_6. Through the point M_6 we draw the straight line M_6M_5 $P - 6$ until it intersects the horizontal O_5O_5 at the point M_5, and so forth. The points $M_1, M_2, \ldots M_7$ will be points on the sought-for isotherm, since this isotherm passes through the fixed point $M_7[f(C_0), C_0]$, and the tangents to the isotherm at any concentration values will have slopes given by Equation (1). This method may be employed to secure as many points as desired. Connecting the points by a smooth curve yields a fairly accurate plot of the isotherm.

The initial section OM_1 of the isotherm $f(C)$ is found by extrapolation. To find the isobars or isosteres we have to record a series of desorption curves for $C = C(V)$ for various temperatures and plot the corresponding family of isotherms by the graphical method outlined above; as we know the families of isobars or isosteres may be readily plotted from the family of isotherms.

This plot is reproduced in Fig. 2. The desorption curves $C_{T_1}(V)$, $C_{T_2}(V)$ ... have been used to plot the corresponding isotherms $f_{T_1}(C)$, $f_{T_2}(C)$ ...for the different temperatures T_1, T_2 ..., $T_1 > T_2 > \ldots$ It is obvious that the intersections M_1, M_2, M_3 of the horizontals O_1O_1, drawn at some distance $C = C_1$ from the axis of abscissas, with the isotherms $f_{T_1}(C)$, $f_{T_2}(C)$ ... are points along the desired isobar $f_{C = C_1}(T)$. In the same way, we see from Fig. 2 that the intersections k_1, k_2, k_3 of the verticals O_2O_2 with the isotherms are points on the isostere $C_{f(C) = a} = C(T)$, representing the constant adsorbed quantity $f(C) = a$.

The converse problem of plotting the desorption curve $C = C(V)$ from a known adsorption isotherm is just as simple (Fig. 3). We divide the isotherm into an arbitrary number of sections Ok_1, k_1k_2, k_2k_3... Through the points k_1, k_2 ... we draw the parallel lines $1 - 1'$, $2 - 2'$, $3 - 3'$, and so forth. We also draw the tangents k_7k_7', k_6k_6', k_5k_5' ... to the isotherm at these points. We lay off the pole distance $OP = Mx_0$ along the concentration axis to the left of O. From P we draw rays PO_1, PO_2, PO_3 so as to make $PO_1 \parallel k_1k_1'$, $PO_2 \parallel k_2k_2'$, and so forth.

Through the point O_7 we draw a straight line parallel to the axis of abscissas until it intersects the vertical $7 - 7'$ (the point M_7). In the same way we draw through O_6 a parallel until it cuts $6 - 6'$ (the point M_6), and so forth. It is readily seen that M_1, M_2 are points on the desorption curve $C = C(V)$, inasmuch as for the several values of concentration C_1, C_2, C_3, the volumes V_1, V_2, V_3 ... will have values that are fixed by Equation (1).

$V_1 = x_0M \frac{df(C_1)}{dc}$, $V_2 = x_0M \frac{df(C_2)}{dC}$, and so forth.

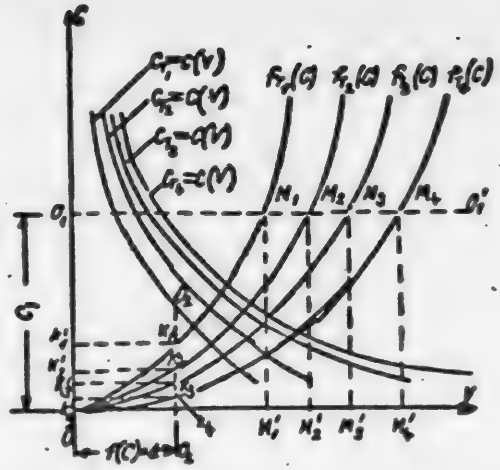

Fig. 2. Construction of adsorption isobars and isosteres from a family of desorption curves recorded at various temperatures.

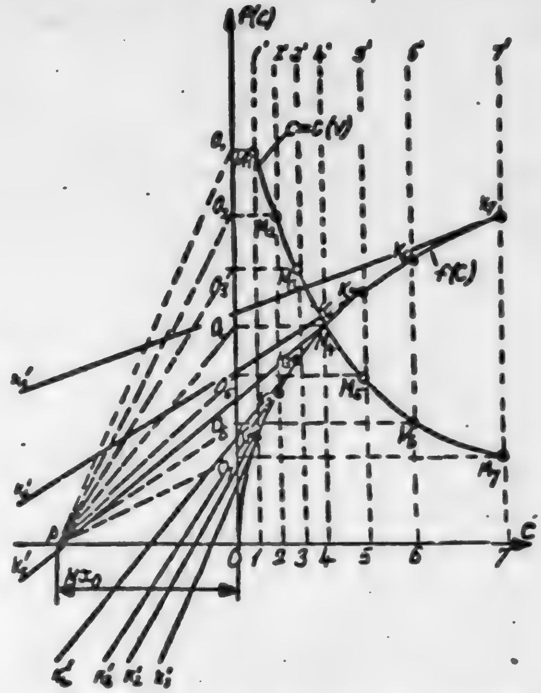

Fig. 3. Graphical method of finding the desorption curve from a given adsorption isotherm.

In the construction of the above graphs we assumed that the length of the adsorption column was the same as that of the adsorption zone, in other words, that the column was completely "spent" at the given concentration $\underline{C} = \underline{C}_0$.

Much more important in chromatographic practice, however, is the case where the length of the adsorption zone, $\underline{Mx}_0$, is much less than that of the column $\underline{Mx}$. The graphic method may again be used to make a rapid analysis of the effect of the principal parameters upon the course of the chromatographic process. Let us determine, for example, how the distribution of the adsorbed substance varies throughout the length of the layer during chromatographic adsorption. It is assumed that we know the adsorption isotherm $\underline{f}(\underline{C})$ (Fig. 4), as well as the volume $\underline{V}_0$ of the solution initially put through until the ring first appears, and the initial concentration $\underline{C}_0$ of the sorbed substance in this solution.

In the isotherm graph we find the point $\underline{M}_0$ with the ordinate $\underline{f}(\underline{C}) = \underline{f}(\underline{C}_0)$, corresponding to the given concentration $\underline{C}_0$. We lay off the axis $\underline{O} - \underline{Mx}$ to the left of the point $\underline{O}$. On this axis we lay off the length $Mx_0 = \dfrac{V_0 \cdot C_0}{f(C_0)}$, which is evidently the initial length of the adsorption zone. Then $\underline{P}_0\underline{P}_0'\underline{A}_1\underline{O}$ represents the initial distribution of the adsorbed substance in the column at the onset of chromatographic adsorption. We are required to find the distribution of the substance at the time the forward edge of the adsorption column is shifted to the end of the column, $\underline{Mx}_1$ long.

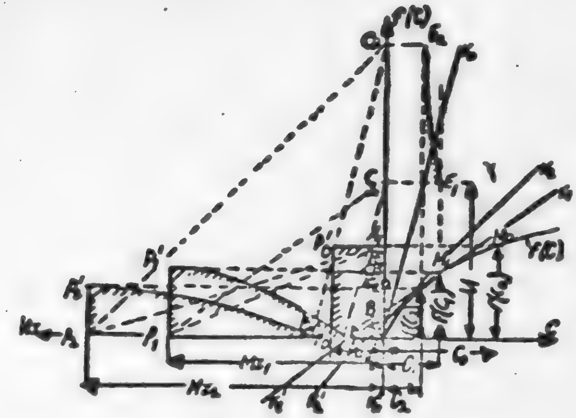

Fig. 4. Separate stages of the "appearance" of the chromatographic ring in a long column.

We draw the auxiliary line PA_1. Through P_0 we pass P_0B_1, P_1A_1. From B_1 we draw k_1k_1' tangent to the isotherm f (C). The ordinate $OE_1 = f(C_1)$ of the point of tangency M_1 is the sought-for value of adsorption at the point Mx_1. To determine the volume of solvent V_1 required to shift the forward edge of the adsorption column to the point Mx_1 we pass the straight line P_1C_1 k_1k_1' through P_1 until it meets the axis of ordinates. The length OC_1 is the desired value of V_1.

To determine the length OD_1 of the column section from which the substance is completely desorbed as the result of the passage of the solvent volume V_1, we draw C_1D_1 from the point C_1 parallel to the tangent k_Hk_H' at the origin of the isotherm ($C = 0$). The length OD_1 is the desired length of the column section. Thus, $P_1P_1'D_1$ roughly represents the distribution of the sorbed substance along the length of the layer. Let us check the correctness of this construction.

We see from Fig. 4 that

$$P_1P_1'E_1O = OD_1P_1'E_1 + P_1P_1'D_1 \tag{3}$$

$$P_1P_1'E_1O = Mx_1 f(C_1); \tag{4}$$

$$OD_1P_1E_1 = \int_0^{f(C)} Mx_1 df(C) = Mx_1 \int_0^C \frac{df(C)}{dC} \cdot dC = Mx_1 \frac{df(C)}{dC} \cdot C_1, \tag{5}$$

$$P_1P_1'D_1 = Mx_\partial f(C_\partial) \tag{6}$$

(since all the substance distributed through the layer must be uniformly adsorbed in the column at the start). Substituting (4), (5), and (6) in (3), we get

$$Mx_1 f(C_1) = Mx_1 \frac{df(C_1)}{dC} \cdot C_1 + Mx_o f(C_o),$$

whence

$$\frac{x}{x_o} = \frac{Mx_o f(C_o)}{f(C) - \frac{df(C)}{dC}} = \frac{OA_1}{OB_1} \qquad (7)$$

This expression (7) follows from the similarity of the triangles OP_1A_1 and OP_oB_1. Thus the point Mx_1, determined by the foregoing construction, satisfies Equation (7). It may be shown just as readily that OC_1 is actually the volume V_1. In fact, it follows from (1) that $V = Mx \frac{df(C)}{dC}$. This relationship between V and x is satisfied in the construction. It also follows from (1) that $OD_1 = V \Big/ \left(\frac{df(C)}{dC}\right)_{C=O}$, so that the length OD_1 actually gives the length of the column section that is wholly free of the adsorbed substance. By plotting the same diagram for a longer layer one can obtain a clear idea of the gradual evolution of the chromatographic ring as it makes its appearance (see the construction for $x = x_2$ in Fig.4).

It follows from Fig.4 that this method can yield the shape of the resulting desorption curve $C = C(V)$ Without going into a detailed exposition of this, we shall merely make the following comments. As long as the volume of solvent put through $V < V_1$, the concentration of the sorbed substance in the solution exiting from a column Mx_1 long will obviously be zero. When $V = V_1$, the concentration jumps to C_1. Thus the point E_1 in Fig.4 is the first point on the desorption curve for a column Mx_1 long. For a column with a length of Mx_2, the initial point would be E_2, etc. It follows that the curve $E_1, E_2, \ldots$ is the geometrical locus of the maxima on the desorption curves of columns of various lengths for a given quantity of the initially sorbed substance $m_o = V_oC_o$.

In Fig. 4 we are dealing with a case in which the column length is much greater than the initial distribution Mx_o. If the difference between the column length Mx_1 and Mx_o is not very great, the construction described changes somewhat, as is seen in Fig.5.

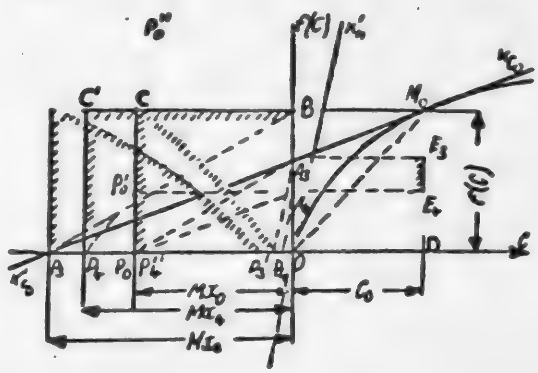

Fig. 5. Initial stage of the "appearance" of the chromatorgraphic ring.

We begin by connecting the point $M_0[f(P_0); C_0]$ to the origin $\underline{O}$. We then pass P_4P_0 through $\underline{P}_4$. This intercept is the desired value of the volume $\underline{V}_4$ required for the forward edge of the adsorption ring to shift to the point $\underline{P}_4$. Through $\underline{A}_4$, which is the projection of $\underline{P}_0$ upon the axis of ordinates, we pass $A_4P_4 \parallel k_Hk_H'$, where k_Hk_H' is the tangent to the isotherm at its origin. The intercept $\underline{OP}'_4$ is the length of the layer that is wholly free of the adsorbed substance. Through $\underline{A}_4$ we also draw A_4P_4 $k_{C_0}k'_{C_0}$, where $k_{C_0}k'_{C_0}$ is tangent to the isotherm at the point $\underline{M}_0$. The intercept P_4P_4'' is the region in which the adsorption substance is distributed uniformly, while P_4 P'_4 is the region of variable distribution. As the adsorption ring advances, the region of uniform distribution gradually grows smaller until the distribution area vanishes completely at the point $\underline{P}_3$ with the abscissa $\underline{Mx_3}$, as shown in Fig.5. The subsequent evolution of the adsorption ring is shown in Fig.4.

The similarity of the triangles OM_0D and $P_4P'_0P_0$ makes it easy to prove that this construction is correct.

$$\frac{Mx_4 - x_0}{P_0P'_0} = \frac{C_0}{f(C_0)} \tag{8}$$

or since

$$P_0P'_0 = V_4,$$

$$M(x_4 - x_0)f(C_0) = V_4C_0 \tag{9}$$

This same equation may be derived from the material balance of the process. Therefore, the intercept P_0P_0' actually is the volume $\underline{V}_4$. Moreover, from (1) the location of the point $\underline{P}_4''$ is given by the equation $x_4 = V_4 \Big/ \frac{df(C_0)}{dC}$ (10), so that if we draw a straight line from $\underline{A}_4$ parallel to the tangent at the point M_0, the intercept $\underline{OP}_4''$ will satisfy Equation (10). Similarly $x_4 = V_4 \Big/ \left(\frac{df(C)}{dC}\right)_{C=0}$ (11), and hence $\underline{OP}_4'$ actually satisfies Equation (11).

In conclusion, it should be said that notwithstanding the convenience and graphic clarity of the method described, its accuracy is wholly determined by the precision of graphic differentiation, which is usually rather low, so that it can be used for rough, approximative calculations.

LITERATURE CITED

[1] E. Gluckauf, Nature, 156, 748-9 (1945).

[2] Smirnov. Treatise of higher mathematics (1948).

Received March 18, 1950.

THE REDUCTION OF CUPRIC OXIDE WITH HYDROGEN

M. M. Pavlyuchenko and Ya. S. Rubinchik

The reduction of cupric oxide with hydrogen is one of the reactions that take place at the boundary of three phases: a gaseous and two solid phases. Hence, an investigation of how this reaction occurs is also of importance in shedding light upon the mechanism involved in other reactions that take place at the boundary of these phases.

Although several papers have dealt with the reduction of cupric oxide [1,2,3], some of the important problems involved in knowing how the reaction occurs remain unclear. One of them is so important a question as the part played by the solid product, copper, in the autocatalysis of the reaction. It has been accepted that the increase in the velocity of topochemical reactions with time is due to the catalytic action of the solid product of the reaction [4,5]. One of the present authors [6] has shown that the autocatalysis of topochemical reactions is the result chiefly of the structure of the initial solid product and may be totally unrelated to the solid product of the reaction. Research on the reduction of cupric oxide from this point of view would be of indisputable interest. In planning the present research we had in mind learning, if possible, the part played by the solid product, copper, in the autocatalysis of the reaction.

According to the literature, there are two points of view regarding the reduction of metals, including copper. Some research workers [7] believe that the reduction involves dissociation of the oxides into the metal and oxygen and that the reducing agents H_2 and CO merely accumulate the oxygen in the gaseous phase, thus shifting the equilibrium in the direction of dissociation. Others [3,8,9] state that reduction does not depend upon dissociation, but involves the reducing agents adsorbed at the surface of the oxides.

Another objective in our investigations was an experimental determination of the part played by dissociation of cupric oxide in the reduction process.

EXPERIMENTAL

Copper oxide was produced in three ways: precipitation with alkali from a solution of copper sulfate, calcination of cupric nitrate, and oxidation of electrolytic copper wire. The oxide was prepared by precipitation with alkali by the method described in the book by Karyagin [10]. In preparing the oxide by calcination, we took triply recrystallized cupric nitrate and calcined it at 600° C for 4 hours. In the last method, the electrolytic copper was heated in air to about 600° C for 20 hours. The hydrogen was produced in a Kipp generator by the action of sulfuric acid upon zinc. It was purified by passing

it through a solution of potassium bichromate in sulfuric acid, through metallic copper chips heated to 300° C, and then through a U-shaped tube filled with anhydrous calcium chloride.

In contrast to Pease and Taylor [1], who employed the dynamic method in exploring the reaction rate, we adopted the static method. The reaction rate was determined by the amount of hydrogen (in cu cm) used to reduce the cupric oxide per unit time. The hydrogen pressure was measured by means of a mercury manometer sealed into the apparatus, and was kept constant during the run. The amount of reacted hydrogen was determined by the change in level of the mercury in the buret.

The reaction vessel, containing a weighed sample of the cupric oxide, was placed in a thermostat, the temperature of which was held constant to within ± 0.6° C. A sample of cupric oxide weighing 0.08 g was placed in an ampoule, which was lowered to the bottom of the reaction vessel. Calcined calcium chloride was placed at some distance from the ampoule, extending as far as the ground-glass connection, to trap the water evolved during the reaction. The calcium chloride was separated from the reaction space by a glass partition that contained minute holes in its side through which the gas could pass freely but which kept back the calcium chloride. The cupric oxide in its ampoule was placed in the reaction vessel, then the partition was put in place, and a layer of granulated calcium chloride was poured in. The air was evacuated from the apparatus by means of a vacuum pump until the pressure was 10^{-1} mm. Evacuation lasted 15 minutes at the temperature of the test to remove adsorbed gases and vapors. After a preliminary run, the valve was closed, and the apparatus was filled with hydrogen until the desired pressure was reached. The time at which the hydrogen filling was complete was taken as the start of the run. The buret was read every 5 or 10 minutes, etc., depending upon the reaction rate.

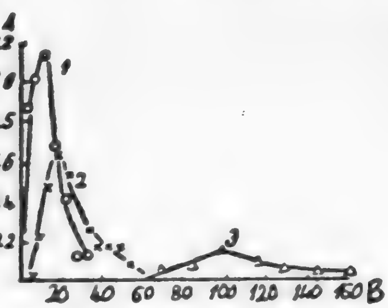

Fig. 1. Variation of the reaction rate in the reduction of cupric oxide with time at 201° C and P_{H_2} = 714 mm.

A – Reaction rate, cu cm/ min; 2 – for cupric oxide produced by calcination of a salt; 3 – for cupric oxide produced by oxidizing copper in air.

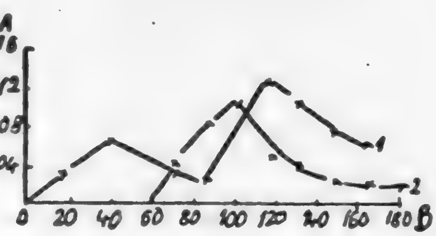

Fig.2. Reduction rate of cupric oxide with hydrogen as a function of time when mercury and its vapor are present.

A – Reaction rate, cu cm/min; B – time, minutes. 1 – Mercury vapor; 2 – liquid mercury.

The curves 1, 2, and 3 reproduced in Fig. 1 give the reaction rate of

reduction as a function of time at 201° C and P_{H_2} = 714 mm for cupric oxides prepared by three methods: precipitation with alkali (1), calcination of a salt (2), and oxidizing copper in air (3). As we see, the cupric oxide produced by the first method was reduced most rapidly, followed by that produced by the second method, and last that by the third method. In the last case, reduction involved an induction period lasting 60 minutes. The reaction took more than 5 hours after the induction period, whereas the cupric oxides produced by the first and second methods were reduced within 40 and 70 minutes, respectively. As we see it, the difference in the reduction rates is due principally to the dimensions of the crystals of the original substance. The most coarsely crystalline product was produced by oxidizing copper. Its color was gray, whereas the product secured by precipitation was dark-brown and more finely disperse. The reaction rate of the oxide produced by calcining the salt increased 100 per cent after pulverization, whereas the reaction rate was quadrupled for the oxide produced by oxidizing the copper wire, and the induction period vanished.

The mean reduction rate of the pulverized and unpulverized oxide obtained by oxidizing copper varies irregularly as the temperature is raised. At 235° C 80% of the unpulverized cupric oxide is reduced within 105 minutes, the same percentage of the pulverized oxide being reduced in 90 minutes. No induction period was observed in either case. The maximum rate in the former case was $3 \cdot 10^{-1}$ cu cm/min, and in the latter $2.5 \cdot 10^{-1}$ cu cm/min.

Thus, the temperature coefficient of the reduction of an oxide produced by a single method depends upon the degree of dispersion of the product. Raising the temperature 34° C increased the mean reduction rate 280% for the unground oxide, and only 50% for the ground oxide. It seems to us that the slight increase in the reduction rate of the ground oxide as the temperature is raised is due to the fact that diffusion of the hydrogen to the place of reaction plays an essential part in the reaction. The rise in the reaction rate with time indicates that the reaction does not begin all over the surface of the crystals, but sets in at individual points and then spreads out into the crystal. The rate of its spread is not the same in all directions, depending upon the crystallographic direction involved. The reaction rate rises to maximum as it crosses certain zones, and then drops off. If the reaction occurred at the boundary between two adjacent solid phases, copper – copper oxide, and the copper exercised a catalytic effect, the presence of the maximum boundary surface between the two phases in the initial product ought to make the reaction rate a maximum at the very outset.

We made the following tests to test the influence of the boundary upon the rate of reduction. Reduced copper powder was oxidized, partially or completely, and then triturated. The amount of oxygen consumed in oxidizing the copper, as well as the oxidation rate, were determined by the same method as used for the reduction rate. Oxidation was done at about 250° C and could be stopped at various copper – oxide ratios. We thus secured a product containing 20, 30, 40, 60 and 100% of copper oxide and 80, 70, 60, 40 and 0% of copper. The copper was in close contact with the oxide formed, being separated from the latter by the boundary surface. Thus we could secure different boundary surfaces, depending upon the degree of oxidation, so that the reaction involved in the reduction of the oxide should have taken place at different rates. No matter whether the oxidation reaction sets in at individual points on the surface

or simultaneously all over the surface of the crystals, in the reduction reaction we should find the reaction rate to be inversely proportional to the time. If the copper begins to oxidize simultaneously all over its surface, during reduction the boundary will shift to the surface itself and will increase until practically all the oxide is reduced. Hence, the reaction rate ought to rise until all the oxide is reduced. If the reaction begins at separate points on the face, the boundary surface will grow during reduction until the oxidation reaction zones are crossed, when it diminishes. Thus, whereas the maximum reaction rate should occur at the onset of the reaction during oxidation, it should lie at the end of the latter during reduction, and vice versa.

In our study of the reduction of partially oxidized copper we always took a sample that contained 0.04 g of the oxide. The reaction rate was the same, within the limits of experimental error, for all the samples, being unaffected by the degree of oxidation of the copper. The curves had the same shape as those secured for the reduction of the oxides produced by calcining a salt and by precipitation with an alkali. These tests lead us to believe that the growth of the reaction rate observed during our experiments is unrelated to the catalytic action of the copper formed during the reaction. Nor did mixing cupric oxide with the product of its oxidation, copper, increase the reaction rate.

According to the literature [1], moisture greatly retards the onset of the reduction reaction. Once the reaction has set in, introducing water vapor into the reaction space does not affect the reaction rate. In our tests the water vapor was introduced into the reaction vessel via a ground-glass stopcock connecting the vessel to another containing water. The entrance of the water vapor into the reaction space could be shut off by turning the stopcock. The vessel containing water was immersed in a thermostat at various temperatures that did not exceed room temperature, so that various water vapor pressures could be secured.

We could observe no effect of water vapor at the start of the reaction or subsequently in tests made at 183° C at various water vapor pressures, using copper oxides produced by precipitation and by calcining a salt.

We were most interested in exploring the effect of mercury and its vapors upon the reaction rate

A sample of cupric oxide was placed in one ampoule, and mercury, ranging in weight from some tenths of a gram to a few grams, was placed in another ampoule. Both ampoules were placed in the reaction vessel. The cupric oxide was in contact with the mercury vapor. The tests were run at 203°C The results of one of these tests are represented by the curve 1 in Fig.2. The reaction rate is more than 10 times smaller when mercury vapor is present and passes through two maxima and a minimum.

In some tests the mercury was mixed directly with the cupric oxide in the reaction vessel. After the mixture had been stirred, the reaction vessel was placed in a thermostat, and the oxide was reduced. The results of one of the tests are shown in Curve 2 of Fig.2. The induction period was found to last some 60 minutes, while the reaction rate was about two-thirds of that in the tests using mercury vapor. The copper powder formed during the reaction amalgamated rather easily. We made use of this property to isolate the reaction product, the copper. After reduction was partially complete, the reaction was broken off by removing the hydrogen. Mercury was added to the reaction vessel,

and the copper produced dissolved in the mercury when stirred with it, the mercury being then removed together with the dissolved copper. The reaction rate, after this mercury processing was the same as when mercury vapor was present.

The sharp drop in the reaction rate in the presence of mercury vapor or liquid mercury seems to us to be due to the fact that the reduction reaction involves adsorbed hydrogen, so that the mercury adsorbed at the surface diminishes the adsorption of the hydrogen.

In this connection we ran tests to explore the effect of the hydrogen pressure upon the reaction rate. The tests were run at the following hydrogen pressures: 200, 350 and 700 mm mercury column. At these pressures there was little difference between the several reaction rates. These tests thus indicate that the reaction involves adsorbed hydrogen, the mercury affecting adsorption considerably and thus obviously affecting the reaction rate.

Evaluation of Results

The reduction of cupric oxide is a reaction in which the crystal lattice of the initial product is disrupted, the crystal lattice of copper being formed. The process involved in the reduction of the oxide and in the formation of crystalline copper may be represented by the following equations:

$$CuO_{cryst.} + H_2 = Cu_{gas} + H_2O + \bar{Q}_1, \tag{1}$$

$$Cu_{gas} = Cu_{Cryst.} + \bar{Q}_2. \tag{2}$$

The latent heat of sublimation of copper, $\bar{Q}_2$, is 81,000 Cal. The heat evolved in the reaction $CuO_{cryst.} + H_2 = Cu_{cryst.} + H_2O$ is 31,300 Cal. Subtracting we find the heat absorbed in the reaction (1) will be 49,700 Cal. The energy of crystallization of copper cannot be utilized to activate the CuO molecule, since the copper is spatially separated from the cupric oxide. Hence, the activation energy of the reaction will at least equal the heat absorbed in the reaction, i.e., 49,700 Cal.

The conversion of the copper into the gaseous phase, followed by its conversion to the crystalline state as specified by Equation (2) seems hardly likely to us, since the former process is highly endothermic, and the energy of the second one cannot be utilized for the first one. It is evident, therefore, that the formation of greater supersaturations of copper in the gas phase, as some researchers assume [11], is not very likely. It is more advantageous, from the energy standpoint, when the resultant copper atoms remain in the two-dimensional space as adsorbed atoms. The heat absorbed in the endothermic reaction (1) is increased by the energy of interaction between the copper atoms and the copper oxide lattice.

Inasmuch as the reaction rate is hardly affected by the hydrogen pressure, the reaction must involve adsorbed hydrogen. This leads us to think that the reaction takes place as follows:

$$CuO + H_2 = CuOH_{2\,ads.} \tag{3}$$

$$CuOH_{2\,ads.} = Cu_{ads.} + H_2O, \tag{4}$$

$$Cu_{ads.} = Cu_{cryst.} \tag{5}$$

The mercury vapor adsorbed at the surface blocks the active centers, resulting in a diminution of the reaction rate. Our findings on the effect of mercury vapor and hydrogen pressure indicate that copper oxide is reduced by adsorbed hydrogen and does not depend upon the entrapment in space of the oxygen evolved during dissociation.

SUMMARY

1. A study has been made of the kinetics of reduction of cupric oxide by hydrogen in the 159-235° C range, the oxide being produced by three methods. The reaction rate was found to increase with time in every case, passing through a maximum and then dropping off.

2. A study has been made of the reduction of cupric oxide, in which a boundary surface between the initial product and the reaction product was established by oxidizing copper powder before the start of the test. The tests did not show that the copper had any effect upon the reaction rate.

3. It has been established that moisture has practically no effect upon the reaction rate.

4. A study has been made of the effect of liquid and vapor mercury upon the reaction rate. It was found that mercury greatly retards the reduction reaction.

5. The rate at which cupric oxide is reduced is only slightly affected by the hydrogen pressure in the 200-700 mm mercury column range. The reduction reaction involves adsorbed hydrogen.

LITERATURE CITED

[1] J. Pease, H. Taylor, J.A.C.S., 43, 2179 (1921).

[2] A. Larson, F. Smith J.A.C.S., 47, 346 (1925).

[3] E. Tatievskaya and G. Chufarov, Izv. USSR Acad. Sci. Div. Tech. Sci. 1946, 7, 1005 .

[4] G. Schwob, E. Pietsch, Z. Elektroch., 35, 573 (1929).

[5] M. Volmer, Z. Elektroch., 35, 555 (1929).

[6] M. Pavlyuchenko, J. Phys. Chem. 23, 800 (1949); J. Phys. Chem. 23, 809 (1949).

[7] A. Lyuban, Izv. USSR Acad. Sci., Div. Tech. Sci. 1943, 9-10.

[8] P. Geld and O. Esin, Izv. USSR Acad. Sci., Div. Tech. Sci. 1946, 6.

[9] B. Averbukh and G. Chufarov, J. Phys. Chem. 23, 37 (1949).

[10] Yu. Karyakin. Pure chemical reagents, 339 (1947).

[11] J. Okayama, Z. Elektroch. 34, 294 (1928).

Received January 20, 1950.

A NEW METHOD OF FORMING THIOINDIGO ON FIBER

V. M. Rodionov, B. M. Bogoslovsky, and Z. S. Kazakova

Laboratory of Dye Chemistry, Moscow Textile Institute

Thioindigo and its derivatives, which possess exceptional fastness to light and chlorine and exhibit good results in tests of other types, have remained important down to the present time. Neither the high price of thioindigo nor the difficulties of dyeing, which are well-known to every dyer and are characteristic of all vat dyes in general, has interfered with this position. Printing with indigoid dyes is not as complicated, to be sure, as their use in unfigured dyeing, but even in printing various difficulties crop up, which often result in spoilage or even in the scrapping of the goods.

In view of the difficulty of printing with indigoid dyes, several methods of applying the dye to the fiber have been proposed at various times, starting directly from the intermediates. The firm of Kalle, for example, placed on the market a compound of the following structure under the name of indigo salt:

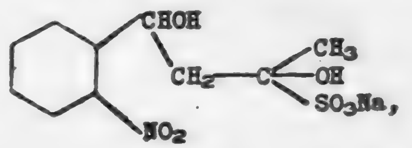

which was rather widely employed at one time for the forming of indigo directly on the fiber. But this product, which required 2-nitrobenzaldehyde for its formation, can be permanently successful only if the cost of production of the latter compound is low, which is not yet the case, as we know. Thus it is not surprising that the subsequently developed indigosols (vat sols), which were sodium salts of bisulfate esters of leuco compounds of vat dyes, were able to displace the indigo salt quickly. Yet, though they possessed a number of positive qualities, among them: dyeing by simple immersion, even and deep dyeing of the fabric, resulting in the color's high resistance to rubbing; the absence of an alkaline medium for dyeing or printing, thus making it possible to employ vat sols for dyeing and printing woolens, vat sols are not free from some very serious disadvantages. The latter include the relatively slight solubility of some vat sols in water, and the high cost of all vat sols, without exception. These factors greatly limit the application of these sols in production, so that they are important only in fabric printing. In the light of all this, we set as our objective the synthesis of compounds from the most easily available intermediates that could be readily converted into thioindigo after they had been applied to the fabric, thus providing a new, cheap, and convenient method of printing thioindigo for the textile industry.

In our research we started with 2-acetyl-3-hydroxythionaphthene, fairly simply synthesized from domestic raw materials, which, as V. M. Rodionov has shown, can be converted, once it has been applied to a fabric together with a thickener, into thioindigo by saponifying the acetyl group, followed by oxidation. But as the conditions governing the splitting out of the acetyl group had not been worked out with sufficient precision at the time, the thioindigo yield was extremely low. Because of this, large amounts of 2-acetyl-3-hydroxynaphthene had to be added to the thickener to achieve an adequate coloristic effect, which made the new printing method of little practical interest. In our research we made a study of the properties of this compound and managed to find a method of quickly and readily splitting out the acetyl group and to work out a method of dyeing and printing with thioindigo, starting out with 2-acetyl-3-hydroxynaphthene. The optimum procedure for saponifying the acetyl group was found to be using a 5% solution of sodium hydroxide, the process being most rapid, according to our observations, at the outset, after which the rate at which the acetyl group is split off falls rapidly. After finding favorable conditions for saponification, we tested the possibility of using it for immersion (unfigured) dyeing and for printing. In the immersion dyeing of fabrics we employed a solution of 3 g of 2-acetyl-3-hydroxythionaphthene in 100 ml of a 5% solution of sodium hydroxide and 5 ml of alcohol. Immersion dyeing lasted 3 minutes at 80°, followed by wringing, drying, steaming for 5-15 minutes, processing with an oxidant – potassium ferricyanide, washing, and drying. Tests in which the oxidizing agent was introduced into the immersion bath indicated that this made it possible to increase the intensity of dyeing, but the samples invariably proved to be heavily soiled, the staining being hard to remove with Turnbull's blue. Adding a catalyst (10 g per liter) to the immersion bath increased the depth of dyeing somewhat. It should be noted that an attempt to substitute other oxidants (H_2O_2, hypochlorite, sodium chlorite, chloramine-T) for the potassium ferricyanide was unsuccessful.

In checking the feasibility of using 2-acetyl-3-hydroxythionaphthene for textile printing we employed a printing ink containing 50 g of 2-acetyl-3-hydroxythionaphthene and 50 g of sodium hydroxide per kilogram of ink. After printing, the samples were dried and treated with potassium ferricyanide. Parallel tests were run in which the oxidizing agent mentioned was added to the printing ink. When this was done, the samples were steamed and then washed for 20 minutes at 80° in a soap solution (3 grams per liter). The same result may be obtained by washing in an acid bath (10 grams of hydrochloric acid per liter, 60°, 15 minutes).

The most intense coloring of the pattern was secured when the potassium ferricyanide was added to the printing ink, though it was then somewhat duller

SUMMARY

1. Our research indicates that our proposed new method of dyeing and printing with thioindigo has proved its worth on a laboratory scale.

2. Certain refinements may be required when the proposed method is used under factory conditions.

Received June 6, 1950

DEVELOPMENT OF A PROCESS OF OXIDATION AFTER A CATALYST HAS BEEN REMOVED FROM THE REACTION ZONE[1]

V. K. Tsyskovsky and N. A. Kiseleva

In our preceding reports we have shown that the catalyst was converted from the quasiherterogeneous (microheterogeneous) state into a herterogeneous state by the action of the reaction products during the oxidation process.

On the basis of the classical concepts [1], according to which a catalyst is able to sorb atmospheric oxygen on its surface during oxidative reactions, producing a complex of intermediate compounds of the peroxide type, it may be assumed that this process would comtinue even when the catalyst was converted into the heterogeneous state. In that case intermediate complexes ought to be formed as long as the catalyst is present in the reaction zone, irrespective of its physicochemical state. As a matter of fact, despite the transition of the catalyst from the quasihomogeneous to the heterogeneous state and the reduction of its active surface by several hundred per cent, the oxidation reaction rate and its course were not affected.

When the catalyst was converted into the heterogeneous state, its active surface was represented by a thin layer of low-molecular metallic salts that settled on the walls of the reactor in the liquid-phase zone and was infinitesimally small compared to the surface of the active particles of the colloidal catalyst. Moreover, the concentration of the active metal in this layer was no longer the same as at the outset, being thousands of per cent smaller (which explains the precipation of the bulk of the modified catalyst).

This, it seemed, was further proof that the catalyst continued to operate after it had become heterogeneous, as if no changes had occurred in its state. None the less, the constancy of the reaction rate and of the course of the reaction does not agree logically with a decrease in the active surface of the catalyst and, hence, with a decrease in the quantity of intermediate complexes formed at that surface. It might have been supposed, in turn, that the active, accelerating action of catalysts ceases in general as soon as they have been converted into a heterogeneous state.

After that, the modified catalyst, which was heterogeneous with respect to its susbstrate, would no longer be able to affect the subsequent course of the oxidation reaction at all and thus could be regarded as an inert substance without any catalytic properties in the given case.

Only the last of these assumptions could be confirmed experimentally. This was done by making two experiments.

In one, oxidation was continued until a certain stage, the modified

1) Report III of a series on the action of colloidal quasiheterogeneous catalysts in the liquid-phase oxidation of kerosene fractions.

catalyst remaining in the substrate to be oxidized until the end of the reaction. In the other, the substrate was oxidized (under the same conditions) until the catalyst had been transformed into a new state, after which the modified catalyst was removed and oxidation of the substrate was continued.

The first experiment was run in the usual manner, while the second one was carried out as follows.

The substrate was oxidized with the catalyst in a glass reactor fitted with a photo-electric cell [2], so that the change in the state of the catalyst could be continuously recorded photocolorimetrically.

When the relative light absorption $\left(\log\frac{I_0}{I_1}\right)$ became a minimum (an indication of the complete replacement of the radical in the high-molecular salt), the oxidation reaction was stopped. The oxidized substrate was discharged from the reactor, cooled, and filtered through a No. 4 porous filter, all the modified catalyst filtering out as a crystalline substance. Not even a trace of the catalyst cation was found in the filtered substrate by spectographic analysis. The filtered substrate, perfectly free of the catalyst, was then oxidized anew under the same conditions as before.

In this test, the total time consisted of two separate intervals: from the onset of oxidation until the emptying of the reactor, and from the recharging of the substrate to the end of the process. This aggregate time equaled the length of the run in which the substrate was oxidized with removal of the catalyst.

When we compare the results of the two tests of oxidation of the same substrate for the same length of time, we readily see that there has been no change in the quantitative results of the reaction (see Table).

End Result of the Reaction Involving Oxidation of a Substrate With the Catalyst Present to the End of the Reaction and With the Catalyst Removed After It had Acquired New Physicochemical Properties

Oxidation conditions	Catalyst concentration, metal as % by weight of the substrate	Residue in the liquid phase after oxidation, % of the substrate	Yield of saponifiable oxidation products, % of the substrate
With catalyst present......	0.04	89.3	14.0
With catalyst taken out....		89.2	12.4
With catalyst present......	0.08	95.5	17.5
With catalyst taken out....		95.7	18.8
With catalyst present......	0.12	95.2	12.5
With catalyst taken out....		94.8	13.2

No appreciable difference in the reaction kinetics was perceptible in this case. A certain discrepancy between the numerical data (increase or decrease) was attributable to the known experimental error.

It is characteristic that the operation of removing the catalyst, involving cooling of the substrate and an interruption of oxidation, did not affect the end result of the experiment.

These experiments have shown that the elements of active catalysis are found only at the outset of the oxidation reaction, which develops thereafter along the given lines autocatalytically, without the catalyst participating.

By following the time changes in the peroxide number of the substrate to be oxidized (Fig. 1) we readily see that the kinetic process of oxidation develops in the same way when a catalyst is present (Curve 1) and after it has been removed from the sphere of reaction (Curve 2), which also explains, at the bottom the identical quantitative results obtained in the two cases. The same holds true when we examine the acid number curves of the substrate, oxidized with a catalyst present (Fig. 2, Curve 1) and then removed (Curve 2), which are also the same.

To exclude the suspicion that the subsequent course of the oxidation reaction involves the catalytic action of the acid products (as some researchers believe), we eliminated the latter from the substrate. This was done by filtering the substrate and then treating it with a 10% aqueous solution of sodium hydroxide until its acid number was zero. To eliminate the sodium ion completely the substrate was then treated with a 10% solution of HCl and washed with distilled water until all the Cl' ion was removed (as shown by a test with $AgNO_3$).

After this operation the peroxide number of the substrate dropped from 0.178 to 0.072.

The substrate subjected to oxidation (Fig. 2, Curve 3) was oxidized somewhat more slowly than in the first two instances. The only possible reason for this is a drop in the total of peroxide compounds.

Hence, this phenomenon enables us to divide the so-called "catalytic" oxidation process into two periods: an initial period of the primary state of the catalyst (or, as it used to be called, the induction period), *i.e.*, the period during which the oxidation reaction is controlled by the catalyst's action; and a second period characterized by the autocatalytic course of the reaction, via the peroxides (with no catalyst present), which exhibits a distinct chain character [3]. This second period may continue for an extraordinarily long time, until the reaction chains are broken by the influence of the wall or an inhibitor.

In its overall complexity, this process is sharply distinguished from the usual process, which is autocatalytic from the very outset (Fig. 1, Curve 3, and Fig. 2, Curve 4).

A very curious fact is the undoubted disproportionality between the acid and peroxide numbers. The accumulation of peroxides in the autocatalytic oxidation process apparently takes place more rapidly than the formation of acid compounds, the concentration of which at the start of the process is extremely small.

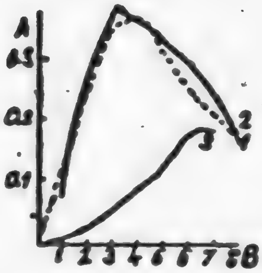

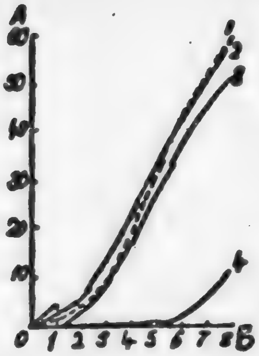

Fig. 1. Dynamics of the evolution of the peroxide numbers.

A – Peroxide number; B – Time, hours.

Oxidation conditions: 1 – with catalyst present; 2 – after removal of the catalyst; 3 – without a catalyst.

Fig. 2. Dynamics of the evolution of the acid numbers.

A – Acid number, mg of KOH per gram; B – Time, hours.

Oxidation conditions: 1 – with catalyst present; 2 – after removal of catalyst by filtration; 3 – after removal of catalyst and treatment of unsaponified constituents with 10% NaOH solution and 10° HCl solution; 4 – without a catalyst.

In the complicated process of joint catalysis the processes of formation of peroxides and acid products are more harmonious.

It may, therefore, be stated that in autocatalytic oxidation, the time during which peroxides are accumulated may be considered to be the induction period.

SUMMARY

1. The concept of a colloid quasiheterogeneous catalyst as a substance that constitutes intermediate complexes of the peroxide type with atmospheric oxygen and remains chemically unchanged itself until the end of the oxidation reaction must be regarded as obsolete.

2. Even if a catalyst should form intermediate compounds with atmospheric oxygen, it does so only at the outset of an oxidation reaction, for a period of time that is infinitesimally short compared to the overall reaction time.

3. An oxidation reaction develops catalytically at the start, but then evolves autocatalytically and exhibits a distinctly chain character.

LITERATURE CITED

[1] "Kinetics of catalysis", Jubilee Symposium of the USSR Acad. Sci., Vol. IV (1937).

[2] V. K. Tsyskovsky, J.Appl.Chem. 27, 7 (1950).[1]

[3] N. N. Semenov. Chain reactions (1934).

Received April 28, 1950.

[1]) See Consultants Bureau Translation, p. 797.

RUBBER VULCANIZATION

N. L. Nemirovsky

Despite the great practical importance of the vulcanizing of rubber, the fundamental process of the rubber industry, the nature of this process is far from certain.

At the present time the "bridge" theory of the formation of a three-dimensional structure is widely accepted and is the prevailing one. This theory asserts that during vulcanization the straight chain rubber molecules are linked together by a vulcanizing agent, forming a sort of sulfur or other "bridges" that "lace" the rubber molecules together, so to speak. The prevailing theory attributes the change in the physical and mechanical properties of rubber when acted upon by a vulcanizer to this constitution of intermolecular chemical bonds. The change in the physical and mechanical properties of rubber are explainable by the formation of three-dimensional structures of this sort. Various experimental findings are hard to reconcile with the "bridge" theory of rubber vulcanization, however.

EXPERIMENTAL

Vulcanization of natural rubber with iodine. The following rubber compound (parts by weight) was used in the tests of vulcanization with iodine:

Rubber (smoked sheets)	100	100	100	100	100	100
Iodine	0.1	0.5	1	3	5	7.5
Ethyl alcohol	10	10	-	-	-	-
$BaCO_3$	25	25	25	25	25	25

The solid iodine was ground in a porcelain mortar with baryta in order to effect more uniform distribution of the iodine throughout the rubber. At low iodine percentages (0.1-0.5%) alcohol was added. Mixing was done in mills using cold rollers. Heating was done in molds. The prepared compound was placed in the mold, using a slight excess to ensure that the mold was well filled and to facilitate the maximum displacement of atmospheric oxygen from the mold. Heating the rubber that contained a high percentage of iodine involved decomposition and the conversion of the rubber into a resinous mass. No vulcanization was perceptible when 0.1-1% of iodine was used. The test results of vulcanized rubbers containing 3-7.5% of iodine are given Tables 1, 2, and 3.

The per cent elongation and the residual elongation changed considerably in all the experiments. The resistance of the vulcanized rubbers to swelling in benzene is worthy of note. The extent of swelling diminished 148% at 160°, being approximately on a par with the swelling of sulfur vulcanized rubbers.

TABLE 1

Effect of the Percentage of Iodine Upon the Vulcanization of Rubber

Heating Time: 10 Minutes; Temperature: 120°

Rubber tests	Per cent iodine 3	5	7.5
Tensile strength, kg/sq cm	9.7	12	13.7
Elongation, per cent	1130	910	403
Residual elongation, per cent	63	51	12
Swelling in benzene after 24 hours, per cent	1068	920	740

TABLE 2

Effect of Changes in Temperature Upon the Vulcanization of Rubber

Per cent Iodine: 7.5%; Vulcanization time: 100 Minutes

Rubber tests	Temperature, °C [illegible]	120	140	160
Tensile strength, kg/sq cm	12	13.7	15.2	36.5
Elongation, per cent	53	403	307	55
Residual elongation, per cent	18	12	5	0
Swelling in benzene after 24 hours, per cent.	[illegible]	740	530	148

TABLE 3

Effect of Heating Time upon the Vulcanization of Rubber

Per cent Iodine: 7.5%; Temperature: 140°

Rubber tests	Time, minutes 10	20	40
Tensile strength, kg/sq cm	15.2	16.1	33
Elongation, per cent	307	120	62
Residual elongation, per cent.	5	1	0

Analysis of the solvent to find the percentage of vulcanized rubber it contained after swelling indicated that the vulcanized rubber did not dissolve in benzene.

These findings on the changes in the properties of rubber due to the action of iodine are evidence that iodine is a vulcanizer of rubber.

As we know, the addition of iodine to an unsaturated hydrocarbon involves the following reaction:

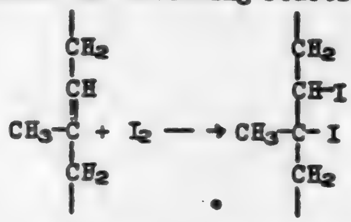

In the light of the foregoing and of this outline of the action of iodine, it must be concluded that the vulcanization effect (the formation of soft rubbers) is produced by the intramolecular reactions in which the double bonds of the rubber are saturated by the vulcanizing agent.

<u>Vulcanization of rubber with large amounts of sulfur</u>. Vulcanizing rubber with large amounts of sulfur enables us to explore the changes in the mechanical properties of rubber throughout the rubber vulcanization process, from the soft rubber to hard, hornlike ebonite.

The rubber compounds had the following compositions (parts by weight):

Rubber (smoked sheets)	100	–
Divinylsodium rubber..	–	100
Sulfur	50	50
Diphenylguanidine	2	2

Vulcanization was done in a steam press at 147° for 1, 3, 5, 7, 10, 15, 20, 25, 30, 40, 50, 60, 80, and 100 minutes.

The results of mechanical tests and analyses are shown in the graphs.

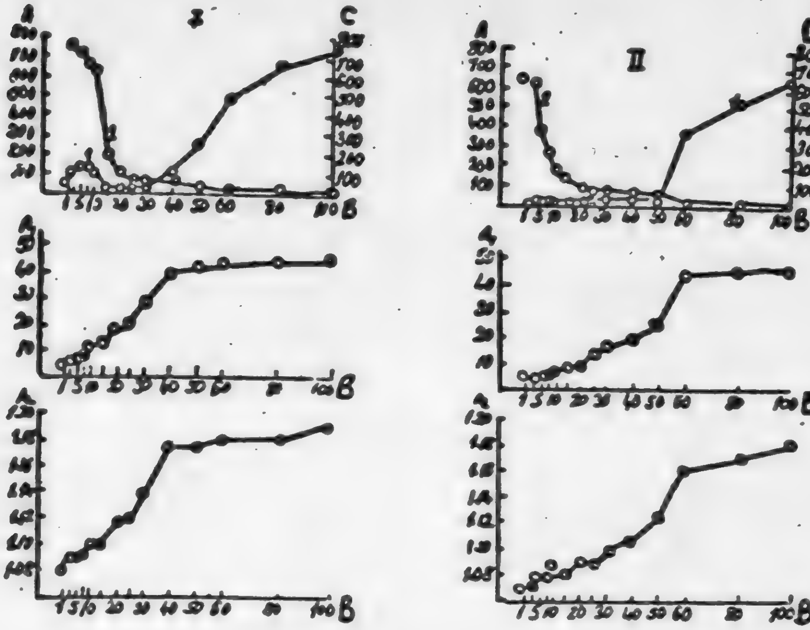

Changes in the mechanical properties of vulcanized rubbers as affected by the combined sulfur and the specific gravity of the rubber compound.

I - Made from natural rubber; II - made from divinylsodium rubber. A - Tensile strength, kg/sq cm; A_1 - Per cent sulfur; A_2 - Specific gravity; B - time, minutes; C - per cent elongation. 1 - Tensile strength; 2 - per cent elongation.

There is but little difference between the mechanical properties of vulcanized natural rubber and those of vulcanized divinylsodium rubber, except in the stage of vulcanization during the first 15 minutes, during which there is a great difference between in their mechanical properties. Nor was there much difference between these vulcanized rubbers in their subsequent processing.

There was hardly any change in the tensile strength (about 20 kg/sq cm) of the natural rubber during the time interval from 15 to 30 minutes or of the divinylsodium rubber (SKB) [RUSSIAN ABBREVIATION FOR THIS SYNTHETIC RUBBER] during the time interval from 1 to 50 minutes, notwithstanding the substantial increase in the percentage of combined sulfur (as much as 26-28% of the rubber). This led us to suppose that there are practically no intermolecular chemical reactions between the rubber and the sulfur (formation of "bridges") for a long period of vulcanization (formation of soft rubber). This point of view is supported by Rebinder and Pisarenko [1]. They assert that "according to the bridge theory, the strength of the SKB vulcanized rubbers ought to be increased by raising the percentages of combined sulfur, but no

increase in strength was observed even when high percentages of sulfur were introduced into the SKB." At the same time, noting that 90-98% of the combined sulfur does not enter into the formation of "bridges", Rebinder and Pisarenko point out the importance of the sulfur that reacts with the rubber intramolecularly, forming polar groups, a formation that they regard as the principle underlying the changes in the physical and mechanical properties of rubber due to vulcanization.

Without denying the importance of polar groups, we still must say that their formation is by no means the basic reason for the change in the properties of rubber during vulcanization.

The formation of polar groups, like that of "bridges", does not explain the i[illegible] lowered strength of the vulcanized rubbers referred to above, despite the substantial increase in the percentage of combined sulfur and, hence, of the polar groups.

The following factors should be borne in mind in this connection, as the authors of the present paper see it:

1) The conditions governing the mutual bonds between the molecules in the rubber, which constitute a system of intertwined long straight-chain molecules spaced close together.

2) The change in form of the straight-chain rubber molecules caused by the interaction with sulfur and, as a result thereof, the shrinkage of the whole system subsequently confirmed by experiment (cf the figure).

3) The establishment of deformed and stressed states within the rubber molecules. Byzov papers [2] on caoutchouc and rubber indicate that he attributed considerable importance to the shrinkage of rubber during vulcanization, believing that the specific gravity of the compound, due to the shrinkage of the whole mass, was the clue to the nature of rubber vulcanization.

The strength increased abruptly and considerably when natural rubber was vulcanized for 30 to 100 minutes and when divinylsodium rubber was vulcanized for 50 to 100 minutes. In this stage of vulcanization the rubber changes from a soft elastic state into a hard, hornlike product (ebonite), possessing exceptionally high mechanical, physical, and chemical properties. In contrast to a soft rubber, the formation of such a product is readily explained by the intermolecular chemical reactions "lacing" the straight-chain rubber molecules into a strong system. This is borne out by the substantial increase in the strength of rubber when the percentage of combined sulfur is raised slightly during the stage in which ebonite is formed.

SUMMARY

The vulcanizing of caoutchouc to a soft rubber may be brought about by intermolecular reactions.

The author wishes to thank E. E. Sorkin, M. M. Kubanov, D. N. Martynenko, N. N. Kanstantinova, and A. T. Sidorinova for the performance of various tasks involved in preparing the rubber and ebonite samples and testing them.

LITERATURE CITED

[1] A. P. Pisarenko and P. A. Rebinder, Light Industry 1950, 8.
[2] B. V. Byzov, Jour. Russ. Phys. Chem. Soc. 53, 103 (1921).

Received January 20, 1950.

THE POLYMERIZATION OF NONENE[1]

B. N. Rutovsky and L. A. Alferova

Central Institute of Wood Chemistry Research

Nonene was polymerized in sealed ampoules (containing 0.9-1.0 gram) on a boiling water bath. Three sets of tests were run: 1) with air present; 2) with nitrogen present; and 3) with benzoyl peroxide present. The polymer was precipitated by methanol from a benzene solution, the precipitation rate being the same for every sample, and the temperature being kept constant at 20°. The polymer was thrown down as white flocs The progress of polymerization at 100° is given in Table 1 and in the figure.

TABLE 1

Polymerization of Nonene at 100°

Time	Polymer yield, % of the initial monomer[2]					
	In air		In nitrogen		With 0.1% of benzoyl peroxide	
	I	II	I	II	I	II
20 minutes	-	-	-	-	6.05	2.83
45 minutes	5.78	2.97	2.52	1.54	8.18	6.05
1.5 hour	7.18	4.91	4.27	2.82	10.75	7.60
3.0 hours	9.13	6.18	6.05	4.01	12.87	8.71
6.0 hours	12.73	8.04	9.22	5.97	16.05	10.59
9.0 hours	15.91	9.62	12.15	7.22	19.54	11.95
18.0 hours	23.05	14.00	20.09	10.89	26.01	16.05

In every case the reaction mixture was a liquid, the viscosity of which rose with the polymerization time. Hence, the polymer is readily soluble in the monomer. When the reaction mixture contained 25% of the polymer, the mixture resembled glycerol at low temperature and was faintly yellowish. The relative viscosity of 1% solutions of the reprecipitated polymer was determined in benzene at 20°, by measuring the rate of flow from the usual capillary viscosimeter.

The results are tabulated in Table 2.

1) Report III of a series on the "Synthesis of 6,6-dimethyl-2-vinylbicyclo-(1,1,3)-heptene-(2) and its polymerization".

2) Physical constants of the monomer: I – d^{20}_4 0.8871; n^{20}_D 1.5045, α^{20}_D + + 12.48°; II – d^{20}_4 0.8864; n^{20}_D 1.5039; α^{20}_D + 8.70°

TABLE 2

Viscosity of a 1% Solution of the Polymer in Benzene at 20°

(Polymerization in Air)

Polymerization time, hours	Relative viscosity
3.0	1.115
6.0	1.111
9.0	1.112
18.0	1.111

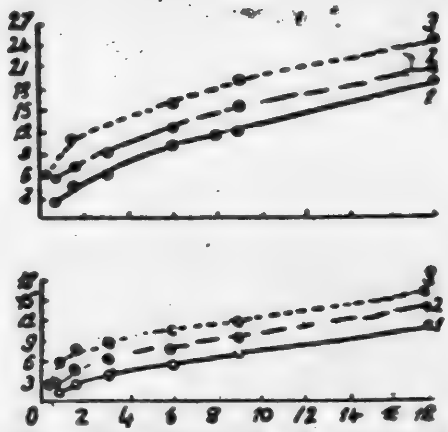

The polymerization of nonene at 100°

Polymerization conditions: 1 – in nitrogen; 2 – in air; 3 – in the presence of 0.1% of benzoyl peroxide.

The polymer produced by polymerizing the nonene in nitrogen was purified by reprecipitating it five times from fresh benzene, after which we determined the specific viscosity of a 1% solution in benzene, the specific rotatory power of the benzene solution, the Kramer-Sarnov softening temperature, and its solubility in various solvents. The approximate molecular weight and the per cent polymerization were determined from the well-known Staudinger equation:

$$\eta_{sp.} = K_m CM,$$

the constant K_m being taken as $1.8 \cdot 10^{-4}$, *i.e.*, equivalent to that of styrene. The results of our analyses and determinations are cited below.

Polymerization in nitrogen at 100°. Specific viscosity of a 1% solution in benzene: 0.145. Molecular weight: 11922. Per cent polymerization: 80. Softening point: 170-180°. Appearance after precipitation: a white powder. Specific rotatory power: $[\alpha]^{27}_{D} + 33.93°$. $\eta_{sp.}/C = 2.146$.

Solubility: partially soluble in ether, with difficulty; slightly soluble in gasoline; soluble in benzene and in chloroform; insoluble in alcohol, ethyl acetate, acetic acid, or water.

3.392 mg subs.: CO_2 11.140 mg; H_2O 3.136 mg.
3.025 mg subs.: CO_2 9.925 mg; H_2O 2.838 mg.
Found %: C 89.57, 89.48; H 10.35, 10.50.
$(C_{11}H_{18})x$. Calc. %: C 89.19; H 10.81.

The specific viscosity and the molecular weight of the polymers produced by polymerization in nitrogen, in air, and in the presence of benzoyl peroxide are listed in Table 3.

TABLE 3

Specific Viscosity and Molecular Weight of Polymers as a Function of the Polymerization Conditions

Polymerization conditions	Specific viscosity, ($\eta_{sp.}/C$)	Molecular weight, M
In nitrogen	2.146	11922
In air	1.702	9455
In the presence of 0.1% of benzoyl peroxide	1.317	7873

SUMMARY

1. Nonene can be polymerized, yielding high-molecular products, thermal polymerization in air yielding a product with a molecular weight approximating 9500, thermal polymerization in nitrogen yielding a product with a molecular weight of about 12000, and polymerization in the presence of 0.1% of benzoyl peroxide yielding a product with a molecular weight of about 8000 (as calculated by the viscosimetric method, assuming K_m to be $1.8 \cdot 10^{-4}$, as for styrene).

2. It has been proved that the polymerization of nonene is a chain-type reaction, since prolonging the polymerization time merely increases the polymer yield while the molecular weight of the polymer secured at various stages of polymerization remains constant.

3. The appearance and solubility of polynonene resemble those of polystyrene, but its softening point is somewhat higher.

Received January 27, 1950.

BLANK
PAGE

CORRECTED TABLES FOR THE ARTICLES BY A. L. ROTINYAN AND V. YA. ZELDES[1]

Report I, JAC 23, 717 (1950)[2]

TABLE 1

Nickel concentration, grams/liter	pH
10.0	5.8
25.0	5.4
39.6	5.3
61.0	5.1

The pH at the onset of hydrate formation drops about 0.26 for every 10° of temperature rise.

All the values of pH cited in Tables 2 and 3 should be diminished 0.4.

TABLE 4

H_3BO_3 concentration, grams/liter	pH at following NaCl concentrations in grams/liter: 5	50
0	5.3	5.2
10	4.7	4.3
20	4.3	4.0
40	3.7	3.4

TABLE 5

Temperature, °C	pH at following nickel concentrations, grams/liter: 21	40	63
20	5.2	5.0	4.8
50	4.4	4.3	4.1
70	3.8	3.7	3.6

Report II, JAC 23, 936 (1950)[3]

TABLE 1

Copper concentration, grams/liter	pH: H_3BO_3 0 g/liter	H_3BO_3 20 grams/liter
0.004	5.3	–
0.05	5.1	–
0.19	5.0	4.2
0.50	4.7	–
0.98	4.5	4.0
3.11	4.3	3.9

TABLE 3

Concentration of ferrous oxide, grams/liter: Before the run	After the run	pH
0.00	0.00	5.3
0.09	0.06	5.0
0.49	0.43	4.7
1.08	1.00	4.4
3.90	1.85	4.3

1) These corrections in no way affect the text or the conclusions of the papers in question.

2) Cf. Consultants Bureau English translation, p. 757.

3) Cf. Consultants Bureau English translation, p. 991.

A. L. Rotinyan and V. Ya. Zeldes

BLANK
PAGE

PLATE

The Physical Characteristics of Fine-Grained Crystalline Masses in Relation to Reactions of Their Mixtures (p. 629).

Fig. 2. Microphotographs of polished sections of powders: a, b, c – grain size 0.088–0.12 mm; d – grain size below 0.035 mm.
a) Anthracite powder (X 50); b) anthracite powder (X 50); c) thoroughly shaken anthracite powder (X 50); d) metallic copper powder, produced by reducing $CuSO_4$ solutions (X 120).

A Method of Eliminating Sulfur from the Precipitating Bath in Viscose Manufacture (p. 681)

1,2) Precipitating flasks; 3) rubber tubing; 4) rubber tubing; 5) air line; 6) overflow flask; 7) separatory flask; 8) outlet to receiver; 9) receiver; 10) unpurified bath entrance tube; 11) siphon tube; 12) supply flask; 13) air discharge tube and condenser.

The Effect of Deformation upon Metal Potentials (P. 687).

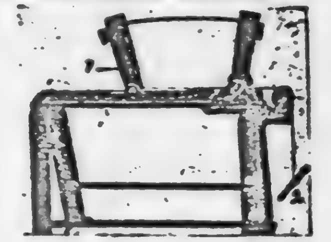

Fig. 1. b) Weighting the device: 1 – blocks; 2 – weight.

The Hydrodynamics of Packed Extraction Columns (p. 699).

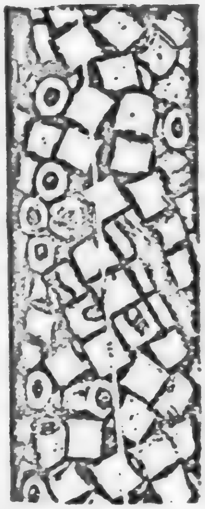

Fig. 2. Liquid flow during film operation.

Fig. 3. Liquid flow in turbulent operation.

Fig. 4. Liquid flow in eddy operation.

Fig. 5. Flooding of the column above the packing.

Fig. 6. Flooding of the column below the packing.

BLANK
PAGE